

EFFECTS OF MANUFACTURING DEFECTS ON THE STRENGTH OF  
TOUGHENED CARBON/EPOXY PREPREG COMPOSITES

by

Luke Everett Turoski

A thesis submitted in partial fulfillment  
of the requirements for the degree

of

Master of Science

in

Mechanical Engineering

MONTANA STATE UNIVERSITY – BOZEMAN  
Bozeman, Montana

July 2000

APPROVAL

of a thesis submitted by

Luke Everett Turoski

This thesis has been read by each member of the thesis committee and has been found to be satisfactory regarding content, English usage, format, citations, bibliographic style, and consistency, and is ready for submission to the College of Graduate Studies.

Dr. Douglas Cairns

\_\_\_\_\_  
(Signature)

\_\_\_\_\_  
Date

Approved for the Department of Mechanical Engineering

Dr. Vic Cundy

\_\_\_\_\_  
(Signature)

\_\_\_\_\_  
Date

Approved for the College of Graduate Studies

Dr. Bruce McLeod

\_\_\_\_\_  
(Signature)

\_\_\_\_\_  
Date

STATEMENT OF PERMISSION TO USE

In presenting this thesis in partial fulfillment of the requirements for a master's degree at Montana State University-Bozeman, I agree that the Library shall make it available to borrowers under rules of the Library.

If I have indicated my intention to copyright this thesis by including a copyright notice page, copying is allowable only for scholarly purposes, consistent with "fair use" as prescribed in the U.S. Copyright Law. Requests for permission for extended quotation from or reproduction of this thesis in whole or in parts may be granted only by the copyright holder.

Signature\_\_\_\_\_

Date\_\_\_\_\_

## ACKNOWLEDGEMENTS

Pascal in his *Pensees* wrote, “Certain authors, speaking of their works, say, ‘My book,’ ‘My commentary,’ ‘My history,’ etc. They would do better to say, ‘Our book,’ ‘Our commentary,’ ‘Our history,’ etc., because there is in them usually more of other people’s than their own.”

My thanks goes out to the entire MSU composites group and my family. Special thanks goes to Boeing, NASA, and the Montana Space Grant Consortium, whose support made this work possible.

## TABLE OF CONTENTS

LIST OF TABLES .....	viii
LIST OF FIGURES.....	ix
ABSTRACT .....	xiii
1. INTRODUCTION.....	1
2. BACKGROUND.....	5
Previous Gapped Composite Research .....	5
Automated Tow-Placed Laminates .....	5
Contour Tape Layup Laminates .....	8
Related or Relevant Research .....	11
Toughened Resin Systems.....	11
Layer Waviness .....	14
Compression Testing.....	15
3. EXPERIMENTAL METHODS .....	20
Material Description.....	20
Panel Gap Configurations .....	21
General Gap Formation .....	21
Specific Panel Configuration.....	22
Sample Selection and Preparation.....	23
Sample Selection .....	23
Sample Preparation.....	24
Characterization Measurements .....	25
Thickness Variations .....	25
Gap Characterizations .....	26
Failure Tests .....	26
Tension .....	29
Unnotched .....	29
Open Hole.....	30
Compression.....	31
Unnotched Samples.....	31
Open Hole Samples .....	32
Loading Methods.....	33
Elastic/Strain Field Tests.....	37

Damage Progression.....	39
4. NUMERICAL METHODS.....	40
Material Properties .....	41
Unnotched Models .....	43
Meshing.....	43
Boundary Conditions.....	45
Hole Models .....	46
Solids.....	46
Stacked Shells .....	47
Meshing.....	47
Gaps Centered Mesh .....	48
Gaps Offset Mesh.....	50
Boundary Conditions.....	51
Various Gap Configurations.....	52
Mesh Independence.....	53
Damage.....	53
Failure Criteria .....	54
5. EXPERIMENTAL RESULTS.....	56
Sample Thickness Measurements .....	56
Elastic Strain Field Tests.....	59
Damage Progression Tests .....	62
Failure Tests.....	66
Tension .....	66
Compression.....	70
Machine Grips .....	70
Fixture .....	76
Comparison of Machine Grips and Fixture.....	78
Tension-Compression Comparisons .....	79
6. NUMERICAL RESULTS.....	81
Unnotched Solid Models.....	81
Open Hole Shell Models .....	85
Centered Gap Mesh.....	85
Offset Gap Mesh .....	91
Comparison of Centered and Offset Meshes.....	95
Experimental and Numerical Comparisons.....	96
Unnotched Compression .....	97
Open Hole Compression .....	98

7. CONCLUSIONS AND RECOMMENDATIONS.....	103
Results .....	103
Experimental .....	103
Numerical .....	105
Design and Manufacturing Recommendations .....	106
Future Work .....	108
REFERENCES CITED .....	110
APPENDICES.....	112
Appendix A Test Results .....	113
Appendix B Quantitative Photoelastic Results .....	121

## LIST OF TABLES

Table	Page
3.1. Specific panel characterization data .....	23
3.2. Experimental Test .....	27
4.1. Ply Elastic Properties .....	41
4.2. Resin Elastic Properties.....	42
4.3. Ply Failure Strengths .....	43
4.4. Numerical matrix.....	55
5.1. Damaged sample data.....	63
5.2. Averaged tension test results and comparisons.....	66
5.3. Unnotched Compression Average Results .....	71
5.4. Machine gripped OHC failure data .....	72
5.5. Statistical data for MTS OHC tests .....	73
5.6. Fixture OHC failure data.....	76
5.7. Statistical data for fixture OHC tests.....	77
6.1. Comparison of failure stresses in centered gap mesh runs, open hole model .....	90
6.2. Comparison of OHC failure stresses in offset gap, open hole model .....	94

## LIST OF FIGURES

Figure	Page
1.1. Formation of gaps.....	3
1.2. Formation of gap interaction regions .....	3
2.1. Fabrication of overlap/gap defects in test laminates. From Sawicki and Minguet. ....	7
2.2. Laminate gap parameters, gap width, stagger distance, and separating plies. Nominal parameter values are indicated by parenthesis. From Edens and Cairns. ....	8
2.3. Graphical summary of Edens and Cairns numerical results .....	10
2.4. Interlayer thermoplastic toughening mechanism. ....	12
2.5. Particulate interlayer toughened prepreg. From Odagiri, Kishi, and Yamashita. ....	13
2.6. Compression strength of layer wave specimens. From Adams and Hyer. ....	15
2.7. Kink band geometry. From Camponeschi. ....	18
2.8. Microstructural compression response. Adopted from Camponeschi. ....	19
3.1. Formation of gap interaction region with four ply orientations .....	21
3.2. Formation of gap interactions in the Boeing panels .....	22
3.3. Gapped regions of interest.....	24
3.4. Grid used for specimen thickness variation measurements. All data points are 12mm (1.5 in.) apart. ....	26

LIST OF FIGURES – Continued

3.5	Unnotched tension sample .....	29
3.6	Open hole tension sample .....	31
3.7	Unnotched compression sample.....	32
3.8	Open hole compression sample with weight attached .....	33
3.9	Compression testing fixture .....	35
3.10	Compression fixture test setup .....	36
3.11	Photoelasticity setup .....	38
4.1	Solid, unnotched mesh. ....	44
4.2	Solid unnotched mesh detail region .....	45
4.3	Boundary conditions for the unnotched solid models.....	46
4.4	Mesh with the gaps centered on the hole .....	49
4.5	Mesh with the gaps offset from the hole .....	51
4.6	Boundary conditions for models with centered gaps .....	52
4.7	Boundary conditions for models with offset gaps.....	53
5.1	Sample thickness variations with an ungapped gauge section.....	57
5.2	Gapped sample thickness variations .....	58
5.3	Photoelastic contours for ungapped sample .....	59
5.4	3 gap photoelastic sample .....	60
5.5	2 gap photoelastic sample sequence .....	61
5.6	Hole edge damage in sample 2gh45 .....	64
5.7	Fiber kinking in a zero degree ply, sample 2gh45 .....	65

LIST OF FIGURES – Continued

5.8.	Damage in a zero ply, sample 2gh45 .....	65
5.9.	Fiber splitting in a zero degree ply, sample 2fg34 .....	66
5.10.	Failed unnotched tension sample .....	68
5.11.	Tension failure results .....	69
5.12.	Open hole tension sample failure .....	69
5.13.	Failed UNC sample .....	71
5.14.	Machine gripped OHC gap comparisons .....	72
5.15.	Typical OHC failure .....	74
5.16.	Stress strain curve for an OHC test .....	75
5.17.	Fixture OHC test comparisons .....	76
5.18.	Typical fixture OHC failure .....	77
5.19.	Comparisons between gripped and fixture tested OHC samples .....	78
5.20.	Tension/compression test comparisons .....	80
6.1.	Strain contours for an unnotched solid model, 3 gap run, zero degree ply .....	83
6.2.	Strain contours for an unnotched solid, 4 gap run, zero degree ply .....	84
6.3.	Longitudinal strain contours for open hole shell model, gaps centered mesh, no gap run, zero degree layer .....	86
6.4.	Longitudinal strain contour detail region for open hole shell model, centered gap mesh, no gap run, zero degree layer .....	86
6.5.	Strain as a function of the distance from the hole edge .....	88
6.6.	Detail of longitudinal strain contours for an open hole model, centered gap mesh, 4 gap run .....	89

LIST OF FIGURES – Continued

6.7.	Strain contours for the loading direction, open hole shell model, offset gaps mesh, ungapped run.....	91
6.8.	Loading direction strain contours for a open hole shell model, offset gaps mesh, 4 gap run.....	92
6.9.	Detail of loading direction strain contours for a open hole shell model, offset gaps mesh, 4 gap run.....	92
6.10.	Zero degree ply maximum stress contour plot of an open hole shell model, offset gap mesh, 4 gap run.....	93
6.11.	OHC stress based numerical comparison.....	96
6.12.	OHC stress based experimental/numerical comparisons .....	99
6.13.	Schematics of samples with varying thickness .....	101
6.14.	Example of layer waviness in a gapped laminate impregnated-sized test results on a common graph.....	102
6.15.	Strength reduction range (shaded area) for gapped samples with out of plane waviness. Adapted from Adams and Hyer. ....	102

## CHAPTER 1

## INTRODUCTION

The aerospace community uses fiber reinforced composite materials extensively in structural designs. Unidirectional composite plies are one layer of parallel continuous fiber reinforcement, with a matrix or binder surrounding the fibers. Composite laminates are made from several layers of variously oriented plies. A description of basic motivations and principles for composite materials is found at the beginning of almost every introductory composites textbook [e.g. Mechanics of Composite Materials, Robert Jones, (1975)].

There are many material options for both the fibers and the matrices. However, the dominant fiber in recent years for structures requiring high stiffness and strength is carbon/graphite [Agarwal and Broutman, (1990)]. Most glass fiber composites are made from dry woven fiber fabrics that are impregnated with resin at the time of the laminate fabrication. These materials are robust in that glass fibers can tolerate high strain to failure. The stiffer, lower strain to failure carbon or graphite fibers abrade or break when woven. The weaving can also introduce waviness and inconsistency in the fibers, reducing the strength of the composite [Pirrung, (1987)].

A preimpregnated ply, or prepreg, requires no weaving of the fabric. The prepreg ply is produced in rolls of tape that contain the unidirectional fibers already impregnated with the matrix. Prepreg materials generally perform better structurally than the

corresponding dry fabric/resin impregnation method as a consequence of better manufacturing controls [Dominguez, 1987]. Due to their success, these materials have been implemented into thousands of applications, including commercial aircraft. The drawback of prepreg is that it can have considerably higher manufacturing costs.

Two manufacturing techniques have been used extensively to fabricate laminates from prepreg materials: hand layup and automated tape or tow-laying. Hand layup affords low initial set up costs and the use of large sheets of prepreg. However, it is labor intensive, time consuming, and can produce an inconsistent quality in final parts [Pirring, (1987)]. All of these factors lead to expensive manufacturing costs and so companies developed machines to automate the process [Williams, (1987)].

Automated tape and tow-laying in composite fabrication has increased significantly in recent years [Grant, (2000)]. Automated tape laying machines use relatively narrow (25-150mm) tapes to build composite parts. Several adjoining tapes are then required to build a large composite part. As the tapes are laid together, three manufacturing conditions arise.

First, the tapes can be laid perfectly beside each other, causing no discontinuity of prepreg material. However, width variance exists in the machine laid tape, so this variance translates to inaccuracy of the tape placements. This leaves two options. Either an overlap or a gap must exist between the adjoining tapes. Previous research on the geometric asymmetries and perturbation of reinforcing fibers caused by fiber overlaps led Boeing to implement a no overlap design specification. This leaves a gap between the tapes as the remaining option, as shown in Figure 1.1.

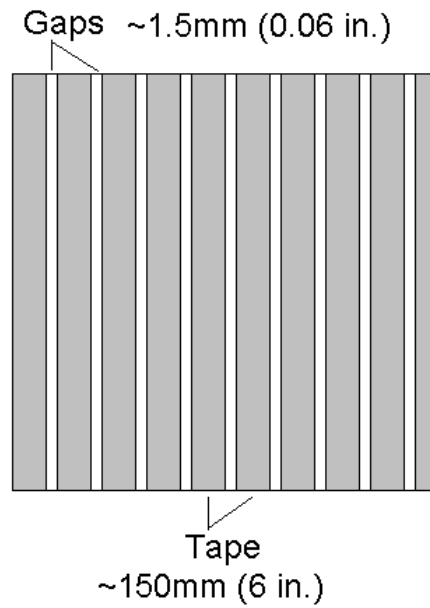


Figure 1.1. Formation of gaps.

As the layup proceeds, the gaps of each ply cross the others. The formation of the gap regions is shown in the two layer, simplified schematic of Figure 1.2.

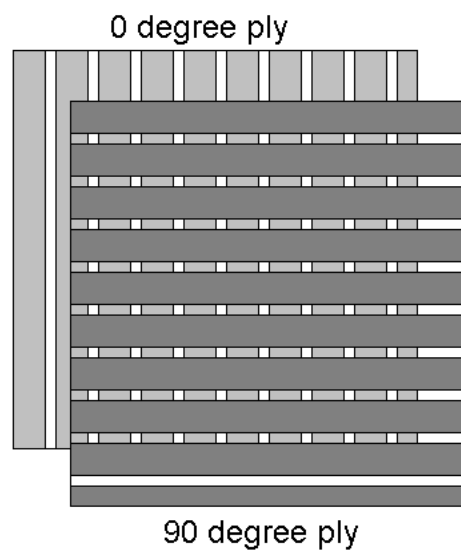


Figure 1.2. Formation of gap interaction regions.

Here, the small white squares represent the gap regions formed as a  $0^\circ$  layer is laminated with a  $90^\circ$  layer. These regions contain no reinforcing fibers and will be comprised of resin, voids, or both. In addition to the resin rich regions, the gaps also perturb the layer geometry; this is manifested in out of plane layer waviness and overall laminate thickness variations.

Little published research and testing have been done on these “gapped” composites, although the manufacturing techniques have been implemented. This lack of knowledge forces companies to conservatively knockdown the composite strengths. This motivates the research presented in this thesis.

The research objectives are to study the effects of the gapped regions on the material behavior with a series of mechanical tests and computer simulations. Then, design and manufacturing recommendations can be made for these gapped material.

## CHAPTER 2

### BACKGROUND

Some work has been previously done in the area of gapped regions created during automated prepreg manufacturing. These provide a background for the work presented in this paper. While none of the work specifically examines the question at hand, it helps develop a better foundation for understanding the problem. Following the survey of similar work, a few areas that became important in the research and results are discussed.

#### Previous Gapped Composite Research

##### Automated Tow-Placed Laminates

Some research was performed on automated tow-placed laminates. These differ slightly from automated tape layup. Instead of prepreg tapes, individual prepreg tows (about 2.54mm (0.1 in.) wide) are laid by the machine. It is obvious that gap and overlap regions are present. In fact, due to the small widths of the laid tows, gap and overlap regions are much more frequent in a tow-placed laminate compared to a similar laminate built with tapes.

Cairns, Ilcewicz, and Walker [(1993)] published data on the effects of the automated manufacturing defects. Notched tension experimental and numerical results were compared. The experimental failure improvement ratio from tape to tow was reported to be 0.795. This improvement was attributed to a larger damage zone in the tow placed laminates at the crack tip. The notched gapped composites were modeled

globally and locally to study the influence of the inhomogeneity on the strain field and damage progression.

A unique finite element method was implemented. Modeling the multilayered composites with solid elements would have been computationally intensive. However, a laminated shell would not allow damage in specific plies of the laminate. So, a stacked shell approach was taken. A set of common nodes could be shared with separate shell elements for each layer. Then, damage was induced by splitting the nodes, giving the required elements separate nodes to act independently from one another, layer to layer.

While numerical results suggested a slight improvement from the effect of the inhomogeneity on the strain field alone, it could not account for the considerable improvement realized experimentally. Damage modeling showed splitting of the  $0^\circ$  ply greatly alleviated the influence of the notch. Delaminations seemed to do the same, and a combination of both provided the most benefit. These analyses showed up to a 36% benefit from these damage combinations.

Possible mechanisms for the experimentally observed improvement due to lap and gap regions for tow-placed composites were shown in this study. However, the improvement was only seen in notched tension samples.

Sawicki and Minguet studied the effect of these intraply gaps and overlaps on compression strength [(1998)]. They also used tow-placed laminates for the study. They studied both unnotched and open hole compression samples. These samples were laid up by hand with a gap and overlap in one of the  $90^\circ$  layers. This is shown in Figure 2.1. Gaps of 0.76mm (0.03 in.) and 2.54mm (0.1 in.) were studied. Again, each of these defects contained both a gap and an overlap. Laminates were nominally about 4-5mm

thick, depending on the layup. Unnotched compression samples 13mm (0.51 in.) wide were tested in a modified IITRI fixture. A Boeing anti-buckling fixture tested samples that were 38mm (1.5 in.) wide with a 6.35mm (0.25 in.) diameter hole OHC.

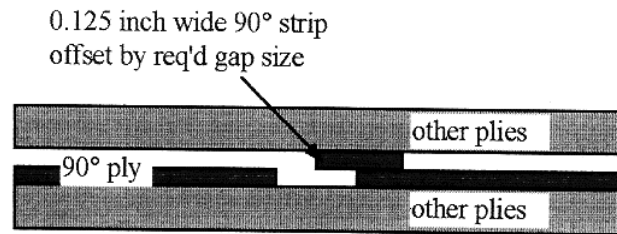


Figure 2.1 Fabrication of overlap/gap defects in test laminates.  
From Sawicki and Minguet.

Unnotched samples with defects produced reductions in mean compression failure strain of 7.5-12.9% for samples at standard conditions. Hot wet samples produced reductions of around 20%. OHC samples produced reductions of 11.6 and 9.5% for standard conditions, and 14.7 and 27% for hot wet conditions. The authors noted that a large reduction was typically seen for the .76mm (0.03 in.) gap, and only a slightly greater one was noticed for the 2.54mm (0.1 in.) gaps. They noted that the hot wet reductions were significantly higher than the standard reductions. They stated that this implied the failure mechanisms which occurred local to an overlap/gap defect were likely to be matrix dominated. The authors discussed previous work studying samples with considerably more frequency of defects in every ply. A significant difference was not observed between the samples with one defect and the work done with samples containing many defects. This indicated that the failures were likely due to out of plane

waviness of the  $0^\circ$  plies, and that this occurred with any defect present [Sawicki and Minguet, (1998)].

Finite element models were also created, modeling the local fiber waviness caused by overlap/gap regions. Failure was most likely driven by interaction of in-plane compression and interlaminar shear stress of the  $0^\circ$  plies. A recommendation was made to reduce the allowable compression strength for materials containing these defects.

### Contour Tape Layup Laminates

Edens and Cairns [(2000)] performed numerical modeling work on gaps in tape laid composites. Solid models of 22 and 28 plies were built for ABAQUS. The work studied the elastic unnotched tensile response of the geometry. No overlaps were modeled because Boeing specifications did not allow them. The research studied peak elastic tensile strains while varying several manufacturing parameters. These parameters are layup, gap width, stagger distance, and stagger number. Variables are shown in Figure 2.2.

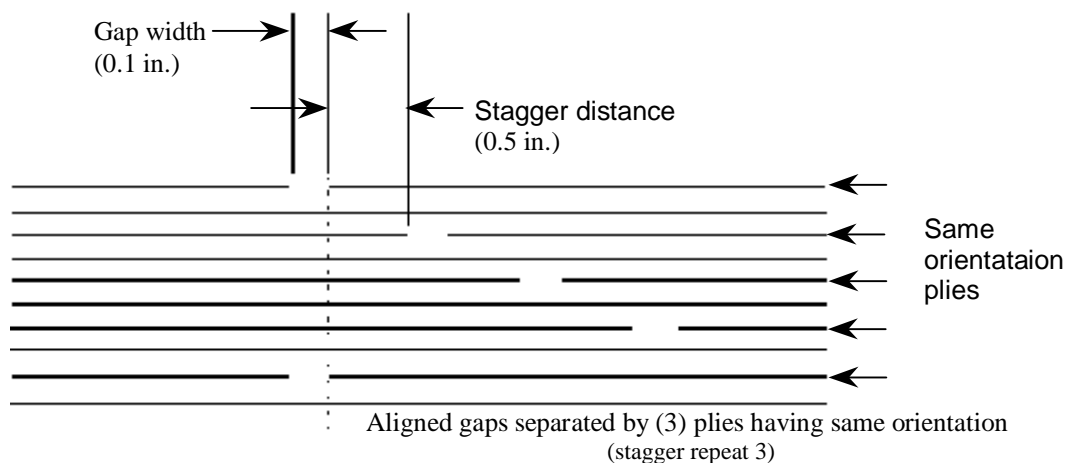


Figure 2.2. Laminate gap parameters, gap width, stagger distance, and separating plys. Nominal parameter values are indicated by parenthesis. From Edens and Cairns.

Gap width refers to the intraply spacing between adjacent tape edges. Distance between the nearest gap edges of two same-orientation plies, when not separated by any other ply of that orientation, is the stagger distance. It is required that before gaps of two different same-orientation plies may align they must be separated by additional same orientation plies with sequentially staggered gaps. This is the stagger repeat number.

The models developed did not include fiber waviness. This was primarily because of the no overlap condition. The overlaps were considered be the predominate cause of the waviness, and so waviness would be negligible in the absence of them. Also, the models were quite complicated and large without waviness. The strain responses were plotted in a bar chart for clarity, shown in Figure 2.3. The following summarizes the effects of varying the mentioned parameters.

- 22&28 ply laminates with a 0.06” gap width  
 $\epsilon(\text{stagger repeat } 2) > \epsilon(\text{stagger repeat } 3)$
- 22&28 ply laminates with a 0.1” gap  
 $\epsilon(\text{ stagger repeat } 3) > \epsilon(\text{ stagger repeat } 2)$
- 22&28 ply laminates with a stagger repeat 2 and 0.06 & 0.1 gap widths  
 stag dist to  $\epsilon$  relation: stag dist  $\uparrow$ - $\epsilon$   $\downarrow$  (small)
- 28 ply laminate with a stagger repeat 3 & 0.06” gap width  
 stag dist to  $\epsilon$  relation: stag dist  $\uparrow$ / $\epsilon$   $\uparrow$  (small)
- 28 ply laminate with a stagger repeat 3 & a 0.1” gap width  
 stag dist to  $\epsilon$  relation: upside down parabola (see data)
- 22 ply laminate with a stagger repeat 3 & a 0.06” gap width  
 stag dist to  $\epsilon$  relation: stag dist  $\uparrow$ / $\epsilon$   $\uparrow$  (very small)
- 22 ply laminate with a stagger repeat 3 & a 0.1” gap width  
 stag dist to  $\epsilon$  relation: upside down parabola
- 22&28 ply with a stagger repeat 3  
 $\epsilon(.1 \text{ gap}) > \epsilon(.06 \text{ gap})$
- 22&28 ply laminates with stagger repeat 2  
 $\epsilon(.06 \text{ gap}) > \epsilon(.1 \text{ gap})$  (small)
- stagger repeat 2 & 3 with 0.06” & 0.1” gap widths  
 $\epsilon(28 \text{ ply laminate}) > \epsilon(22 \text{ ply laminate})$

- Except for “weird” mesh, strains within 8% of nominal (12% for weird mesh).

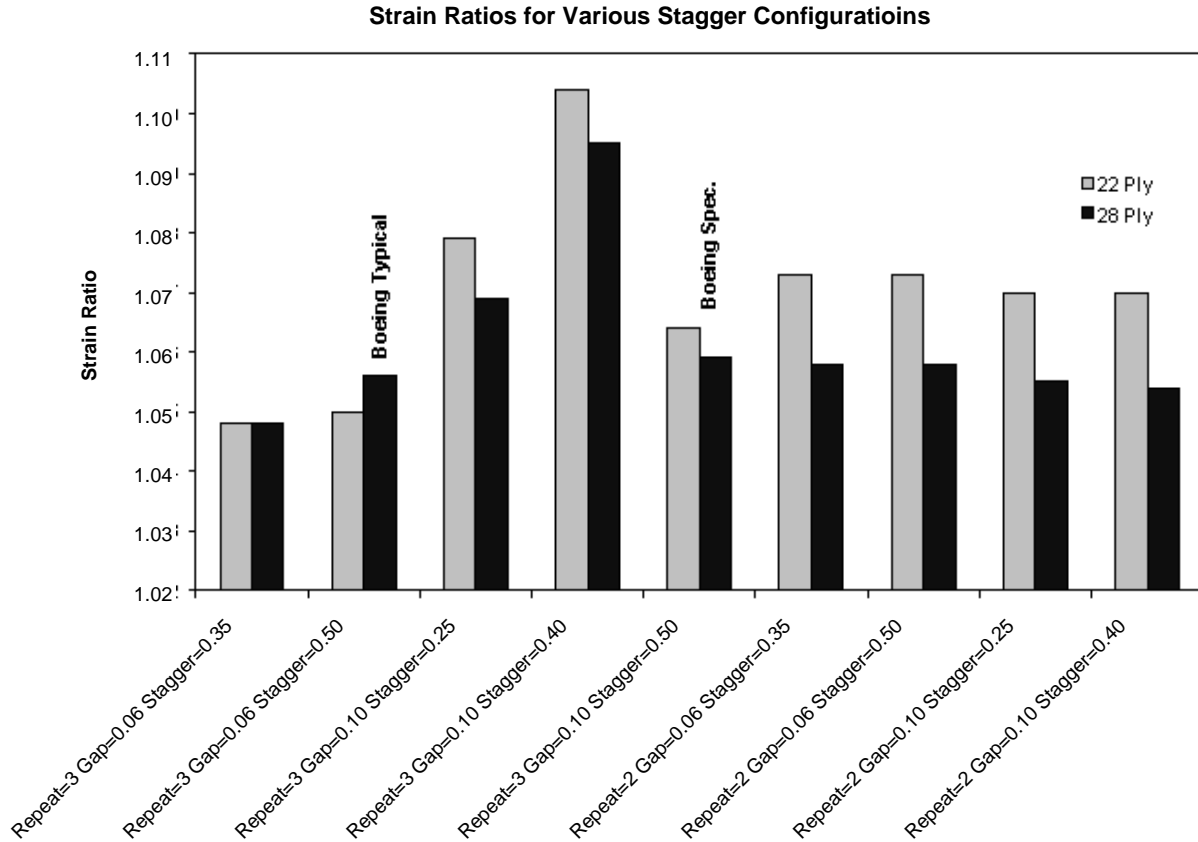


Figure 2.3 Graphical summary of Edens and Cairns numerical results.

All of the gap configurations had higher strains than a nominal, ungapped case. This was the result of the material inhomogeneity alone. No failure or damage was studied. This result points the opposite direction from that of Cairns, Icelwicz, and Walker. They found a decrease in maximum strain with the introduction of gaps. The source of this

difference is unclear, but it should be noted that one studied tow placement with notches, while the other unnotched tape. The geometries modeled were quite different.

### Related or Relevant Research

#### Toughened Resin Systems

Many early composites, and several used extensively today, use a relatively brittle matrix system. These systems provide good properties at a low cost. However, their brittleness is illuminated in a dynamic, impact event. A localized impact can happen various ways in manufacturing and applications. One such way is if a tool is dropped onto the composite surface during maintenance. The composites industry, encouraged by aerospace manufacturers, began to address this issue with alternative resins.

Thermoplastics were studied and implemented as an alternative. However, these were denser than thermosets, and reduced the weight savings associated with the materials. They also typically had lower modulus, less chemical resistance, higher viscosities, and their properties degraded at high temperatures [Gosnell, (1987)]. Some research also indicated a limit of composite toughness that became independent of resin toughness after the resin reached a certain toughness level [Cairns, (1990)]. This showed that although the damage or process zone for an exceedingly tough resin may be quite large, it is constrained in a composite by the layer interfaces. This led to alternative toughening mechanisms.

Several companies developed interlayer toughened systems. Although the manufacturing techniques vary, these techniques generally place particles of thermoplastic into the thermoset resin. These particles resist fracture, causing the fracture

path to circumvent the particles. This has been called a torturous crack path, making the crack grow in a non self-similar fashion than in traditional crack growth

Boeing utilized the TORAYCA T800H/3900-2 version of these toughened materials. This is illustrated in Figures 2.4 and 2.5. Odagiri, Kishi, and Yamashita [(1996)] reported that most delaminations due to impact happen along ply interfaces. Therefore, they (Toray) dispersed the thermoplastic particles along the ply interfaces. This is the material used for the laminates tested in this research.

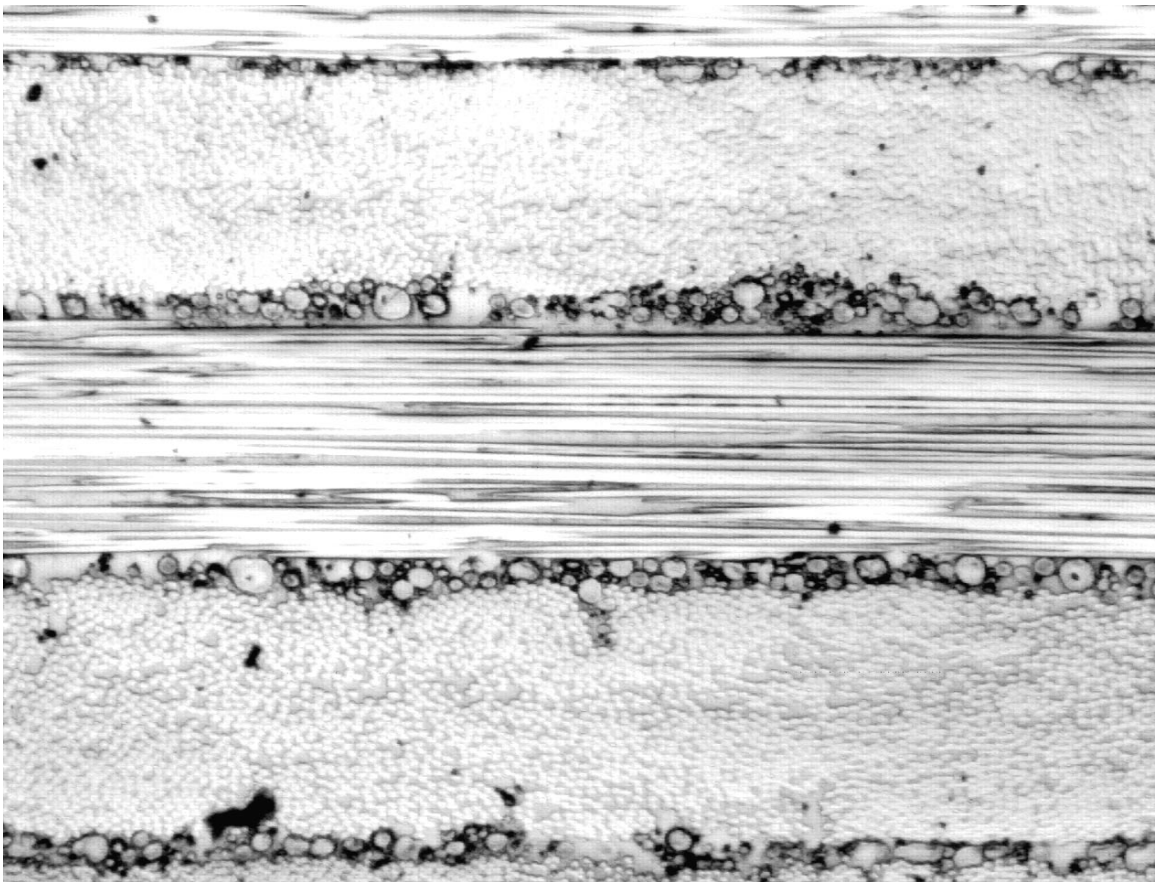


Figure 2.4. Interlayer thermoplastic toughening mechanism.

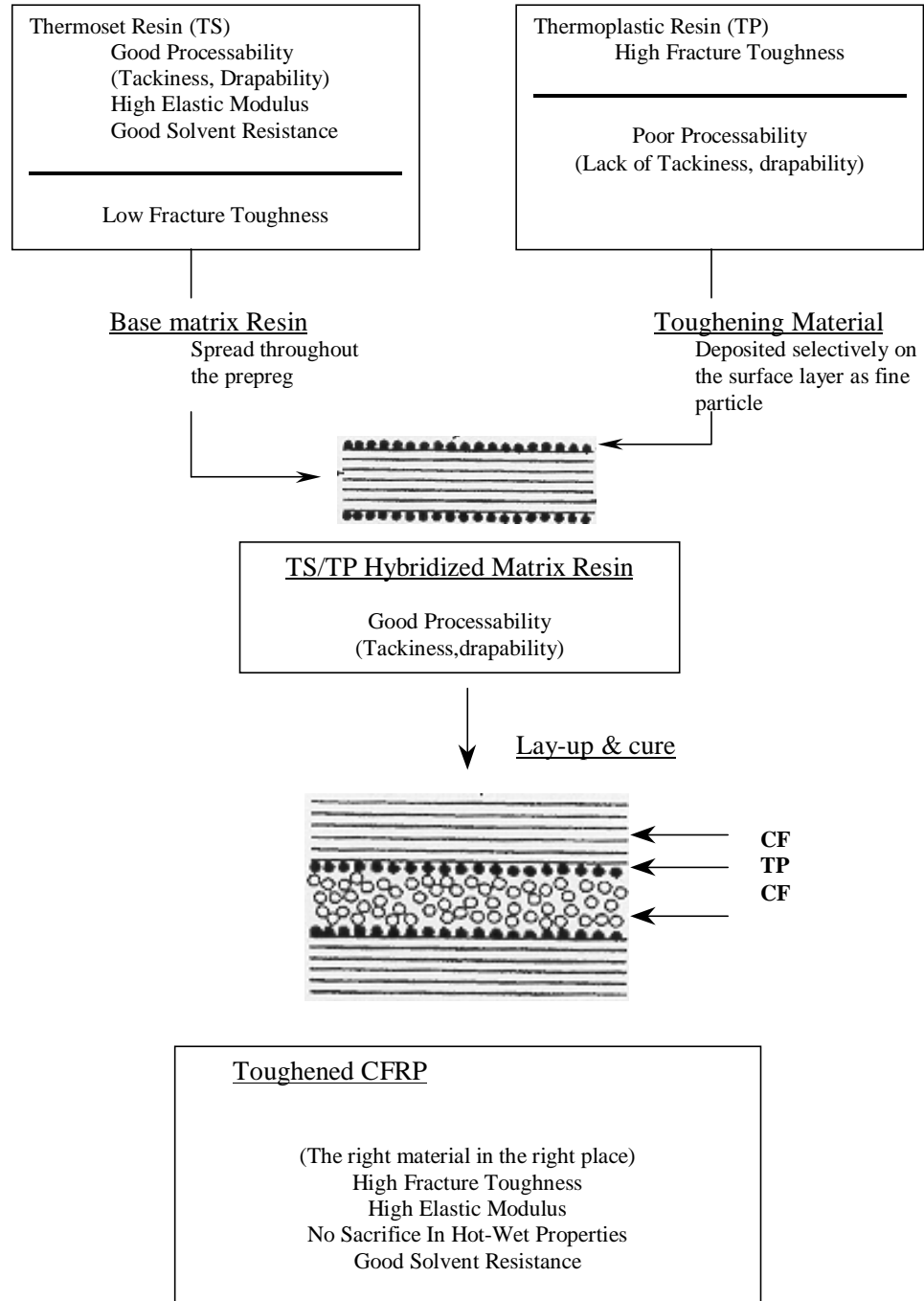


Figure 2.5. Particulate interlayer toughened prepreg. From Odagiri, Kishi, and Yamashita.

### Layer Waviness

Layer waviness is out of plane displacements of the plies caused during manufacturing. It is most common in thick section composites. Waviness is especially a problem in composites that contain overlaps and gaps [Sawicki and Minguet, (1998)]. Some work has been done characterizing the response of these defects.

Most work has been done on the effects of waviness in cylindrical structures. However, Adams and Hyer [(1994)] have considered the effects on flat panels. One single wavy  $0^\circ$  ply was introduced into the specimens. The waviness was preformed into the layer, and then three  $90^\circ$  tows were placed so the  $0^\circ$  ply wove through them. Several different levels of waviness were introduced. Samples were tested statically and in fatigue. The static results showed a decrease in strength from 1 to 36%. The results are shown in Figure 2.6. This was interesting, because the wavy ply only accounted for 20% of the laminate strength. Slightly waved specimens broke at the reinforcing tabs in the gripped section and at the wavy ply. More severely waved specimens broke only at the imperfection.

This work demonstrated significant strength reductions. Reductions of one wavy ply exceeded the load carried by that ply. This shows that even an analysis that removed the wavy ply in its strength calculations may be nonconservative.

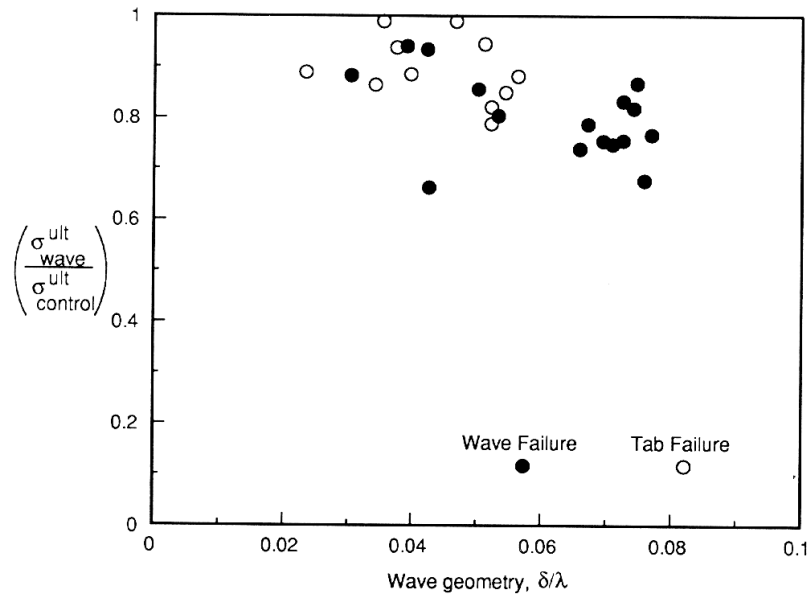


Figure 2.6. Compression strength of layer wave specimens.  
From Adams and Hyer.

### Compression Testing

The research goal and a special interest by Boeing led compression testing to be the predominate test performed. There are many unanswered questions about compression, especially in laminates with manufacturing defects. The editors of the first ASTM D30 symposium devoted to compression stated [Groves and Highsmith, (1994)],

“There is still considerable need for additional study of failure processes under compressive loading and for further study of the influence of fabrication/processing flaws on compression performance.”

Compression testing is not trivial. It is always a structural test with a complicated interaction between local failures and structural instabilities [Herakovic, (1998)]. A few generalized testing methods and theories will be presented next.

Camponeschi [(1991)] reviewed the status of compression. The following is a summary of his review. The first question asked is what is compressive strength or failure. This seems to be an often overlooked question. Many researchers today assume that it is the compressive failure of the composite on a microstructural level. Indeed, this can be seen by the great lengths taken in material testing to produce such a failure. The author notes that if this response requires such coercion in the controlled environment of the laboratory, can this response be expected in service? Further, he cites strength data from an IITRI compression fixture. Strength is plotted against a length/thickness parameter. The result is a curve of compression strength that is steep and not constant. Therefore, the ASTM standard with the IITRI fixture, arguably the most widely accepted compression test, is simply a narrow band of the output of a quickly changing curve. Despite these difficulties, methods to compare and quantify composites are needed, and so methodologies are discussed.

Four questions that guide compressive strength research are these.

1. How should composite materials be tested in compression?
2. How do composite materials fail under a compressive load?
3. What failure theories describe these failures?
4. What compression data are available for composite materials?

Due to the experimental aspect of this research, the answer of the first two questions will be primarily addressed.

Test methods are broken down into the variations on two main categories. The first is gauge length restraint. The gauge length of the test is the unclamped portion of the

sample. Most tests either support the gauge length, or they leave it free. If the goal of the compression setup is to eliminate buckling, a supported gauge length obviously precludes this.

The second variable is load introduction. This is the method that the load was transferred to the sample from the testing machine. The two main options within this are load by shear or end loading. Shear loading clamps the sample faces and end loading pushes on the sample ends. To help ensure accurate results, test consideration recommendations are made.

For shear loaded tests,

1. The flatness and parallelism of tabs,
2. The upper and lower limits on gauge length,
3. Poisson and free-edge effects in laminates, and
4. No stress concentrations or bending induced by the fixture.

For end loaded compression tests,

1. The flatness and perpendicularity of specimen ends,
2. Provisions to prevent end-brooming,
3. The upper limit on gage length,
4. Poisson and free-edge effects in laminates, and
5. No stress concentrations or bending induced by the fixture.

General failure mechanisms were also summarized. The first is fiber buckling. These are based on the stability of the fibers in the softer matrix. For low fiber volumes, the fibers buckle somewhat randomly. This is out of phase (randomly) and is called the

extensional mode. For higher fiber volumes (above 30%) the fibers buckle in phase (ordered), and it is called the shear mode. Transverse tension or shear is another failure mechanism. This is failure due to Poisson effects or very slight waviness and usually happens in unidirectional composites or composites with considerably low transverse strengths. The final failure mechanism discussed is fiber kinking, shown in Figure 2.7. The failure mechanisms are detailed nicely in Camponeschi's Figure 2.8.

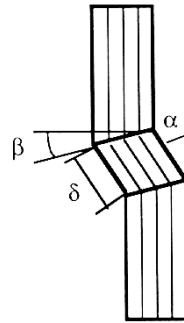


Figure 2.7. Kink band geometry. From Camponeschi.

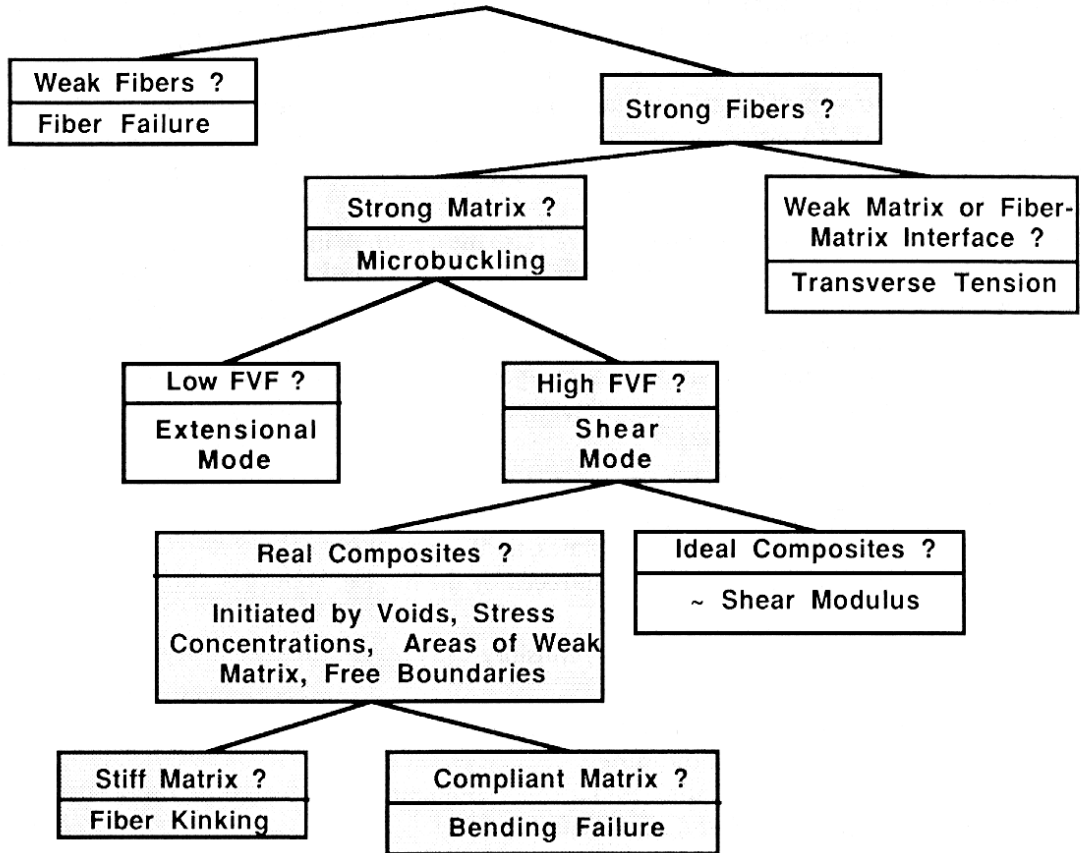


Figure 2.8. Microstructural compression response. Adopted from Camponeschi.

## CHAPTER 3

## EXPERIMENTAL METHODS

All of the experimental work done is detailed in this chapter. First, it includes a description of the material. Then, some specialized measurements are described. Next, sample preparation is described. Finally, motivations for experiments run and descriptions of each test are presented.

Material Description

The Boeing Company manufactured the carbon/epoxy laminated material for all of the samples tested. This material finds application in the manufacture of the Boeing 777 for the fin torque, stabilizer torque box, and floor beams (internet site). The material was Torayca T800H/3900-2, a thermoplastic toughened thermoset resin polymeric matrix composite. This consisted of T800H high strength carbon fibers and 3900 high toughness epoxy resin with improved impact resistance. Additionally, thermoplastic particles applied between layers increased delamination resistance (as described in Chapter 2).

Boeing provided three 1.4 m (55 in.) by 1.4 m (55 in.), 31 ply composite panels for testing. The layup for each panel was the same, and was

[(45/90/-45/0)3/45/0/-45/0/-45/0/45/(0/-45/90/45)3].

However, the panels were not identical, due to different resin gap configurations.

## Panel Gap Configurations

### General Gap Formation

Boeing manufactured the panels using an automatic tape layup machine. This machine used 150 mm (6 in.) wide, 0.2 mm (0.0758 in.) thick tapes of prepreg lamina. The gaps were formed during manufacturing similar to the description in Chapter 1, Introduction. However, the laminates were built with the 31 ply layup described in the previous section. Gaps formed with four ply orientations are in Figure 3.1.

Definitions and descriptions of gap width, stagger distance, and stagger repeat number are found in the summary of Edens' work in Chapter 2.

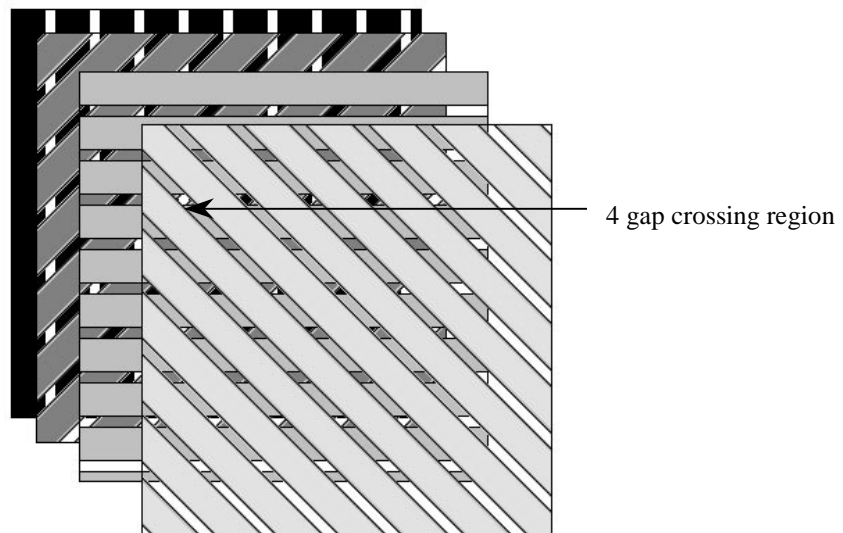


Figure 3.1. Formation of gap interaction region with four ply orientations.

### Specific Panel Configurations

Each panel measured 1.4m (55 in.) square. Gap configuration varied for each panel, but generally, the gaps were configured similar to Figure 3.2.

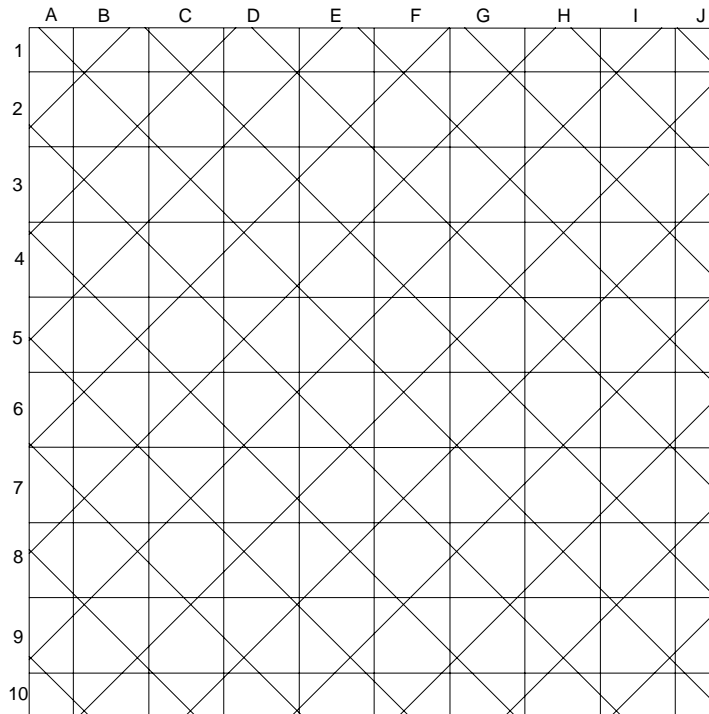


Figure 3.2. Formation of gap interactions in the Boeing panels.

Lines represent ply gaps, and where lines cross represent gap interaction regions. The primary difference between the panels was the stagger. Each ply for each panel is listed in Table 3.1 with the stagger arrangement specified.

Table 3.1. Specific panel characterization data.

Panel	Ply	Gap Width	Stagger Repeat #	Stagger Distance
1	45	0.06	4	0.5
	90	0.06	4	0.5
	-45	0.06	2	0.5
	0	0.06	1	0.5
2	45	0.06	0	NA
	90	0.06	0	NA
	-45	0.06	0	NA
	0	0.06	0	NA
3	45	0.03	1	0.3
	90	0.03	0	NA
	-45	0.03	0	NA
	0	0.03	0	NA

### Sample Selection and Preparation

#### Sample Selection

The motivation for the research was to study the effects of gaps on the material strength, and so the first characteristic selected for the samples was the gap configuration. As previously described, the gaps in each layer crossed with gaps in other layers to form gap interaction regions. A complete analysis required testing of various gap interactions.

First, samples were selected with no gaps present. This was both for a control group within the given panels, and also to verify the testing methods and machines used against published data. Second, gapped regions were selected for testing. These regions included samples with one gap, two gaps, three gaps, and four gaps crossing. All of the gap crossings were selected with various orientations. For example, a sample with one

gap has four possible orientations:  $0^\circ$ ,  $45^\circ$ ,  $-45^\circ$ , and  $90^\circ$ . Similarly, there are multiple combinations in each category of crossings: 2, 3, and 4 gaps. Examples of each of these types of crossings are highlighted in Figure 3.3.

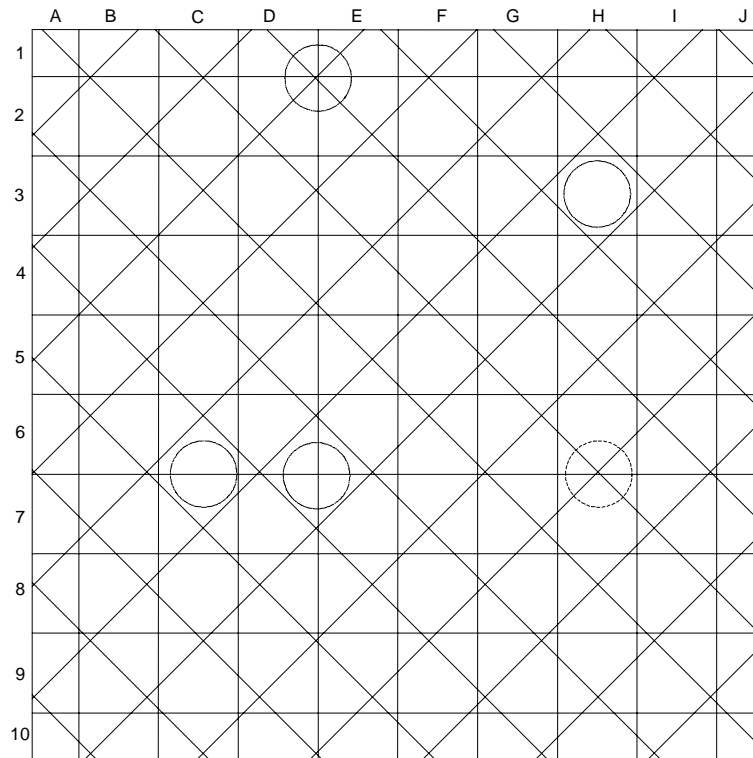


Figure 3.3. Gapped regions of interest.

### Sample Preparation

The sample geometry varied depending on the desired test: tension, compression, open hole, etc. Templates were cut for each type of test (discussed later in this chapter) with oversized dimensions for a final cut. These templates were located on the panels at the desired gap crossings, and traced directly on the panels.

The panels were too large to cut samples on a standard saw. Samples were also needed from the interior of the panels, and so this eliminated the use of several other

possible cutting methods. Many methods were tried; but the best was a pneumatic cutoff saw. This enabled samples to be cut relatively quickly from anywhere on the panel. It also cut the composite aptly, leaving no visible tears or delaminations in the samples. It was, however, quite noisy, and prompted more than one phone call from irritated faculty. Additionally, cuts wandered, leaving a somewhat irregular sample edge.

The water cooled/lubricated diamond blade tile saw accurately cut the samples to their final dimension. This produced clean, straight edges. Any further drilling or routing was then done. For most samples, 1.59mm (0.063 in.) thick fiberglass tabs (G-10) were glued with a Hysol epoxy to the gripping area of each sample. A majority of the samples were mounted with strain gauges for the final step. Gauges used were a HBM 350 ohm 6.35mm (0.25 in.) by 3.18mm (0.125 in.) gauge.

### Characterization Measurements

After the samples were cut and prepared, each one needed to be measured. All of the samples were measured for thickness, width, and length with digital calipers. A few special measurements were made on selected parts for detailed information about sample thickness and gap geometry.

### Thickness Variations

Bending in some of the test results surfaced questions about sample irregularities, especially in the thickness direction. A grid of points was mapped onto the samples in question. This is shown in Figure 3.4. Then, a device was set up to measure the thickness at the mapped points. This utilized a precision granite slab, a screw-in post,

and a digital depth gauge (accuracy of 0.00245mm) with a small, spherical bearing point. The depth gauge was zeroed, and then samples were located under the gauge at each designated location. These were recorded, and plotted, and are discussed in Chapter 5.

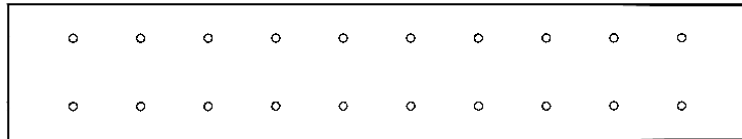


Figure 3.4. Grid used for specimen thickness variation measurements.  
All data points are 12mm (1.5 in.) apart.

### Gap Characterizations

Samples of representative gap sections were also studied. The samples were cut to about 20mm (0.787 in.) square. They were encased in a clear resin, and polished for microscope study. Microscope pictures were taken at various magnifications.

### Failure Tests

The effect of the gaps upon ultimate load was Boeing's foremost interest. That data would be critical in developing new and modifying existing design specifications. This led to the majority of the tests run for ultimate load. A full spectrum of tests was desired to completely study the gap effects. All of the useful tests performed are listed in Table 3.2.

Table 3.2. Experimental Test

<b>Loading</b>	<b>Notch</b>	<b>Gaps</b>	<b># samples</b>	<b>Motivation</b>
Tension Failure	None	None	3	Establish baseline tensile material properties and compare with Boeing database
		3	3	Observe overall effect of gaps on tensile failure in unnotched case and compare with ungapped case
	6mm (0.25 in) Hole	None	3	Establish baseline OHT failure properties to compare to Boeing experimental and theory
		3	3	Check for observable effect of gaps on OHT failure from ungapped tests
Compression Failure	None	None	5	Establish baseline compression material properties and compare with Boeing database
		3	4	Observe overall effect of gaps on compressive failure in unnotched case and compare with ungapped case
	6mm (0.25 in) Hole	None	20	Establish baseline OHC failure properties to compare to Boeing experimental and theory
		1 2 3 4 staggered	8 9 26 2 14	Check for observable effect of gaps on OHC failure from ungapped tests

Table 3.2. Experimental Test Matrix (Continued)

<b>Loading</b>	<b>Notch</b>	<b>Gaps</b>	<b># samples</b>	<b>Motivation</b>
Fixture Compression Failure	6mm (0.25 in) Hole	None	5	Eliminate bending induced by machine head misalignment and sample asymmetry. Establish baseline OHC failure properties to compare to Boeing experimental and theory
		1	5	Check for observable effect of gaps on fixture OHC failure from ungapped tests
		2	5	
		3	5	
OHC Photoelastic	6mm (0.25 in) Hole	None	1	Find ungapped strain field to compare to FEA and establish baseline
		2	1	Compare results to ungapped tests and FEA to find strain field disturbance of gaps
		3	1	
OHC Damage Progression	6mm (0.25 in) Hole	3	6	Look for effect of gaps on damage progression

This included tension, compression, unnotched, notched, ungapped and gapped tests. However, compression and open hole compression tests often drive Boeing composite designs. Since a limited amount of material was available, emphasis was placed on open hole compression tests, with fewer samples of the others.

### Tension

Various tensile tests were performed. Generally, they were broken down into two categories: unnotched and open hole.

Unnotched. Both virgin (containing no gaps) and gapped samples were tested in unnotched tension (UNT). Initially, the sample geometry used was rectangular (140mm (5.5 in.) by 38mm (1.5 in.)) with a short (~38mm (1.5 in.)) gauge length. This geometry was identical to the compression geometry (discussed later), and simplified variables. These samples failed at the grip/sample interface, and so invalidated the tests.

The successful geometry was a longer, smoothly dogboned specimen. The reduced dogbone section forced failure to occur in the middle of the sample, away from the gripping area. This geometry was taken from a template used at MSU. Specimens were initially cut to a rectangular section, and then routed along the edges to the template size. The specimens were about 203mm (8 in.) long and 21.6mm (0.85 in.) wide (at the narrowest section). They were also reinforced with fiberglass tabs in the gripping areas (Figure 3.5).



Figure 3.5. Unnotched tension sample.

Three samples of virgin material were tested. They represented a control to compare to gapped tests and to compare to data from Boeing's internal tests. Gap orientations of three gaps were chosen for UNT testing. The secondary importance of these tests limited tests to only three gap orientations. The three gap orientation was chosen because a worst case scenario was desired, but there were not enough four gap regions. The types of three gap orientations were mixed, because it was not feasible to locate identical orientations for each sample. Perfect gap crossings were few, and so samples were selected as near to that as the panels allowed.

Open Hole. The other tension tests were open hole tests. Lessons learned from the unnotched tests led the geometry to follow the ASTM standard D 5766 [ASTM, (1997)] immediately. The desired hole size was 6.35mm (0.25 in.) (a common Boeing hole size). The ASTM standard recommended a width/diameter ratio of at least six. This sized the sample width to 38.1mm (1.5 in.). Again, the length of the sample was about 203mm (8.0 in.). Tabs were not used because the centered hole provided a stress concentration so the sample would not fail in the grips.

Special care was taken while drilling the sample holes. Careless drilling with inappropriate drill bits easily damaged the composite. In previous work, delaminations near the drilled hole elevated the failure strength of the samples [Phillips and Parker, (1987)]. Experienced personnel in the composites industry suggested a specialized bit called a dreamer [Whishart, (1999)]. The Carbro dreamer drilled and reamed a 6.35mm +0.0254mm (0.25 in +0.001 in) hole in one operation. Various cutting speeds and a water coolant were tried. A hole cut dry at a moderate speed was used.

Similar reasoning as for the unnotched tests was used for selection of virgin and 3 gap samples. The geometry is shown in Figure 3.6.

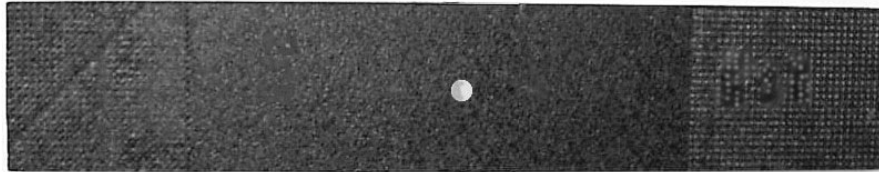


Figure 3.6. Open hole tension sample.

### Compression

“The compressive response of fiber-reinforced composite materials has been the subject of investigation since the development of these materials. Even with this long-term interest, this area is still one of the least understood in the field of composites today.” [Camponeschi, (1991)]

Compression tests were exceedingly more difficult to conduct than tension tests as a result of difficulties stated previously. This is due to a larger sensitivity to geometry perturbations. Murphy’s law required these tests to be of most interest to Boeing.

Unnotched Samples. Geometry for the unnotched samples was selected first. After some preliminary calculations and a few trial tests, rectangular, 25.4mm (1.0 in.) wide samples with a 38.1mm (1.5 in.) long gauge length were selected. Typically, testing machine grips were limited to a ~51mm (2.0 in.) grip length. This, along with the desired gauge length, required a sample about 140mm (5.5 in.) long. This complimented the natural divisions in the samples that occurred with the 150mm (5.9 in.) wide prepreg tapes. Glass tabs were glued to the gripping areas, and strain gauges were mounted on

several of the samples. Two gauges were mounted back to back, which allowed detection of bending during the test. This geometry is shown in Figure 3.7.



Figure 3.7. Unnotched compression sample.

Open Hole Samples. Holes in composites are used for a variety of purposes. Obviously, they serve for connecting main joints or accessory hardware with bolts. Equally as important, they provide access from one side of the laminate to the other. So, many aerospace applications require holes. The stress concentration associated with these holes can become the driving factor in a design. This leads to investigation of the effect of holes in laminates.

A 6.35mm (0.25 in.) hole in a 38.1mm (1.5 in.) wide laminate was used, similar to the open hole tension tests. But in compression, the gauge length needed to be much smaller. A gauge length of 38.1mm (1.5 in.) was chosen. This allowed the overall sample length to be shorter than the tension tests, and was the same as the unnotched compression, about 140mm.

Open hole compression was the largest set of tests. A full spectrum of tests were run, including 0, 1, 2, 3, and 4 gaps. An example of sample geometry is in Figure 3.8.

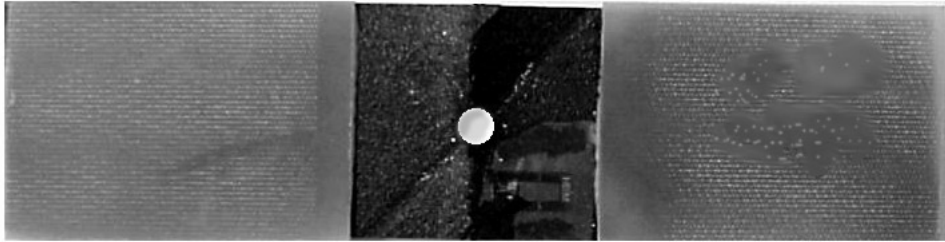


Figure 3.8 Open hole compression sample

Loading Methods. A loading method was needed for all of the compression tests. A review was provided in Chapter Two for the various forms of load introduction and gauge length support. The first method tried was an unsupported gauge section with load introduced by shear. This was done using a hydraulic grip, 55 kip hydraulic actuated MTS 880 machine with Instron electronics. The MTS was selected for its high load capacity, precision alignment, hydraulic grips, and a high overall stiffness to resist buckling loads. Gauged samples tested in this manner revealed enough bending to cause concern. This led to the development of another test method.

A fixture for compression testing was desired. There were several criteria for the fixture.

- Resist any out of plane forces that would cause bending loads
- Reduce or eliminate the effects of machine head misalignment
- Accommodate both unnotched and open hole samples
- Accommodate various widths of samples
- Be compatible with MSU testing machines
- Have low cost and ease of manufacture

While several standard fixtures exist in the industry, they would not accommodate the sample size that was desired for testing, and were designed for a specific use and were not flexible enough to accommodate a wide variety of samples. So, a fixture was designed and built.

The considerable thickness and high ultimate loads of the test material made a purely shear loaded design difficult. Testing unnotched samples in the fixture eliminated the end load only option. A fixture that both end loaded and shear loaded the sample seemed it would provide the desired results. Some published work in this area contained fixture designs that were of this type [Lessard and Chang, (1991)] and [Coguill and Adams, (2000)].

These conceptual ideas were designed and sized into a fixture that accommodated samples for this project. Details of this fixture are shown in Figure 3.9. Four steel plates were the base of the fixture and provided the clamping surfaces of for load transfer through shear. Four steel sliding rods aligned the top and bottom plates and prevented out of plane movement or forces on the sample. Twelve bolts were used to provide the clamping force on the sample. After design, the fixture was machined and built by the author in the mechanical engineering/college of engineering machine shop.

The fixture required some specialized sample preparation. If the fixture loaded the ends of the sample, they needed to be machined flat and parallel to each other. This provided uniform loading over the entire sample thickness, and helped eliminate eccentric loading. This was done on a standard, vertical end mill with a sharp, carbide bit moving at a high cutting speed. A vacuum was also used to collect all of the carbon dust

during the process. After the samples were prepared suitably, they were loaded into the fixture.

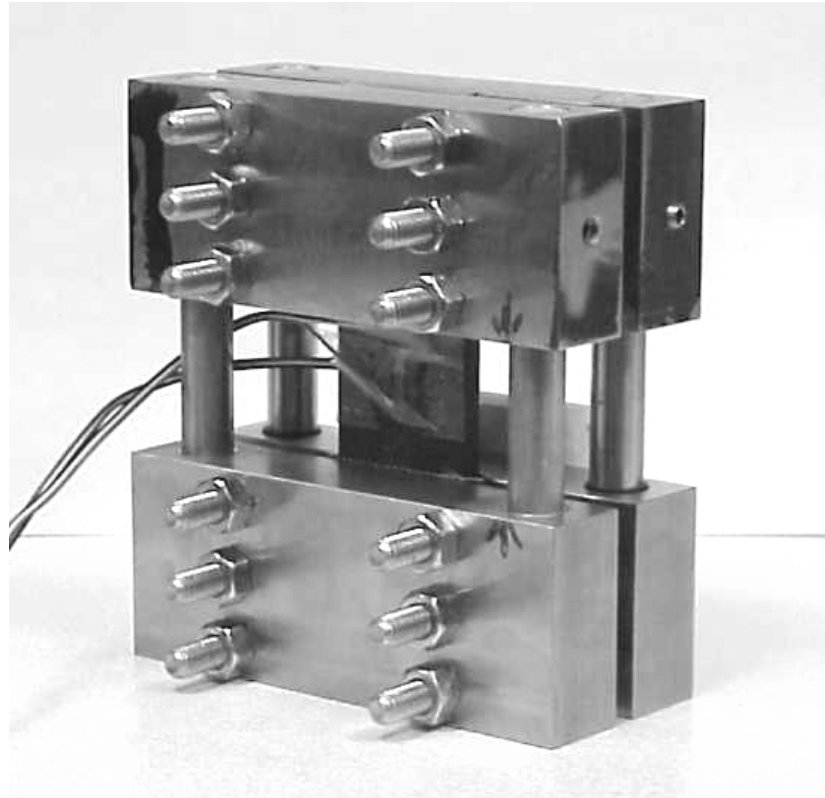


Figure 3.9. Compression testing fixture.

The fixture had sandpaper bonded to the interior, loading faces. This provided the loading from shear. The fixture was placed on flat, machined steel pads. The sample was loaded into the fixture, with the sample ends aligned flush with the fixture top and bottom surfaces. Then, the fixture was placed into the testing machine. The machine used was the Instron 4206 double screw machine. This was selected for its high load capability and it was the easiest to adapt for a fixture. The entire bottom head was removed, so that a flat base was used to set the fixture on. The top, actuator attachment was a circular, flat plate that screwed into the load cell. Three additional steel plates were used in the setup. One went underneath the fixture, between the machine base and the

fixture bottom. This plate was shimmed parallel to the top loading surface with shims. The two other plates were placed between the top of the fixture and the actuator loading surface. Sandwiched between these plates was a thin rubber pad. This allowed for correction of any misalignment or rotation of the actuator head. A picture is in Figure 3.10.

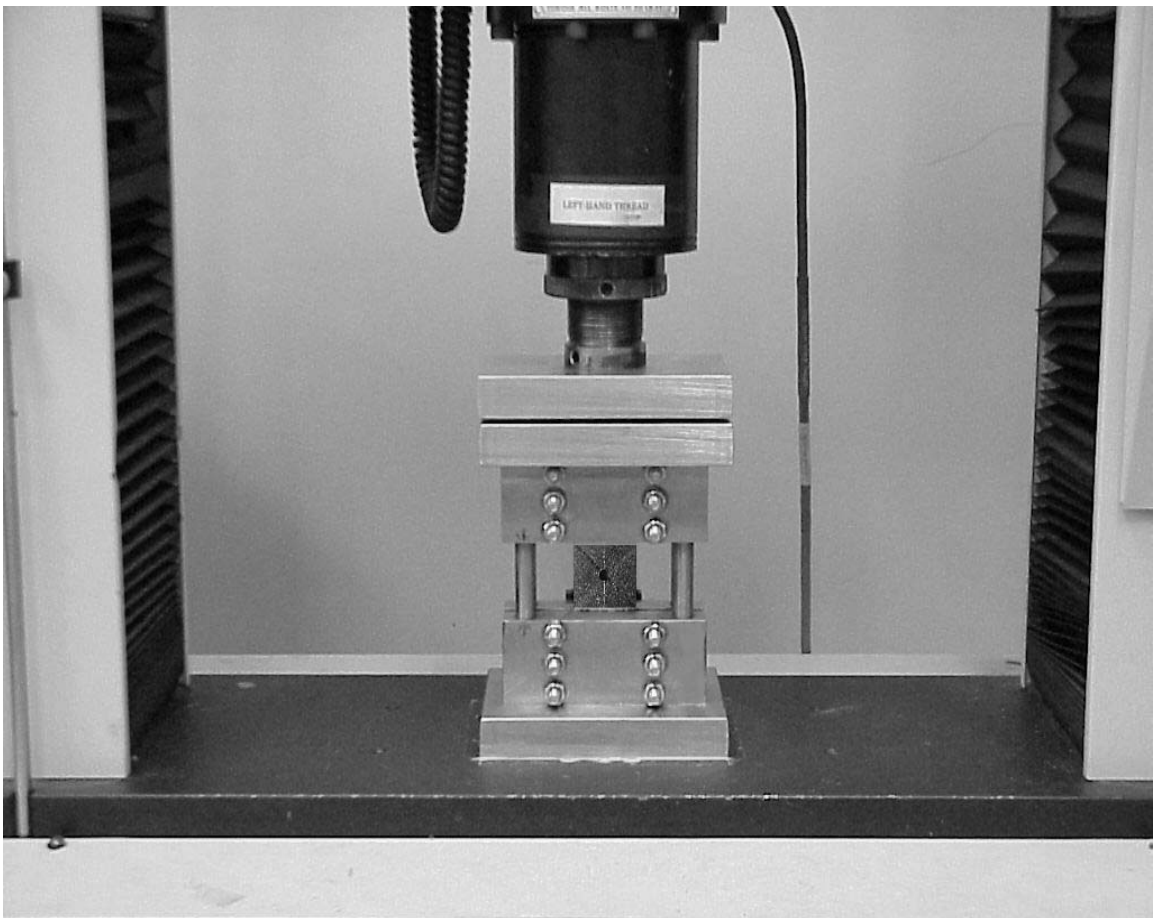


Figure 3.10. Compression fixture test setup.

### Elastic/Strain Field Tests

Strain gauges were used on a majority of the samples tested to failure. However, these provided only one data point for the strain field in the sample. In the open hole tests there was considerable strain gradient from the hole geometry as well as from various gaps and gap crossings. A method to measure these strain fields was desired. Strip or chain strain gauges were tried. Small gauges were required to get enough strain points to be worthwhile, and were expensive. The size made precision alignment of the gauges hard to obtain. Additionally, the gauges did not always bond adequately with the inconsistent sample surface. These factors made the data from the gauges not worth the time and expense required to obtain it. Photoelasticity was found to provide a full field strain measurement of the sample with relative ease in testing and setup.

Open hole samples were prepared as described in the failure tests section in this chapter. Open hole samples were the only tested with this method. This was due to limited time and the priority interest Boeing had in open hole compression tests. The final step was to apply a photoelastic coating onto the surface of the part. The coating was purchased in flat sheets, and it is a clear plastic with one side painted silver. The silver coating helps to reflect the polarized light passing through the strained plastic. The coating was cut just oversize of the part. It was then bonded onto the part with an epoxy with a reflective powder mixed in it. Again, this epoxy helped to reflect the polarized light. After the epoxy cured, the coating edges were sanded smooth to the parts, and the center hole was drilled through the coating. The coating could not get hot during any of the preparation. If it did, the plastic material would be left with residual strains, which could be seen later in the measurement process.

The sample was then loaded. A Measurements Group 031 polariscope was used to emit polarized light to the sample in question. The sample was viewed through another filter on the polariscope. Here, the fringes were viewed to see the strain contours. A digital camera was used to take photographs of the stressed part through the filters. An image of the setup is in Figure 3.11.

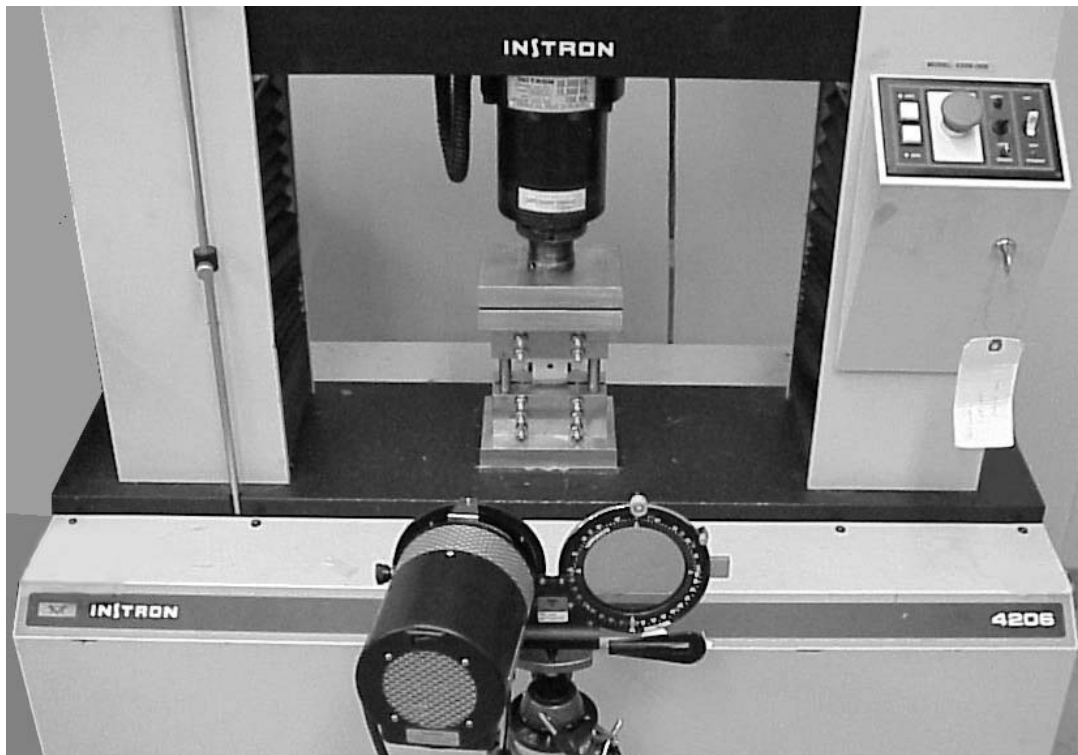


Figure 3.11. Photoelasticity setup.

### Damage Progression

In order to understand the failure mechanisms in the samples better, it was desired to see the damage progression to failure of the samples. This data could then also be compared to predicted failures in the finite element models. Again, these tests were only performed on open hole compression tests, for reasons stated previously.

It was relatively difficult to partially damage an open hole compression sample. This was because nearly all of the damage happens extremely close to the failure load. Additionally, damage in a compression test was unstable. This afforded little reaction time to stop and unload the sample before ultimate failure occurred. Initially, loading at a high percentage of failure was calculated, such as 90% and 95% of ultimate. This approach proved unsuccessful, because the failure of each particular sample was unknown and the uncertainty of the failures was enough so that 95% of failure of one sample may have been 100% of failure for another. Therefore, the method used was to gradually load the sample until a “significant” amount of damage was heard during the final stages of loading. This was difficult, and a few samples were failed in the process.

After the samples had been damaged, a nondestructive damage detection technique was tried. The samples were placed in a CT scanner and scanned. The scanner used x-rays, which detects density differences. It was hoped that the scanner would see delaminations and cracks in the specimens. However, the cracks must have closed significantly during the damage. Only vague, minimal damage was noted. Therefore, the samples were cut slowly using the diamond blade saw. They were then polished and placed in the microscope for analysis and documentation with digital photographs.

## CHAPTER 4

## NUMERICAL METHODS

The careful use of finite element methods has proved to be a valuable tool in engineering design. A cursory look at the engineering design industry and the multi-billion dollar FEA industry affirms its impact and usefulness.

These methods are applied to material research for several reasons. Test scenarios can be modeled in finite elements to predict the general behavior of the material and the test. This information can then be used to design a more intelligent, informed test from the start. Test results can also be compared to the FE models for validation. If the models are validated (i.e. they accurately predict the response and failure of the material), they can supply information (for instance, failure mechanisms and progression) about the test that would have been difficult or impossible to obtain through experimental measurement.

Often, the aerospace community creates computer models of an entire structure. Typically these models are large and complex, but substructure and material details cannot be included. This is because the models would be overly time consuming to build, and because the computer resources needed to model that detail on such a large scale are either impossible or costly to procure. So, an analysis that models structure globally may miss certain details on the material or substructural level. These details have the possibility of being critical design aspects.

Smaller, local FE models include the substructural and material details that the global models miss. Then, the local models assess if these details are indeed a significant factor in the overall design. Finally, guidelines and design specifications are applied to the global models and designs. These are the motivations for building the finite element models presented here.

### Material Properties

The material properties used were the same for all of the models created. The properties input into the models were properties of a single, fiber-reinforced ply. The finite element code used these properties to build the laminate properties.

Elastic properties were needed for the elastic response of the models. All of the elastic properties were obtained directly from Boeing. These are the same properties Edens used in his work, and they are printed below in Table 4.1. The first set of properties describe the reinforced composite prepreg. These are the predominate material properties used in the models. The second set of properties is for the resin only. They include no reinforcement, and so are low. These are input into the model where resin gaps are present, and are listed in Table 4.2.

Table 4.1. Ply Elastic Properties.

Property	Value	Units
$E_1$	142 (20.6)	GPa (msi)
$E_2$	7.79 (1.13)	GPa (msi)
$G_{12}$	4 (0.58)	GPa (msi)
$G_{13}$	4 (0.58)	GPa (msi)
$G_{23}$	4 (0.58)	GPa (msi)
$\nu_{12}$	0.34	

Table 4.2. Resin Elastic Properties.

Property	Value	Unit
E	3.5 (0.507)	GPa (msi)
$\nu$	0.45 (assumed)	
Elongation	4.1	%

Failure strengths were needed to predict laminate failure. Failure data was more difficult to obtain. This is because a single ply's strength is dependent on the laminate that surrounds it. Surrounding plies may constrain some of the damage in a given ply, affording it higher failure strength than in a unidirectional test. So, unnotched tension and unnotched compression failure strains were obtained from Boeing for the specific laminate under consideration. If the strain is equal in all plies, and the ultimate failure reflects failure in the  $0^\circ$  layers, the failure strain for a  $0^\circ$  ply is known for both tension and compression. These failure strains were transformed to strengths using the elastic properties.

If the failures that occurred in the laminates are fiber dominated, then these strengths will be critical for predicting failure. The other ply failure strengths are not so easily extracted from the test data. Tests of the given laminate would be required where failure occurred for each of the ply strengths: transverse tension, transverse compression, and shear. These tests were not readily available. It was also noted that most likely the failure mechanisms would be fiber dominated. If this is the case, the other matrix and transverse direction strengths have a secondary importance in predicting the laminate failure. Therefore, the strengths other than fiber direction tension and compression were taken from material properties of IM7/8552 reported in the laminated theory program Laminate Analysis. These properties are reported in Table 4.3. Strength properties for

the resin region were assumed to be the same as the 2 direction properties of the composite plies.

Table 4.3. Ply Failure Strengths.

Property	Value	Units
$S_{1t}$	2.39 (346)	GPa (ksi)
$S_{1c}$	1.64 (238)	GPa (Ksi)
$S_{2t}$	7.93 (11.5)	GPa (Ksi)
$S_{2c}$	1.72 (25)	GPa (Ksi)
$S_{12}$	8.41 (12.2)	GPa (Ksi)

### Unnotched Models

#### Meshing

Finite element work done by Edens and Cairns was mentioned in chapter two. A considerable amount of work was done creating solid ABAQUS models of various stagger repeats, stagger distances, and gap widths. However, two of the three panels for testing had no stagger or little stagger, but a no stagger finite element model had not been created. Edens input a no stagger, unnotched mesh case into the meshing program he had written. Then, this mesh was adapted to the 31 ply panel layup. This enabled solid modeling of an unnotched gapped sample with no stagger. Details of these models are shown in Figure 4.1. A detail region of the gap intersection is shown in Figure 4.2.

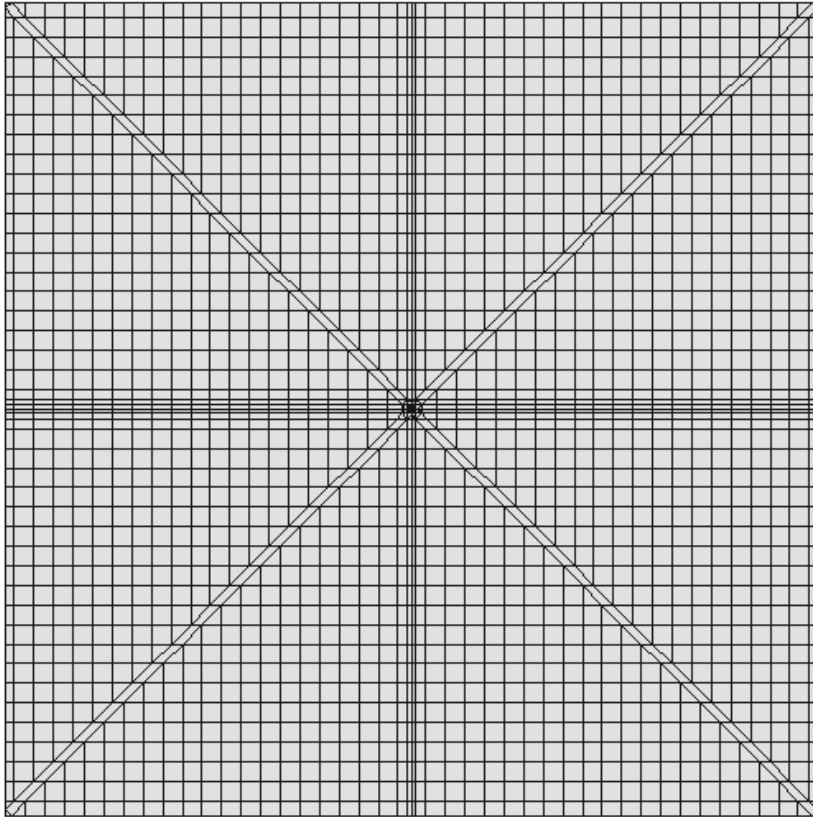


Figure 4.1. Solid, unnotched mesh.

An interesting idea was used to mesh each layer of these composites. Instead of using a different mesh with the proper gap orientation for each separate layer, a mesh was created that accommodated a gap in any of the four ply orientations found in the panels:  $45^\circ$ ,  $90^\circ$ ,  $-45^\circ$ , and  $0^\circ$ . Then, this mesh was used for all of the layers, and the different gap orientations were assigned by choosing matrix material properties for the proper gap in each layer. This assured node connectivity from layer to layer. This simplified the laminate meshing process, and allowed greater ease in changing layups.

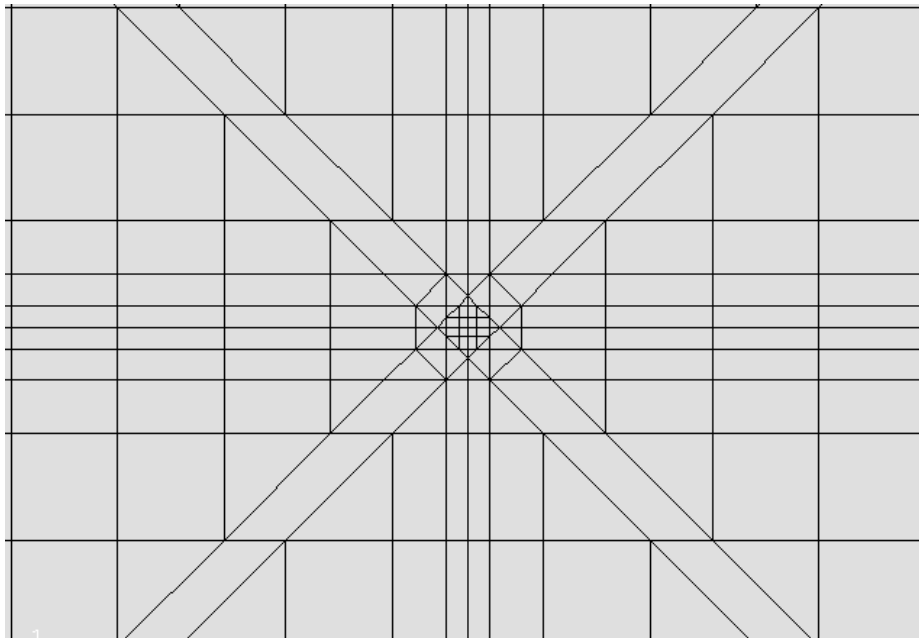


Figure 4.2. Solid unnotched mesh detail region.

### Boundary Conditions

Boundary conditions were then applied to the model. These are detailed in Figure 4.3. The model was constrained on the left side with a zero displacement condition in the  $0^\circ$  direction (x direction). The transverse (y) direction was not fixed, so that Poisson effects were not present. The lower left hand corner was fixed in all directions so the model was stationary. A constant displacement load was applied in the x direction on the right edge of the model.

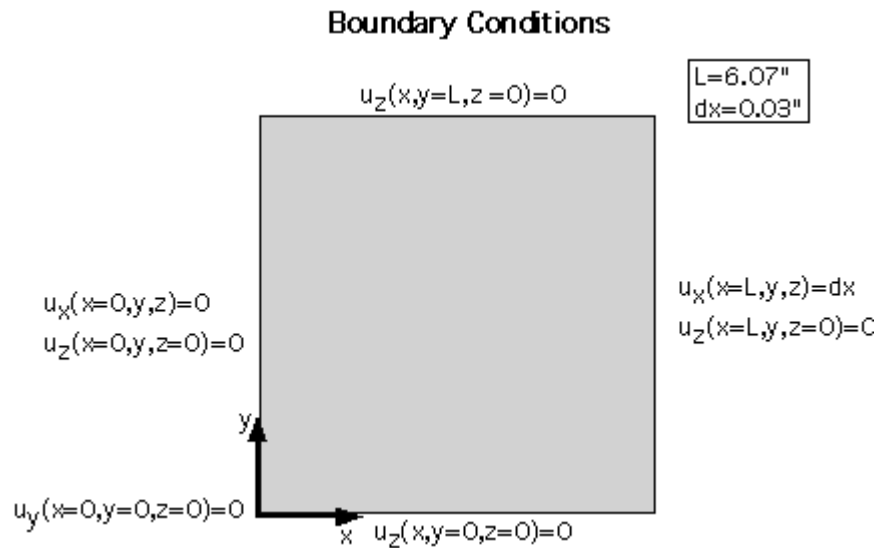


Figure 4.3. Boundary conditions for the unnotched solid models.

### Hole Models

Models that contained holes were desired to compare to the OHC experimental tests. Several variations were desired, including various gap runs, and varied relationships between the hole location and the gap locations. Solid and shell model approaches were examined.

### Solids

Next, a model containing a hole was built. It was recognized that the unnotched solid models took considerable time to solve. Also, the mesh was somewhat coarse and there was a concern about a high aspect ratio in the mesh. So, a more detailed mesh with faster running times was desired. The primary attempt to achieve this was to decrease the overall dimensions modeled. The previous runs had modeled a 150mm by 150mm (6 in. by 6 in.) block of the gapped material. However, the material tests performed had a

38mm by 38mm (1.5 in. by 1.5 in.) gauge section. So, the model section was decreased to the experimental section. A new preliminary mesh was created of the smaller geometry. It did not model all of the gap details, but it contained a refined mesh, and also incorporated a 6.35mm (0.25 in.) hole. The run times of this model were still quite long, and its mesh was even a simplified gap case. This led to a different approach to modeling this three dimensional geometry.

### Stacked Shells

A stacked shell method was employed similar to that of Cairns et al. [(1993)]. This was briefly described in chapter two. This method of stacking shells creates a quasi-three dimensional model. The benefits of this modeling technique were many. The first was a considerable reduction of solution times compared to 3D solid models. It modeled every ply distinctly, which enabled the resin gaps to be modeled accurately. The biggest limitation of the stacked shells was that no through the thickness properties were available. Another limitation was that all of the layers affected one another equally, and so the effects of the ply stacking sequence could not be determined.

Meshing. The Patran user interface was used for modeling. This interface was used primarily because it had the capability to create both ABAQUS and ANSYS decks, although an ANSYS deck was never written successfully by PATRAN. Due to the gaps that needed to be included, the meshing became complicated.

Two main meshes were selected for analysis. One had the hole center and the center of the gaps aligned. The other aligned the center of the gap crossings with the hole edge. These two cases seemed they would represent the gap/hole interactions adequately.

Gaps Centered Mesh. Before the mesh was created, the geometry was set up to incorporate all of the gapped areas. The gap width selected for modeling was Boeing's maximum allowable, at 2.54mm (0.1 in.). Several areas were created to accommodate all of the gap and composite sections of the model. Then, a circle was created in the model. The meshing technique was like the solid models. The mesh template incorporated all of the gap orientations, and it was used for all of the layers. A half symmetry model was used. The symmetry axis ran through the middle of the sample (and the hole) and was parallel to the loading direction.

When the hole was centered, its perimeter nearly matched with a gap intersection. Because this was so close, a very small triangular area was formed at the hole edge. This area was considerably smaller than the surrounding elements, and so the diameter of the hole was increased slightly to eliminate the small element. The hole diameter input because of this adjustment was 6.604mm (0.260 in.). This caused concern about the influence on the results. So, the stress at the hole edge was calculated and averaged for the 6.35 mm (0.25 in.) and the 6.6 mm (0.26 in.) hole size cases. A stress distribution for an orthotropic plate with a hole, corrected for finite width was used [Agarwal and Broutman, (1990)]. The stress was averaged over a distance of 1.42 mm (0.056 in.). The stress for the larger hole was only 1% higher than the normal hole. Therefore, the

slightly larger hole size was not greatly influencing the models. Once the geometry was in place, the model was ready to be meshed.

As previously stated, this mesh aligned the centers of the gap region and the hole. The meshing of the model was not trivial because the mesh transitioned from a curved edge on the hole perimeter to a straight edge on the model boundary. High stress and strain gradients were expected at the hole. So, a refined mesh was desired along the hole perimeter. It was not necessary for the entire model to have such a refined mesh; a course mesh in the areas of low stress would help reduce model size and solution times.

PATRAN provided precise control of meshing. Mesh seeds were manually applied to a majority of the model area edges. A weighted mesh seed command was used to have dense mesh seeds on one part of an area (near the hole), while having a lower density on the other end (near the model edge). This tool was extremely helpful in achieving proper mesh refinement. Once mesh seeds were created, the mesh tool in PATRAN was used to fill in the model with quadratic shell elements. The mesh for this case turned out quite clean, and can be seen in Figure 4.4.

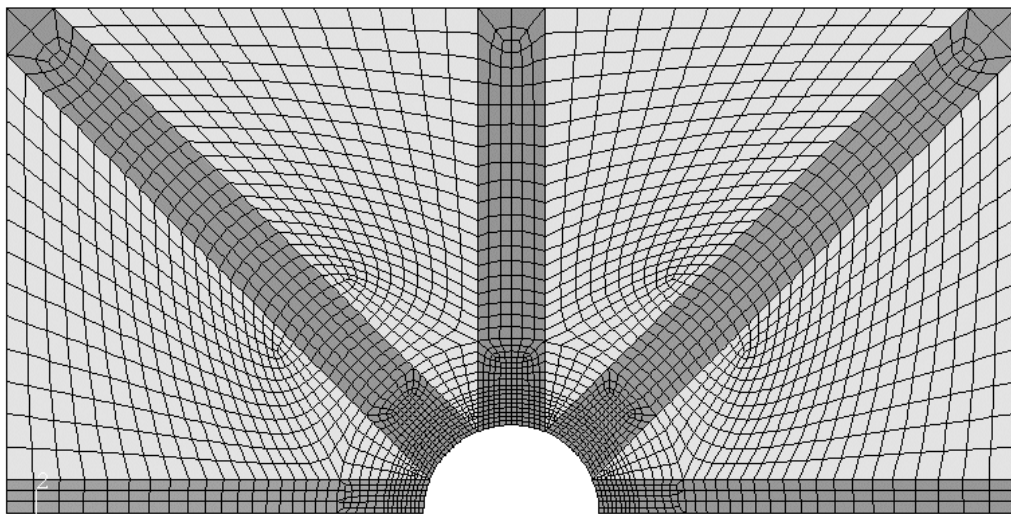


Figure 4.4. Mesh with the gaps centered on the hole. (Potential gap sites shaded.)

This created one layer of the composite. Since the mesh for all of the layers was the same, this layer was copied to create the 31 ply laminate. Each layer was copied directly on top of the previous, so there was no real thickness of the model. Now, the model contained 31 plies of separate nodes and elements. This model was saved for later use when damage needed to be included. This is discussed later. For an undamaged case, the layers needed to be connected to each other. This was done by equivalencing, or combining all of the nodes that laid on top of one another. This left the model with one layer of nodes, from which 31 layers of elements were constructed.

Gaps Offset Mesh. The initial geometry was set up as in the previous mesh. The same gap width and hole size were used as before. This geometry did not allow for half symmetry, so the entire sample was modeled. The gaps were offset of the sample center so that the center of the gapped region aligned with the edge of the hole. This case was selected because it placed the largest part of the resin region at the same location as the highest stress concentration caused by the hole. Once all of the gapped areas and the hole were setup, meshing proceeded similar to the gaps centered case. Weighted mesh seeds were created, and then PATRAN was used to mesh the model with quadratic shell elements. This model contained more gap interaction, and the mesh created was not as smooth and clean as the previous. The meshed geometry is shown in Figure 4.5. This mesh was then copied to form the 31 layer laminate in the same way described in the section above.

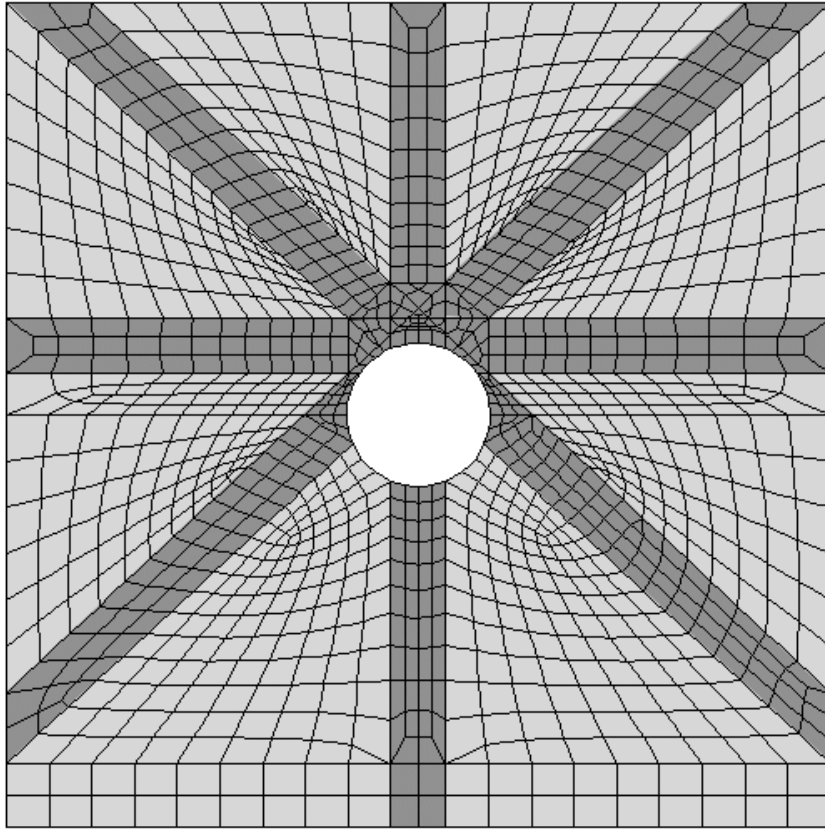


Figure 4.5. Mesh with the gaps offset from the hole.  
(Potential gap sites shaded.)

Boundary Conditions. After meshing, boundary conditions were applied. Since one of the meshes made was symmetric, a half symmetry boundary condition was applied to the center surface. The other boundary conditions for both shell models were on the ends. One end was fixed, and the other had a displacement applied to it.

On the fixed end, all degrees of freedom were constrained to zero except for displacements perpendicular to the load direction. This was not constrained so that Poisson effects would not be present at the ends due to that constraint. Models were run with that degree of freedom (DOF) constrained, and it added minor stress concentrations at the boundary.

On the displaced end, all of the boundary conditions were the same as the fixed, except the displacement in the loading direction was set to various values. The shell models had both displacements and rotations constrained. The boundary conditions for each of these models are shown in Figure 4.6 and Figure 4.7.

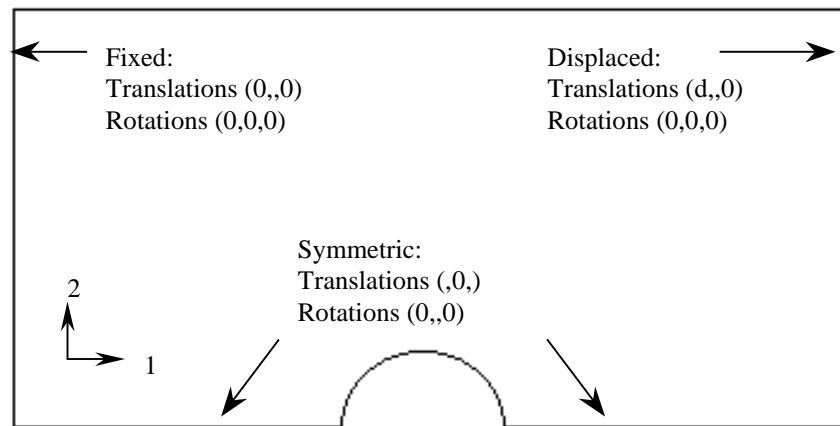


Figure 4.6. Boundary conditions for models with centered gaps.

Various Gap Configurations. Gap configurations were varied by changing the material defined in each gap region. Either the meshed gap material was defined with resin only properties, or it was defined with composite ply properties. In this manner, models were run with no gaps all the way up to 4 gaps. These corresponded to experiments.

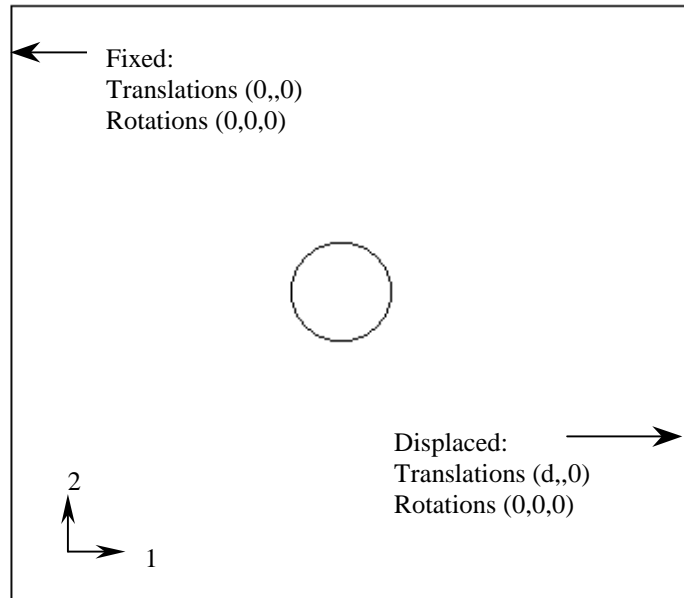


Figure 4.7. Boundary conditions for models with offset gaps.

Mesh Independence. Isotropic material properties were input for every element in each of the meshes. This helped determine if there was any mesh dependencies. The isotropic runs were studied for any discontinuous behavior at element boundaries or at difficult geometry transitions. The results could be easily verified because the isotropic behavior of the hole geometry has been well characterized. [Peterson, (1974)]

Damage. For an undamaged model, all of the overlapping nodes were equivalenced. After the damage locale was determined from the undamaged model and the failure criterion, a copy of the unequivalenced model was equivalenced for all of the nodes except those in the damaged areas. Then, these nodes were independent from the surrounding nodes, and so modeled the damage as either a split or a delamination from

the structure. A damage site within a single ply (intraply) is termed a split. Damage between two or more plies (interply) is termed a delamination.

### Failure Criteria

The final task was to determine when failure occurred in the simulations. This was done by applying failure criteria to the model. Failure strengths of the composite material had been input. This was described earlier in the chapter. ABAQUS provided several options for predicting failure. The most fundamental one used was a maximum stress criterion. This predicts failure when any of the stresses (in local ply coordinates) exceed the maximum strength input. This criterion is accurate when the failure is dominated by one particular stress. However, it lacks accuracy when more than one stress component is significant.

Another failure criterion used was the average stress Whitney-Nuismer failure criterion. This criterion is a laminate criterion, and it works well with fiber dominated failures. It uses a known, notched laminate strength, to predict other notched strengths within the same material system [Agarwal and Broutman, (1990)]. This criterion assumes that the laminate failure is dominated by the failure of a critical volume in front of the notch. This will be described further when it is used in Chapter 6.

All of the finite element models were discussed. A listing of all of the models created and solutions run are listed in Table 4.4.

Table 4.4. Numerical matrix.

<b>Geometry</b>	<b>Mesh</b>	<b>Runs</b>	<b>Motivation</b>
Unnotched	Mike's solid	Isotropic	Check for mesh dependancies
		Ungapped	Compare to ungapped experiments/Boeing standards
		3 gaps 4 gaps	Look for effects of gaps, compare to experiements, gain insight on failure mechanisms
Open Hole	Stacked shells, gaps centered	Isotropic	Check for mesh dependancies
		Ungapped	Compare to ungapped experiments/Boeing standards
		1 gap 2 gaps 3 gaps 4 gaps	Look for effects of gaps, compare to experiements, gain insight on failure mechanisms
	Stacked shells, gaps offset	Isotropic	Check for mesh dependancies
		Ungapped	Compare to ungapped experiments/Boeing standards
		1 gap 2 gaps 3 gaps 4 gaps	Look for effects of gaps, compare to experiements, gain insight on failure mechanisms

All models are available in Turoski [(2000)].

## CHAPTER 5

### EXPERIMENTAL RESULTS

Experimental results and comparisons are presented next. This includes comparisons of the effects of differing parameters within the testing regimen. They include both geometry measurements, as well as measurements taken during testing. The results are also compared to one another, and these comparisons are evaluated to determine the effects of the varied parameters.

One point deserves reiteration. The gaps in the samples are designated 1gap, 2 gaps, etc. A sample designated 1 gap does not include only 1 gap; one gap designation implies that gaps are present in every ply of one of the ply orientations. For instance, if the gap designation is 1 gap  $0^\circ$ , gaps were present in *every*  $0^\circ$  ply.

#### Sample Thickness Measurements

A few samples were measured to examine the effects of the gaps on the thickness variations of the samples. None of the samples' gap geometries were identical, so a few samples were measured to show general trends. After the measurements were taken, the data points were plotted to show trends. The measurement was not concerned with how deep the gap itself was, but how the gap changed the thickness of the sample globally. This was representative of the thickness difference that was present in the test machine or fixture while gripping the sample. Therefore, if a measurement data point laid directly in a gap, this data point was not used to calculate the maximum thickness difference. Eight

samples were measured. Four contained gaps, the others did not. A sample was designated ungapped if it did not contain gaps within the gauge section. This did not restrict gaps from being in the tabbed areas. This was done out of necessity, because few samples were present in the panels that contained no gaps throughout.

The samples that were ungapped all contained gaps on one end in the grip area. The trend from all of the thickness plots showed a decrease in overall laminate thickness on the end that contained the gaps. The average, maximum thickness difference for these four samples was 0.292mm (0.0115in.), or about 5% of the average thickness. A sample thickness plot is shown in Figure 5.1. The x coordinate is along the length of the sample, while the y coordinate is transverse to that.

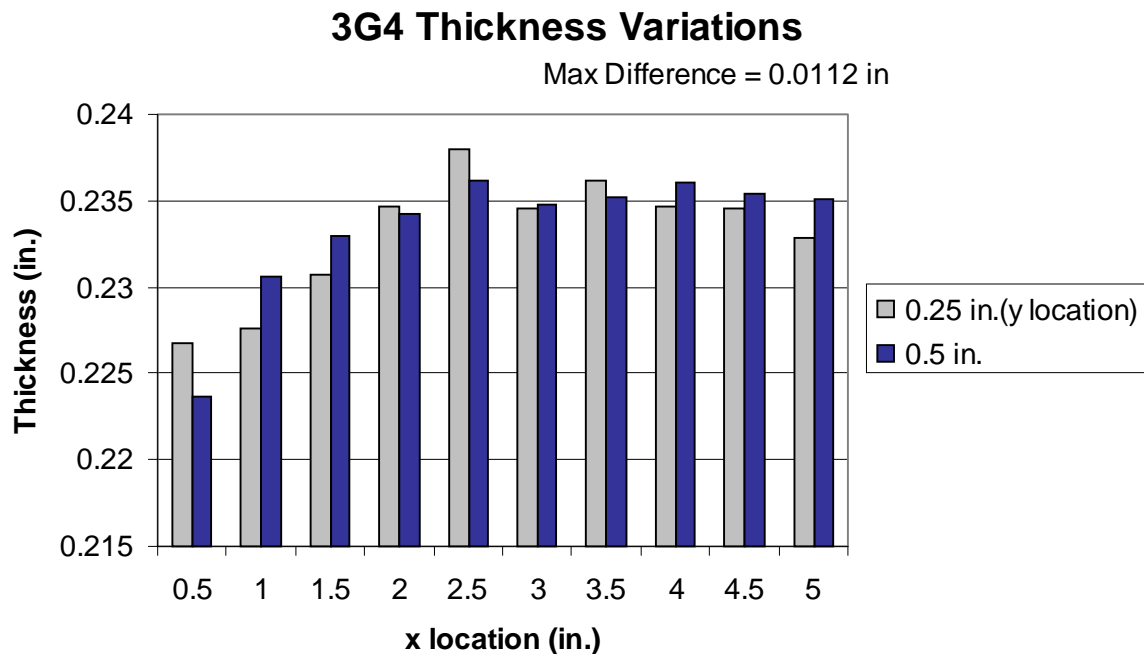


Figure 5.1. Sample thickness variations with an ungapped gauge section.

The remaining four samples each contained three gaps in the gauge section. Some of the grip areas contained gaps, but the highest concentration was in the gauge section. All of these samples were the thinnest around the gaps in the gauge section. The average, maximum thickness difference for these samples was 0.273mm (0.0108in.), again about 5% of the average laminate thickness. A typical plot is shown in Figure 5.2.

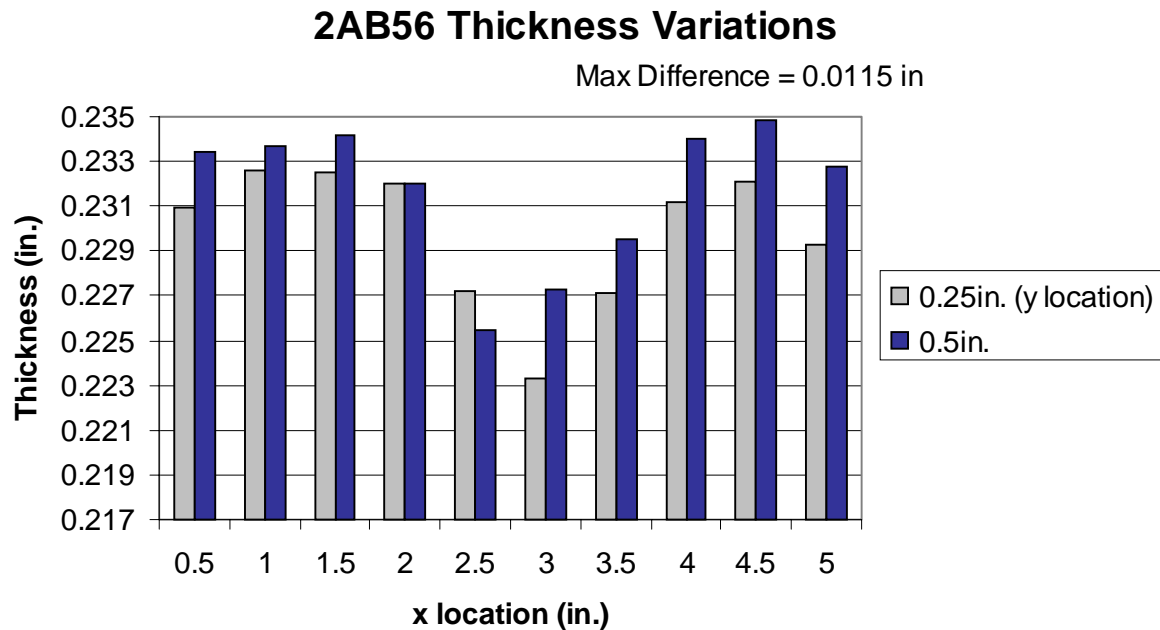


Figure 5.2. Gapped sample thickness variations

These thickness differences seemed large enough to disturb the sample symmetry significantly. Published research indicated that compression tests are notorious for being sensitive to geometry perturbations [Camponeschi, (1991)]. This raised the question of how good the sample test results were expected, especially with respect to the amount of bending present in compression tests. This will be discussed more later after the testing results have been presented.

Elastic Strain Field Tests

Photoelasticity was used to compare the elastic strain fields of ungapped and gapped samples. The fixture was used to eliminate bending in the samples. In the strain gauged tests, the fixture was adjusted until the back to back gauges aligned well. This could not be done in the photoelasticity tests. So, it was not assured that the samples were being loaded evenly throughout. Therefore, the trends from the tests were important, but the overall magnitudes of the values were not as accurate. Three samples were tested, as shown in Table 3.2. The first sample tested was the ungapped sample. Its contours are shown in Figure 5.3.

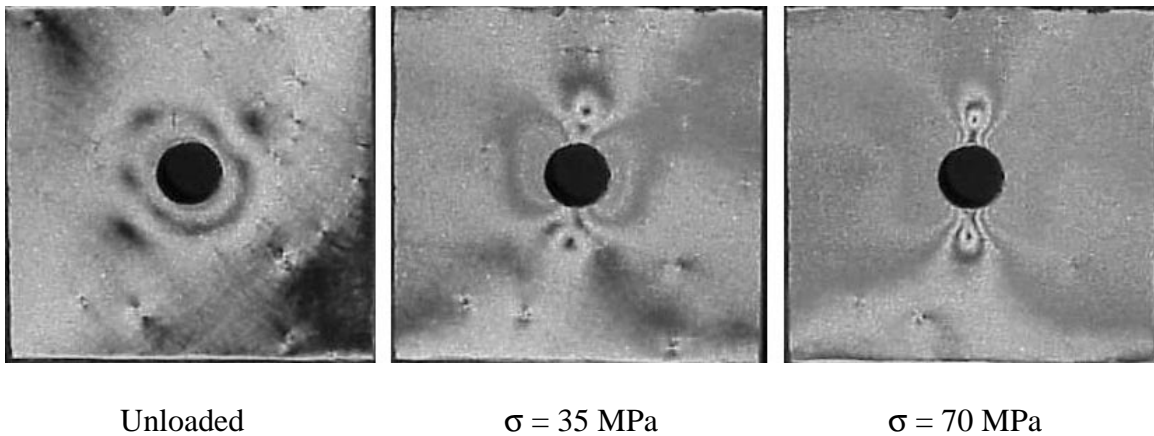


Figure 5.3. Photoelastic contours for ungapped sample.

The first frame is the unloaded sample. The low order fringes that are parasitic. They were caused by the coating material heating up during the drilling operation, and residual stresses formed during cooling. These may have distorted the quantitative measurements made, and will be discussed later.

The second frame is the sample loaded to 9000 N (2000 lbs). The contours were as expected, except for the upper right hand quadrant. This quadrant is asymmetric compared to the others, and had an overall higher strain field. The cause for this was unknown. The final frame was the sample loaded to 18000 N (4000 lbs). The same contours are as in the second frame, but there were more, indicative of the higher loading.

The next sample tested had 3 gaps. The gap configuration and the loading sequence are shown in Figure 5.4.

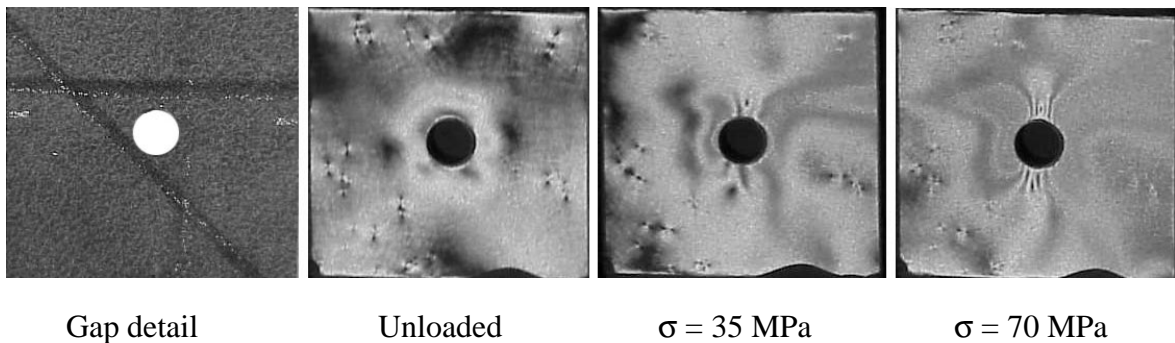


Figure 5.4. Three gap photoelastic sample.

The gaps in the sample were located horizontally across the top of the hole, at a 45 degree angle, and vertically on the right side of the hole (this gap was faint in the picture). Again, the unloaded sample had some parasitic fringes (frame two). The next two frames of the picture are 9000 and 18000 N (2000 and 4000 lbs.). The influence of the gaps is apparent. In all three of the loaded frames, the horizontal gap is easily seen. Additionally, the gap interaction in the lower right quadrant is also apparent. Finally, the gap interaction in the upper left quadrant on the edge of the part is seen in the last two frames. In all of these cases, the contours around the hole edge (those of higher strain) were stretched into the gapped regions. This indicated higher strains present in the gapped regions than what would have been there in the ungapped case.

The final sample tested was one with two 45 degree gaps. These gaps, along with the photoelastic images, are shown in Figure 5.5.

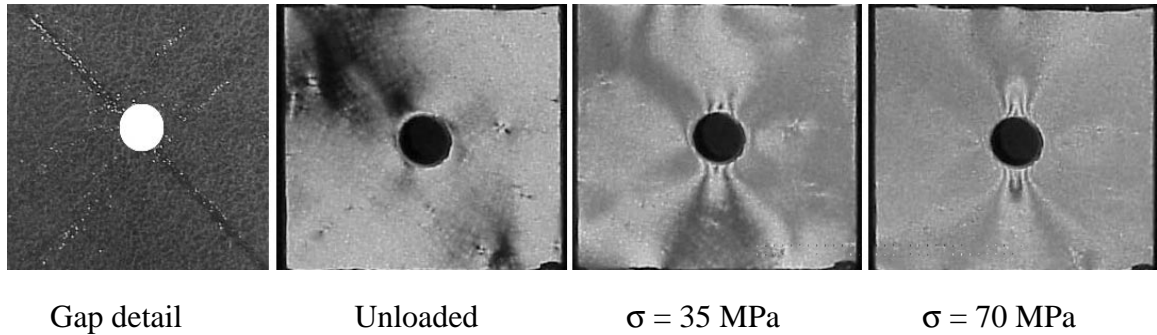


Figure 5.5. 2 gap photoelastic sample sequence.

The gap that angled to the right was difficult to see. More care was taken when drilling the hole in the photoelastic coating. Therefore, the unloaded case in the second frame of the figure did not have significant parasitic fringes. The sample was then loaded to 9000 and 18000 N (2000 and 4000 lbs), shown in frames three and four of Figure 5.5. The “x” pattern formed by the gaps was reflected in these images. Similar to the last sample, the strain contours started to follow the gaps, although it was less obvious.

The photoelastic method indicated a difference in the strain field of the gapped samples compared to the ungapped samples. More quantitative data was desired, and was obtained using the strain interpretation techniques outlined by Dalley and Riley [(1965)], and in the polariscope manufacturer handbook [Measurements group, (1992)]. Strain was measured at points along the ligament from the hole edge to the sample edge for contours of the no, 2, and 3 gap samples at a gross stress of 70 MPa. The data generally showed the expected trends, but only a few points were obtained, and a strain calibration was not conducted, hence the trends did not have a great amount of detail.

The photoelastic strains were compared to the FEA strains, and are shown in Appendix B.

It was interesting to see multiple gaps influencing the strain field. This was not expected, considering that the photoelastic method was only a surface measurement technique. That indicated that the gaps were affecting the sample through the thickness, not just within the ply.

One argument for a source of error in these measurements was made. The gaps, as stated earlier, caused divots in the surface of the part. The multiple gap effect seen in the figures above could have been due to the divoted surface of the part not mating precisely with the flat photoelastic coating. This would cause a thicker bondline of epoxy in these areas, which may have affected the strain transferred to the photoelastic coating.

### Damage Progression Tests

Tests were also conducted to see if the damage formation was influenced by the presence of the gaps. Unpolished samples were examined under the microscope first. Some damage was seen, but not clearly. The samples were then mounted in clear plastic and polished. Two different areas were polished. First, the samples were sanded down so that the edge of the hole with the highest stress concentration was exposed for polishing. Then, one of the samples was cut along the ligament from the edge of the hole to the edge of the sample. These areas were polished and studied under the microscope for damage. Six samples were tested. They are presented in Table 5.1.

Table 5.1. Damage progression test data.

<b>OHC Sample</b>	<b># Gaps</b>	<b>Damage Load</b>	<b>Average Net Normalized Stress MPa (ksi)</b>	<b>Percentage of average 3 gap failure strength</b>
2fg34	3	15.59	369(53.5)	101
2gh45	3	13.79	337(48.91)	92.1
2hi56	3	14.29	341(49.45)	93.1
3g12	3	12.67	313(45.35)	85.4
2de7	3	13.02 (failed)	327(47.43)	89.3
2de3	3	11.81	358(51.92)	97.8

Damage was suspected in the zero degree plies and around the gapped areas. Most of the damage was seen in the zero degree plies. Typical compressive fiber failures were seen [Jones, (1975)]. Some delamination was also observed in the zero degree plies. No true interply delaminations were observed. This was attributed to the toughening material applied between the plies during manufacturing.

A picture of a damaged hole edge is shown in Figure 5.6. Black dots above the layer signified a zero degree ply. Nearly all of the damage was observed in the zero degree plies. Some matrix cracking was seen in the cross plies, but it was small compared to the zero ply damage. Details of these failures are shown in Figures 5.7 to 5.9.

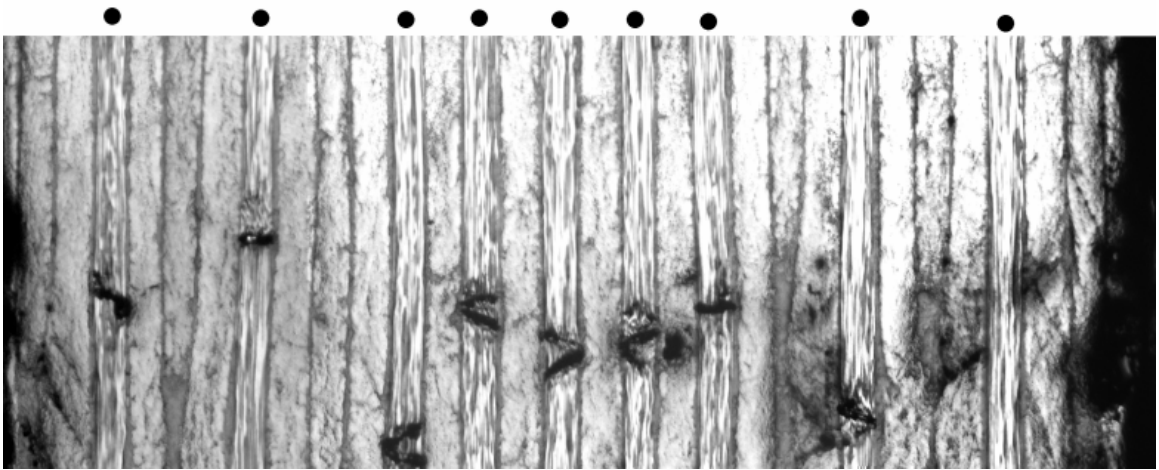


Figure 5.6. Hole edge damage in sample 2gh45.

Fiber kinking of a zero degree ply is shown in Figure 5.7. No matrix cracking that bridged to the zero damage was observed around this failure, which implied that the failure was initiated in the zero ply. Delamination was observed in the zero ply shown in Figure 5.9. Again, no other cracking was observed around this damage. The gap in the ply directly above the delamination was also interesting. A curve into the gap of the zero ply was noticed. The failure corresponded directly to the location of the gap above it. This suggested that the ply curvature caused by the gap was causing the failure. Fiber buckling and splitting was observed in the ply in Figure 5.8. Although matrix cracking was seen in the surrounding plies, they did not bridge to the zero degree plies to suggest that those cracks initiated the damage in the zero plies. Few cracks were seen in the gapped regions of the composites. This implied that the cracks were not failure initiation sites. Their role in reducing the failure strength of the laminates seemed to be restricted to the geometry perturbations that they created and any strain redistribution they caused.

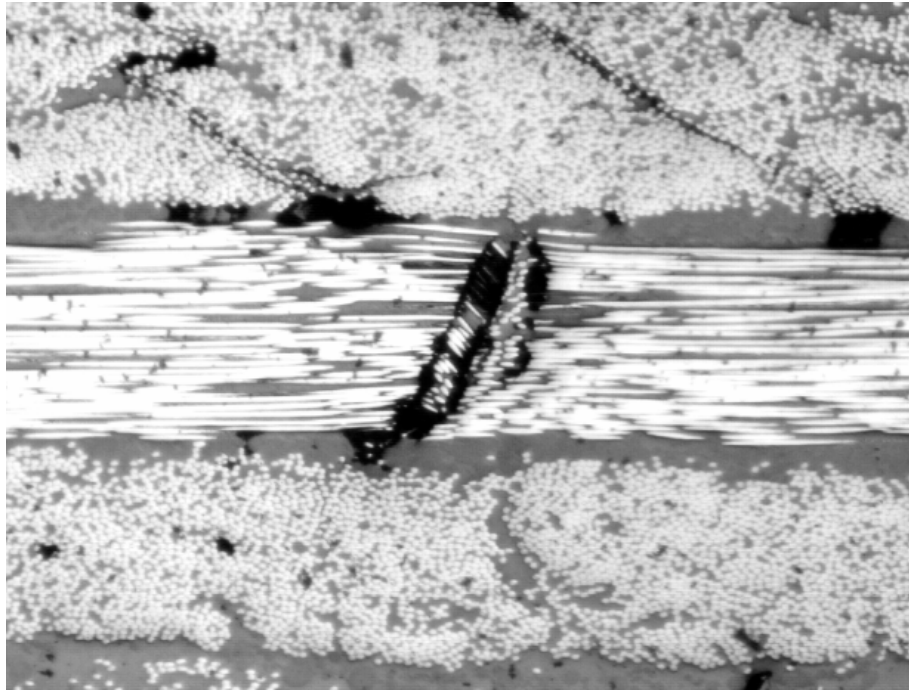


Figure 5.7. Fiber kinking in a zero degree ply, sample 2gh45.

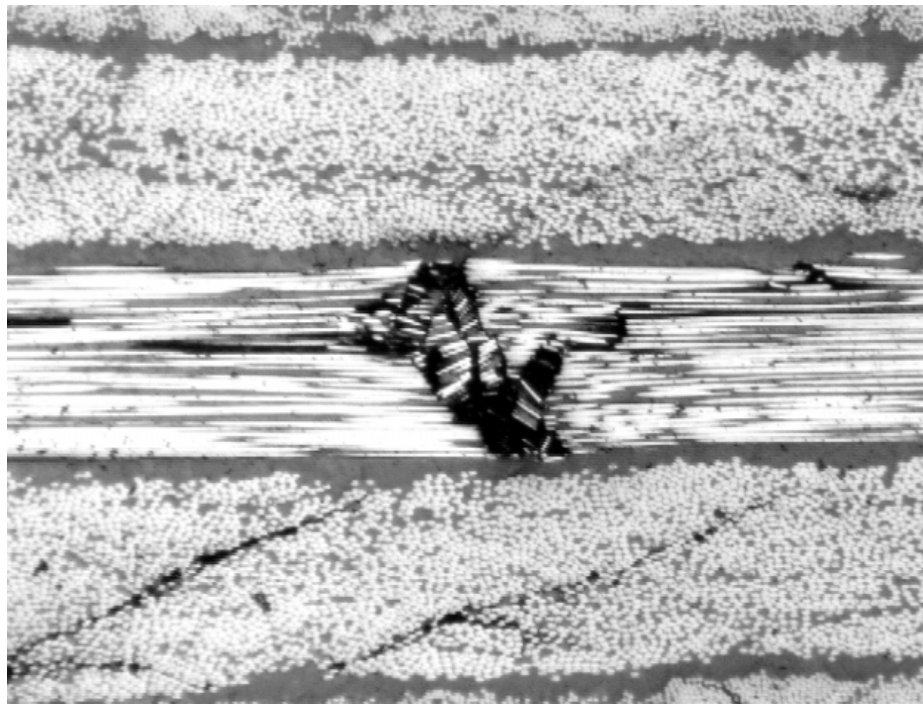


Figure 5.8. Damage in a zero ply, sample 2gh45.

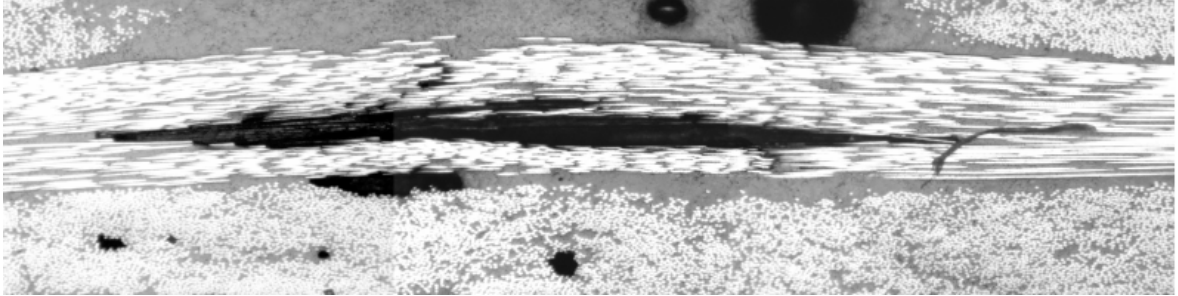


Figure 5.9. Fiber splitting in a zero degree ply, sample 2fg34.

### Failure Tests

Failure tests were the majority of tests conducted. Several specimens with holes and gaps were failed in both tension and compression.

#### Tension

The first samples tested in tension were unnotched, ungapped samples. Motivations and the number of samples in each category were listed in Table 3.2. These tests gave strengths to compare to Boeing test data [Avery,(1999)], and were also used to compare to later gapped tests. The results are listed in Table 5.2.

Table 5.2. Averaged tension test results and comparisons.

Gap Configuration	Notch	Test	Average Net Normalized Stress MPa (ksi)	Strength percentage of no gap case
no gaps	none	tension	982(142.46)	100
3 gaps	none	tension	829(120.19)	84.4
no gaps	6.35 mm (.25 in) hole	tension	488(70.79)	100
3 gaps	6.35 mm (.25 in) hole	tension	489(70.94)	100.2

The average normalized failure strength of these samples was 980 MPa (142 ksi). The term normalized stress indicated that the load was divided by the thickness of a nominal laminate. This thickness was obtained by multiplying the average thickness of a ply, 0.193mm (0.00758 in) by the number of plies in the sample. This helped eliminate the effect of processing variation on the thickness. This was justified by reckoning that a ply's weight from the carbon fibers was highly controlled and nearly constant, and so the amount of reinforcement in the plies was nearly equal. The unnotched ply tensile strength was reported from Boeing as 2390 MPa (346 ksi) (see Table 4.3). This strength was put in to laminated plate software, and the average composite stress at predicted failure was 972 MPa (141 ksi), less than 1% difference. This validated the unnotched tension.

The next set of tests were the unnotched gapped samples. As stated before, only a three gap configuration was used because of time and material constraints. These results are also listed in Table 5.2. The average failure stress for this set of samples was 827 MPa (120 ksi). This was a reduction of slightly more than 15% from the ungapped tests. Both ungapped and gapped failures happened in the narrowest part of the gauge section. A failed sample is shown in Figure 5.10. This was where failure was expected. Some damage accumulated during the tests, but the failures were sudden and no significant softening was seen in the stress strain curve. The next tests were run to determine if a similar reduction happened in a tension sample with a hole.

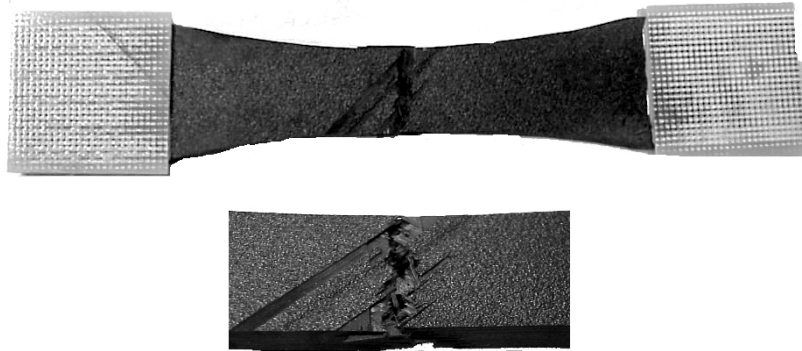


Figure 5.10. Failed unnotched tension sample.

Similar configurations of ungapped and gapped samples as the unnotched tests were run with holes in them. They are also presented in Table 5.2. The average normalized net failure stress for the ungapped specimens was 585 MPa (85 ksi). Net failure stress or strength implied that the area of the sample was calculated without the area of the hole. The specimens containing three gaps had an average net normalized stress of 587 MPa (85 ksi). Therefore, no statistically defensible difference existed between the ungapped and gapped groups. The failures in these tests were from the edge of the hole to the edge of the sample. Again, this was the expected and accepted failure mode, and so the tests were valid. The results of all the tension tests are shown in Figure 5.11. A failure example is shown in Figure 5.12

## Tension Comparisons

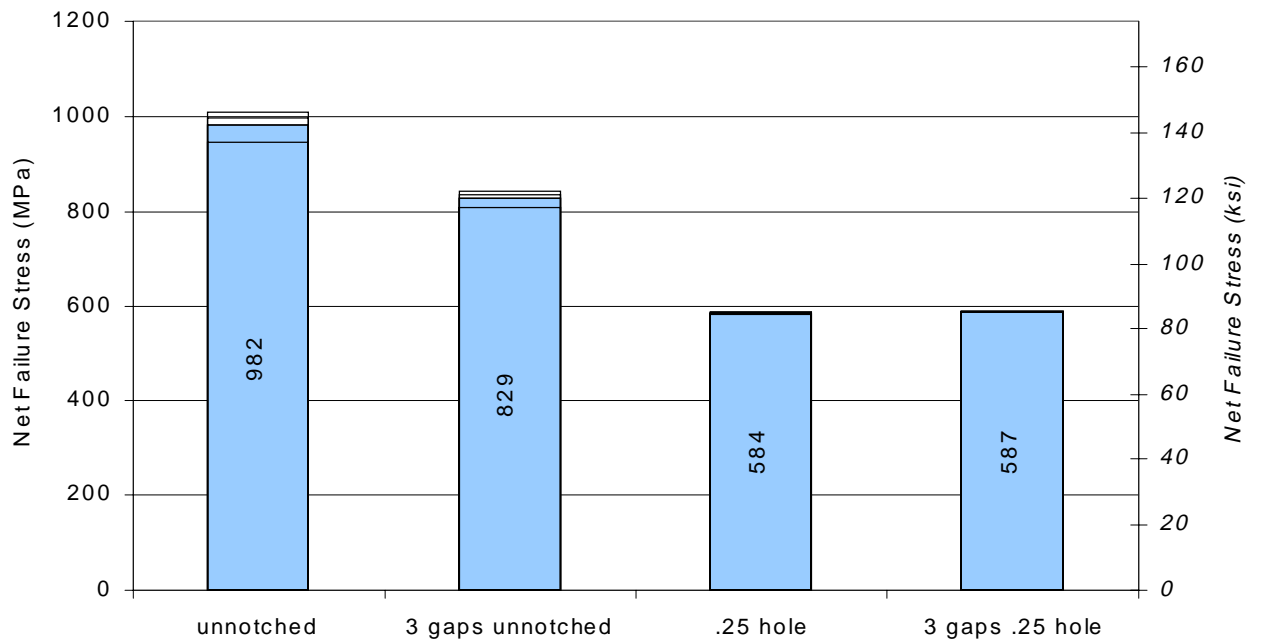


Figure 5.11. Tension failure results.

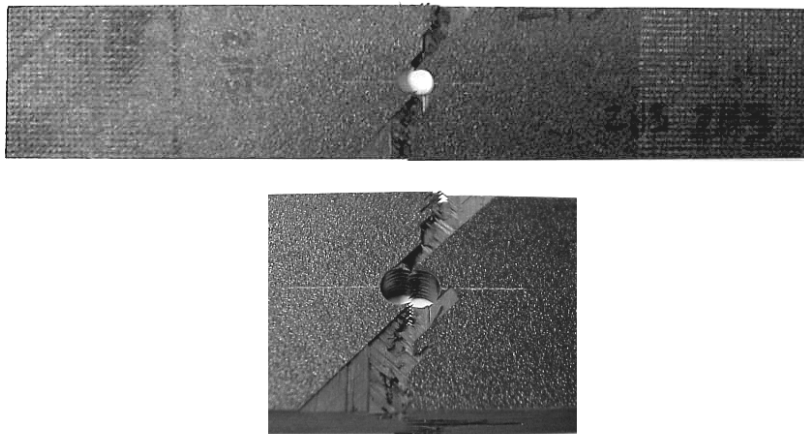


Figure 5.12. Open hole tension sample failure.

These results were interesting. The unnotched tests produced a reduction of over 15%, but the open hole tests saw no reduction whatsoever. This indicates, at least for the tension case, that the gaps played a large role in the failure of the unnotched samples. However, the hole geometry and free edges dominated the open hole tests; the small material defects had little significance on the failure. Next, compression tests were run to see if similar results occurred.

### Compression

Several compression tests were run. Two main categories of testing were loading in the grips and loading in the fixture. Each of these contained several subcategories. After each test results section, comparisons were made to highlight the effects of the various gap and hole geometries in compression. The first set of results that will be discussed are the machine grip tests.

Machine Grips. A full spectrum of unnotched and open hole tests were run. These results are presented and then comparisons are made. Motivations and the number of samples tested were listed in Table 3.2.

Unnotched tests in the machine grips were tested with no gaps and with a three gap configuration. The average failure strength for the samples without gaps was 544 MPa (79 ksi). The average failure strength for the three gap configuration was 498 MPa (72 ksi). The reduction for the gaps was about 9% of the ungapped strength. Failure was catastrophic with no audible damage before final failure. Some of the samples failed by brooming in the middle of the gauge section. This was perceived as the best failure mode, because the failure was not affected by the grips. Most of the samples broke at the

termination of the glass tab. Although not as clean as a pure gauge section failure, this failure is an accepted ASTM failure mode. A picture of a typical failure is presented in Figure 5.13. These figures are reported in Table 5.3.

Table 5.3 Unnotched Compression Average Results

Gap Configuration	Notch	Test	Average Net Normalized Stress MPa (ksi)	Strength percentage of no gap case
no gaps	none	compression	544(78.84)	100
3 gaps	none	compression	498(72.19)	91.5

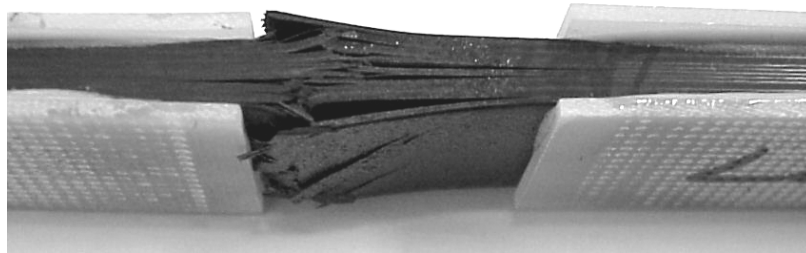


Figure 5.13. Failed UNC sample.

Boeing also reported typical failure data for the unnotched compression of this laminate [Avery, (1999)]. They reported a compressive strength of 671MPa (97.3 ksi) for ungapped material. The experimental results obtained at MSU are 19% lower than the reported unnotched compressive strength. This indicated that bending in the samples might have been significant.

For most of the compression tests, the amount of bending was measured with back to back strain gauges. Bending was present in these samples, possibly due to specimen asymmetry. This will be discussed more at the end of this section.

The next tests were open hole compression (OHC) tests. All gap configurations were tested: no gaps, 1 gap, 2 gaps, 3 gaps, 4 gaps, and stagger. These results are included in Table 5.4. Additionally, they are plotted in Figure 5.14.

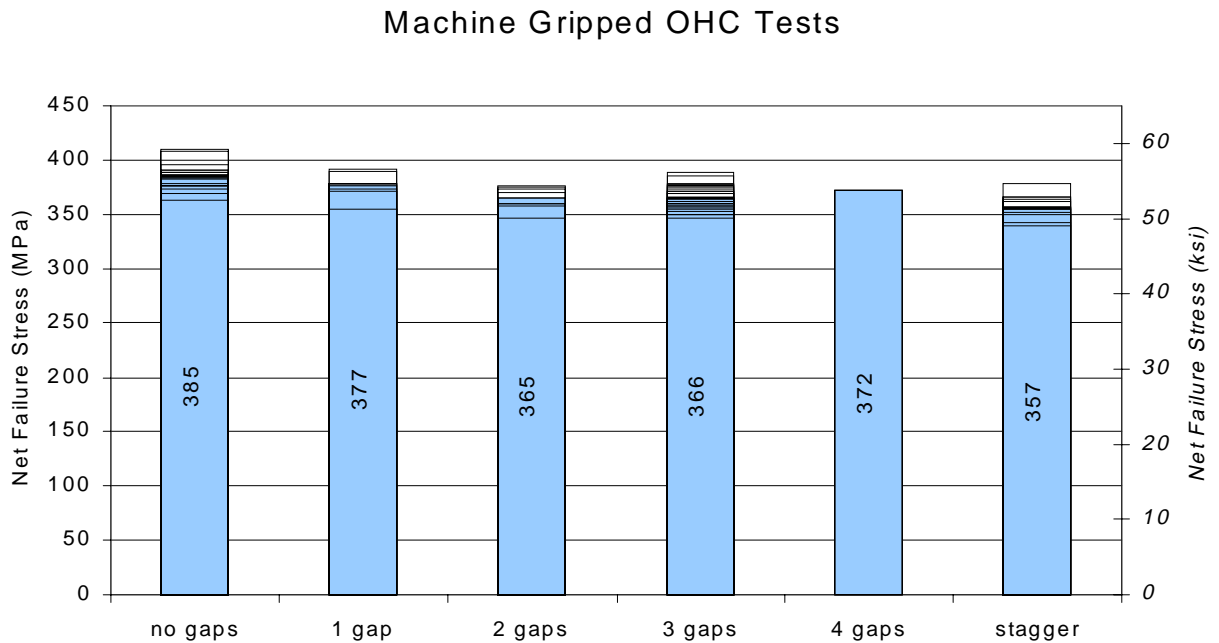


Figure 5.14. Machine gripped OHC gap comparisons.

Table 5.4. Machine gripped OHC failure data.

Gap Configuration	Notch	Test	Average Net Normalized Stress MPa (ksi)	Strength percentage of no gap case
no gaps	6.35 mm (.25 in) hole	compression	385(55.86)	100
1 gaps	6.35 mm (.25 in) hole	compression	377(54.68)	97.9
2 gaps	6.35 mm (.25 in) hole	compression	365(52.99)	94.8
3 gaps	6.35 mm (.25 in) hole	compression	366(53.09)	95.1
4 gaps	6.35 mm (.25 in) hole	compression	372(53.99)	96.6
stagger gaps	6.35 mm (.25 in) hole	compression	357(51.79)	92.7

The trend seen in Figure 5.14 was generally highest on the left, with reducing strengths moving to the right. The exception was the four gap orientation, but this sample set only had two data points, so it was weaker statistically than the other samples.

Although there was a trend present, it was a relatively small one. The maximum difference between the no gap and stagger sample sets was about 7%. All of the other differences were smaller than that.

Enough samples were tested in this group of tests to perform statistical analyses to see if statistical differences existed between the groups. These were performed using SigmaStat, and the results are presented in Table 5.5.

Table 5.5. Statistical data for MTS OHC tests. (alpha=0.05)

Gap geometry	Mean Failure MPa (ksi)	Std Dev MPa (ksi)	Difference from no gaps MPa (ksi)	Statistically significant difference
No gaps	385 (55.9)	11.2 (1.63)	NA	NA
1 gaps	377 (54.7)	11.4 (1.66)	8.1 (1.18)	no
2 gaps	365 (53.0)	9.6 (1.39)	19.8 (2.87)	yes
3 gaps	366 (53.1)	11.3 (1.64)	19 (2.77)	yes
Stagger gaps	357 (51.8)	10 (1.46)	28 (4.07)	yes

A t-test was performed between each of the sample groups. The result returned was that either the two groups were significantly different or not. The differences of the means was usually small, so these analyses helped determine the significance of the test results.

Another topic of interest was to see if the data for the OHC ungapped tests agreed with ungapped OHC data from Boeing. The OHC strength for this laminate reported from Boeing is 412 MPa (59.7 ksi) [Avery, (1999)]. Tests run gave an OHC strength of 385 MPa (56 ksi), which was about 6% lower than Boeing's data. This questioned the validity of the failures.

All of the OHC specimen data reported failed in a brooming manner in the middle of the gauge section. Nearly all of the failures had no obvious signs of a bending failure; a

few of the samples had a slight bias to one side of the sample, which hinted at bending. A typical failed specimen is shown in Figure 5.15. Many of the OHC samples were gauged with back to back strain gauges to detect bending. A typical stress strain curve is shown in Figure 5.16.

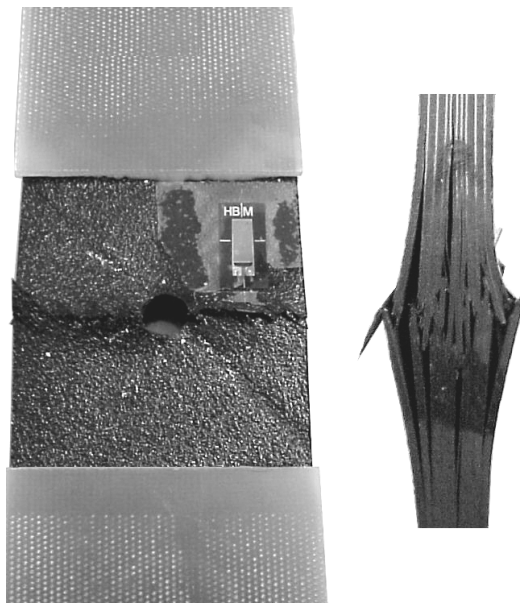


Figure 5.15. Typical OHC failure.

These curves showed enough bending to cause further study. Since geometry variations had been seen, the bending needed to be separated into bending due to sample asymmetry and bending due to machine head misalignment. To test for head misalignment, an aluminum sample was machined to the same outer dimensions as the OHC samples. Two strain gauges were mounted back to back, and the sample was loaded in the testing machine. The stress strain curves aligned nearly perfectly. This

indicated that the bending due to machine head misalignment was small or nonexistent, and that the bending was dominated by sample asymmetry.

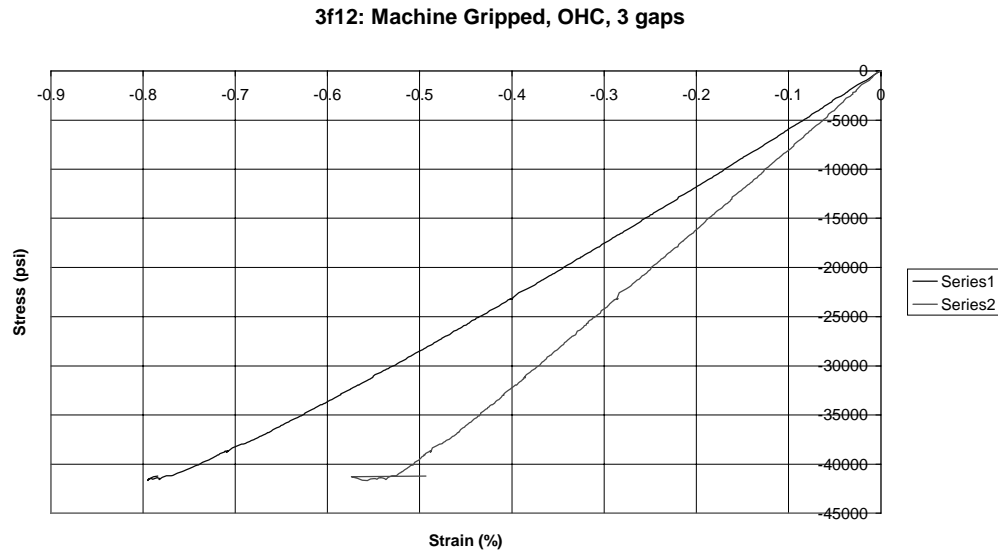


Figure 5.16. Stress strain curve for an OHC test .

This was not surprising, considering that a no gap sample that had gaps in the tabs averaged about 0.254 mm(0.01 in) thinner on the gapped side. The thickness measurements (detailed earlier in the chapter) showed that considerable asymmetry was present in the samples, which could have easily introduced bending in the tests. A fixture was used to try to eliminate some of this bending.

Fixture. The results of the fixture tests are presented next. Only open hole compression tests were run in the fixture. The tests and number of samples were listed in Table 3.2. Comparisons are made between different gap groups tested in the fixture. Then, the fixture results are compared with the machine gripped results.

Tests were performed for no, 1, 2, and 3 gaps. The results are listed in Table 5.6, and are shown graphically in Figure 5.17.

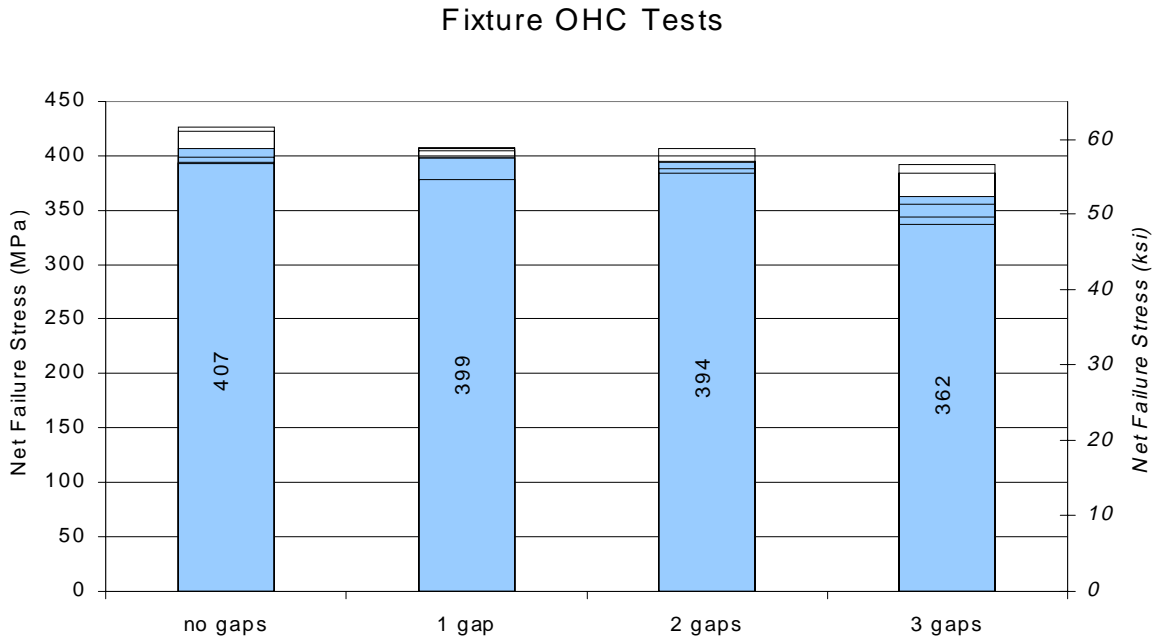


Figure 5.17. Fixture OHC test comparisons.

Table 5.6. Fixture OHC failure data.

Gap Configuration	Notch	Test	Average Net Normalized Stress MPa (ksi)	Strength percentage of no gap case
no gaps	6.35 mm (.25 in) hole	fixture comp	407(59.03)	100
1 gaps	6.35 mm (.25 in) hole	fixture comp	399(57.83)	98.0
2 gaps	6.35 mm (.25 in) hole	fixture comp	394(57.10)	96.8
3 gaps	6.35 mm (.25 in) hole	fixture comp	362(52.56)	88.9

The trend was similar to the machine gripped OHC results. The ungapped case had the highest strength, while strength decreased with increasing gaps. The largest strength decrease from ungapped specimens was the 3 gap case, with an average 11% below the ungapped case. This is a significant decrease, and indicates that the gaps can have a

significant effect on the strength of the material. Statistical tests were performed, and the results are shown in Table 5.7.

Table 5.7. Statistical data for fixture OHC tests.

Gap geometry	Mean Failure MPa (ksi)	Std Dev MPa (ksi)	Difference from no gaps MPa (ksi)	Statistically significant difference
no gaps	407 (59)	16.2 (2.36)	NA	NA
1 gaps	399 (57.8)	12.5 (1.81)	8.3 (1.20)	no
2 gaps	394 (57.1)	10.4 (1.51)	13.3 (1.93)	no
3 gaps	363 (52.6)	23.9 (3.47)	44.6 (6.47)	yes

The fixture ungapped OHC strength was compared to the strength provided by Boeing. The strength reported by Boeing was 412 MPa (59.7 ksi). This was nearly the same as the fixture test strength of 407 MPa (59 ksi). This gave some confidence to the fixture tests. All of the failures from the fixture broomed in the middle of the gauge section, as shown in Figure 5.18. The back to back strain gauges generally aligned well with one another. However, the samples were adjusted until the best strain gauge data was obtained. Some differences were noted between the machine grips and fixture tests.

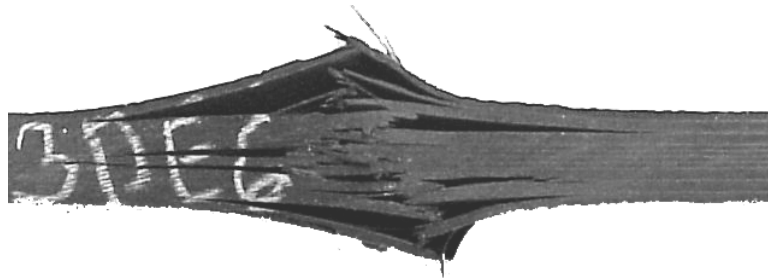


Figure 5.18. Typical fixture OHC failure.

Comparison of Machine Grips to Fixture. Differences and similarities were observed during the OHC testing between the grips and the fixture. A graph comparing the failure strength using both testing methods is in Figure 5.19. First, the ungapped results differed considerably. The machine grip ungapped tests were about 5% lower than the corresponding fixture tests. This indicated that the fixture was constraining some of the sample geometry asymmetries and so resisted the onset of buckling on a global scale. One gap and 2 gap samples were also notably higher for the fixture method. However, the 3 gap case differed. The machine grip average failure stress for 3 gaps was 366 MPa while the fixture average was 362 MPa. So, while the fixture had higher failure strengths with samples with no or few gaps, when the number of defects became high, the strengths became similar. Several scenarios might have caused this.

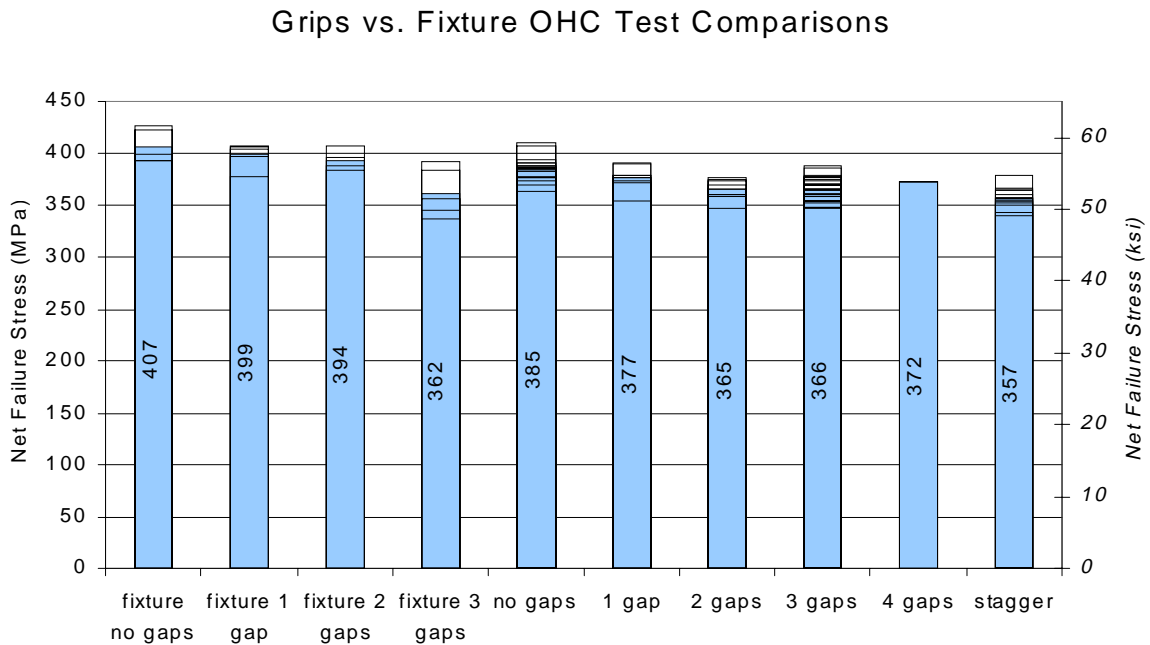


Figure 5.19. Comparisons between gripped and fixture tested OHC samples.

First, the geometric asymmetries in the high gap samples may have been too great for the fixture to compensate and resist the bending that the defects caused. Therefore, the two test methods were similar in the 3 (high) gap case. Another possibility was that the actual strength reduction of the 3 gap samples in the fixture happened to be the same as the strength of the 3 gap samples that experienced more bending in the machine grips. Generally, this did not make sense. If the fixture eliminated bending, and the samples tested in both the fixture and the grips were the same gap orientation, the samples with more bending applied (the machine gripped samples) should have broken at a lower stress.

The ungapped results varied from one test method to the other. This affirmed that various compression test methods can give different results. There is no agreement among researchers which of the methods are correct [Camponeshi, (1991)]. Some hold to the fact that the real failure happens at the microstructural level; others say the meaningful failure happens somewhere between global buckling and microstructural failure. Whichever criterion one prefers, the important question to ask is how is the strength value going to be used, and will the end analysis predict the in service performance correctly. In contrast to the ungapped results, the gapped results are clear. Regardless of the testing method, the OHC samples with a high number of gaps failed around an 11% lower stress than the Boeing OHC data.

#### Tension-Compression Comparisons

A graph of no gap and 3 gap test results for UNT, OHT, UNC, and OHC is presented in Figure 5.20. The unnotched tension tests produced a considerable decrease in failure

strength, while the open hole tension tests were unaffected. Unnotched compression saw reductions from ungapped to 3 gaps as well. The reduction from the MSU ungapped to MSU gapped tests is approximately 9%. However, the reduction was quite large from the Boeing ungapped data to the MSU gapped tests, at around 25%. This comparison was not completely accurate, because the Boeing and MSU tests methods were not the same.

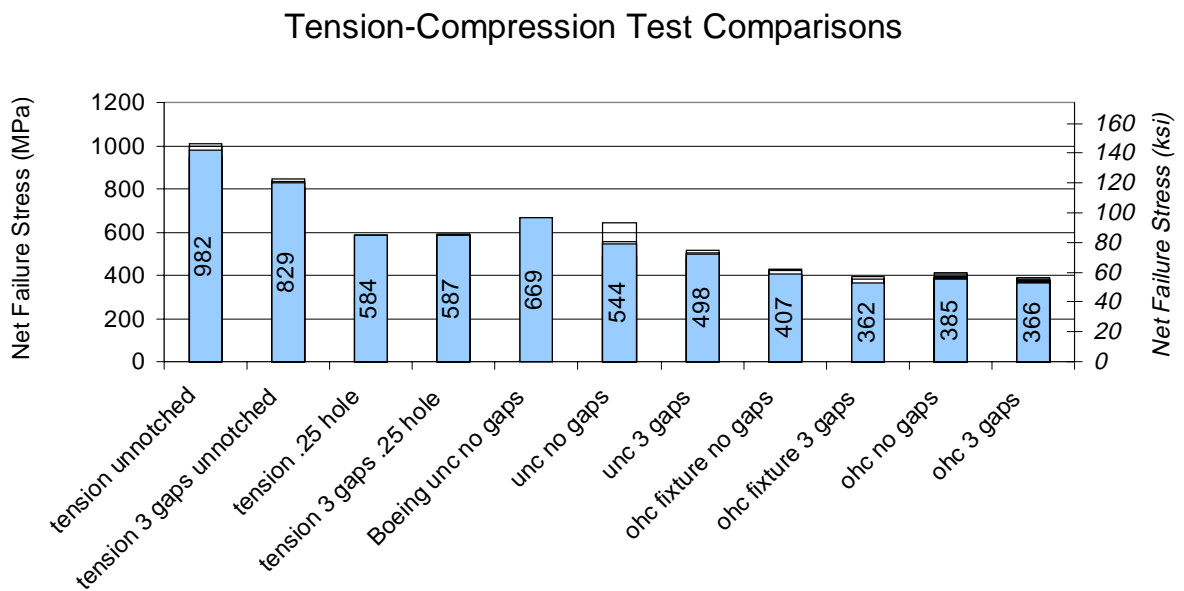


Figure 5.20. Tension/compression test comparisons.

Consequently, while the OHT tests were unaffected by the gaps, the OHC tests were affected. Depending on the ungapped strength used, the 3 gap OHC strength was reduced 5-10%. This demonstrates that the unnotched compression strengths are more sensitive to the gaps than the OHC tests. The same trend is apparent in tension, but overall the compression tests are more sensitive to the gap defects than the tension tests. This was expected, based on the bulk of the published research on compression testing.

## CHAPTER 6

## NUMERICAL RESULTS

The results of the finite element analyses performed are discussed in this chapter. Each model's results are discussed and compared to the results of the different runs performed within that model. This includes solid, unnotched models as well as the stacked shell models with holes, which were described in Chapter 4. Each of the different models were run with a variety of gap configurations. Model motivations and run descriptions were provided in Table 4.4. Those various gap runs are compared to each other, within a model. Factors compared are overall strain field, damage initiation load and location, and failure load and location. Then, the models are compared to one another using the same variables. Finally, the numerical results are compared to the experimental tests.

Unnotched Solid Models

The first models run were unnotched solid models. The mesh used for this model was shown in Chapter 4. The model was first input with isotropic material properties. This was done to check for mesh dependence. A displacement of 0.76 mm (0.03 in) was applied at the boundary condition. The strain throughout the entire model was easily calculated by strength of materials and classical laminated plate theory at 0.494% linear strain. The model was run, and the strains were plotted for all of the layers. Any mesh

effects would have been seen as a nonuniform strain distribution. When the strain was plotted, the value was constant, at -0.00494. This gave confidence that the mesh did not cause any artificial effects.

Next, composite material properties were input. Only the reinforced material was used. No gaps were present, although the mesh still contained the gapped areas. Strength of materials calculations were used to determine the displacement that corresponded to failure. The model was run with the composite material properties, and the model behaved correctly, producing a constant strain throughout the zero degree ply of -0.0116, the unnotched compression (UNC) failure strain from Boeing. This combined with the isotropic run validated the mesh, so gap properties were input for investigation.

Three and four gap runs were made. The three gaps were run because several samples of that configuration were tested. The four gap configuration was run because it contained the most gaps, and so was the most severe.

The three gap case was loaded with a displacement loading of -0.07 in. This produced an overall nominal strain of -0.01156, corresponding to the longitudinal failure strain for the composite ply. Any differing strains from gaps were compared to this strain. The strain contours of a 0° ply are shown in Figure 6.1.

The darker, yellow orange color was the color of the bulk of the ungapped model. The strain that corresponded to these colors was about -0.0116. This was the expected nominal strain. There were some strain gradients associated with the gaps. One of the 45° gaps was not perturbed. That gap was filled with composite properties, not resin only (because it was a 3 gap case). The lighter yellow (which indicated a higher compressive

strain) was seen in three of the gaps. This strain was slightly higher than the nominal. The center gapped region had more strain perturbations.

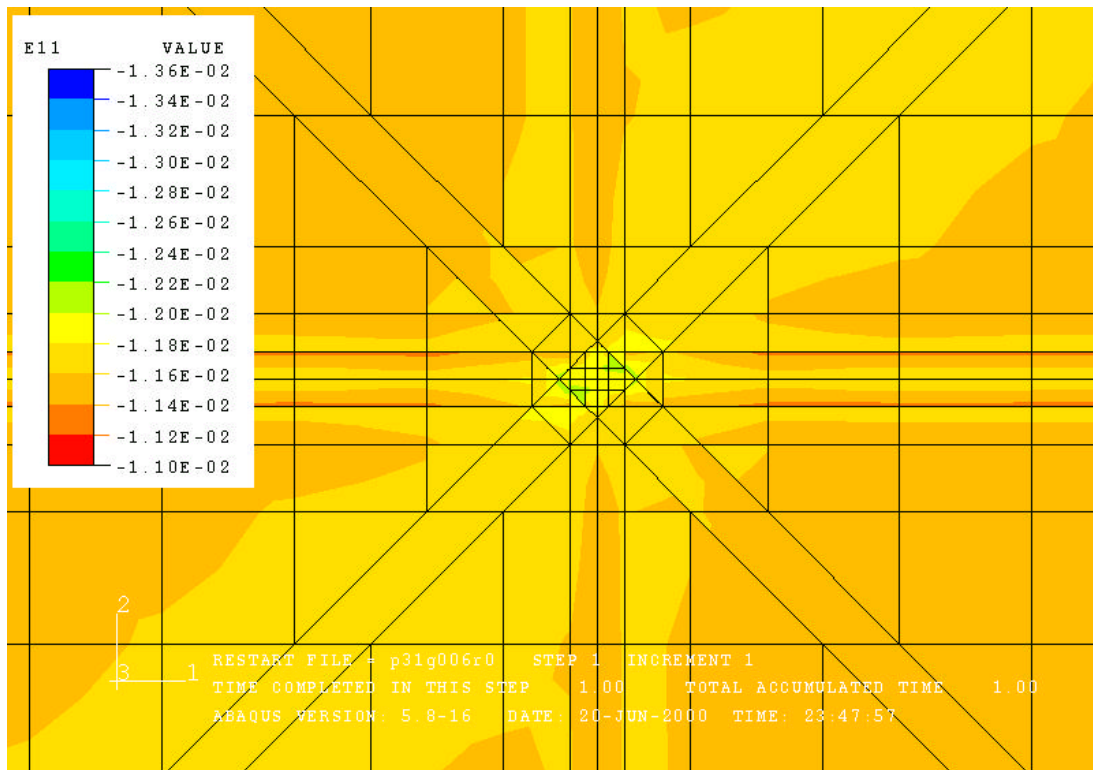


Figure 6.1. Strain contours for an unnotched solid model, 3 gap run, zero degree ply.

The green contours seen indicate a strain around  $-0.0124$ . This was about 7% higher than the nominal. The higher strain in the gapped areas did not necessarily mean failure. The resin has a higher strain to failure than the laminated composite. The gaps raised the strain locally in the fibers surrounding the gapped region. (Note that the gapped region in this  $0^\circ$  layer was the horizontal gap.) This is seen as light yellow contours. This increase is only slight, with the highest strain at  $-0.0119$ . Next, reaction forces from the edge nodes of the model were extracted. These were summed, and then divided by the cross section area. Finally, this stress was scaled linearly so that the maximum strain in the model was equal to the maximum failure strain. The resultant

stress was 4% lower than the ungapped predicted UNC failure. So, if the failure was dominated by the  $0^\circ$  plies, the 3 gap composite would be predicted to fail at around 4% lower than an ungapped specimen.

The four gap sample was similar, but the strain increases were more severe. The  $0^\circ$  ply strain contours are shown in Figure 6.2. The model was also run with a displacement of  $-0.07$  in., producing a nominal strain of  $-0.01156$ . All four gap areas of the mesh were at slightly higher strains, corresponding to each gap assigned with resin properties. The center gap crossing had the highest strains.

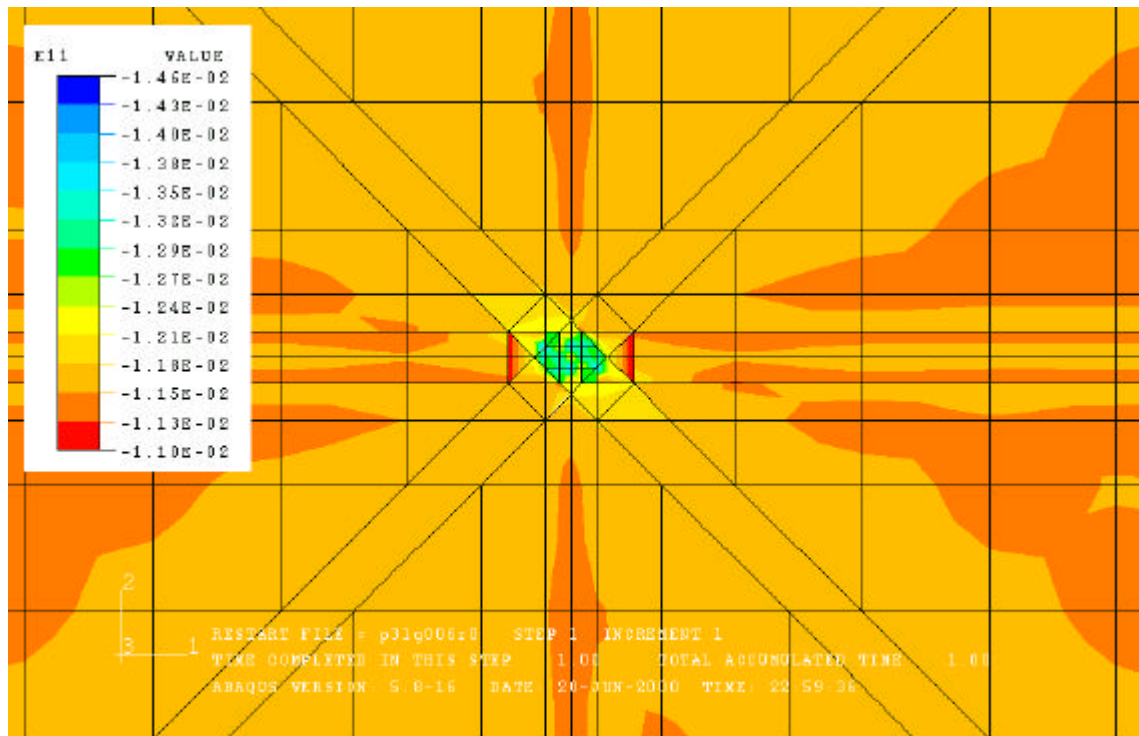


Figure 6.2. Strain contours for an unnotched solid, 4 gap run, zero degree ply.

Elements in the center region had strains as high as -0.01381. This was 19% higher than the nominal strain. Although high, a strain of -0.01381 corresponds to a -103 MPa (-15.6 ksi) stress. This is considerably lower than the Boeing reported compressive failure strength of the resin, which is -172 MPa (-25 ksi) [Avery, (1999)]. However, the composite surrounding the gaps was increased in strain. The highest strain calculated in the ply near the gaps was -0.01227. Again, the stress was calculated, as in the 3 gap case. The 4 gap predicted failure stress is 7% below the ungapped failure stress.

### Open Hole Shell Models

The next models were open hole shell models. The stacked shell method that was used to create these models was described in Chapter 4. Again, the first run was done with all isotropic material properties. The results were checked with previously know analytical solutions. In addition, with no gaps present, the isotropic runs were expected to have smooth stress and strain contours. If they did not, that indicated that the mesh influenced the results. This was done for both of the open hole shell meshes: centered gaps and offset gaps.

#### Centered Gap Mesh

The isotropic run with the centered gap mesh produced the correct results. The contours showed no anomalies, and the strains were correct. The next run was to use composite material properties for an ungapped run. Strain contours for a 0° ply are shown in Figures 6.3 and 6.4. These contours are smooth and no mesh anomalies were seen.

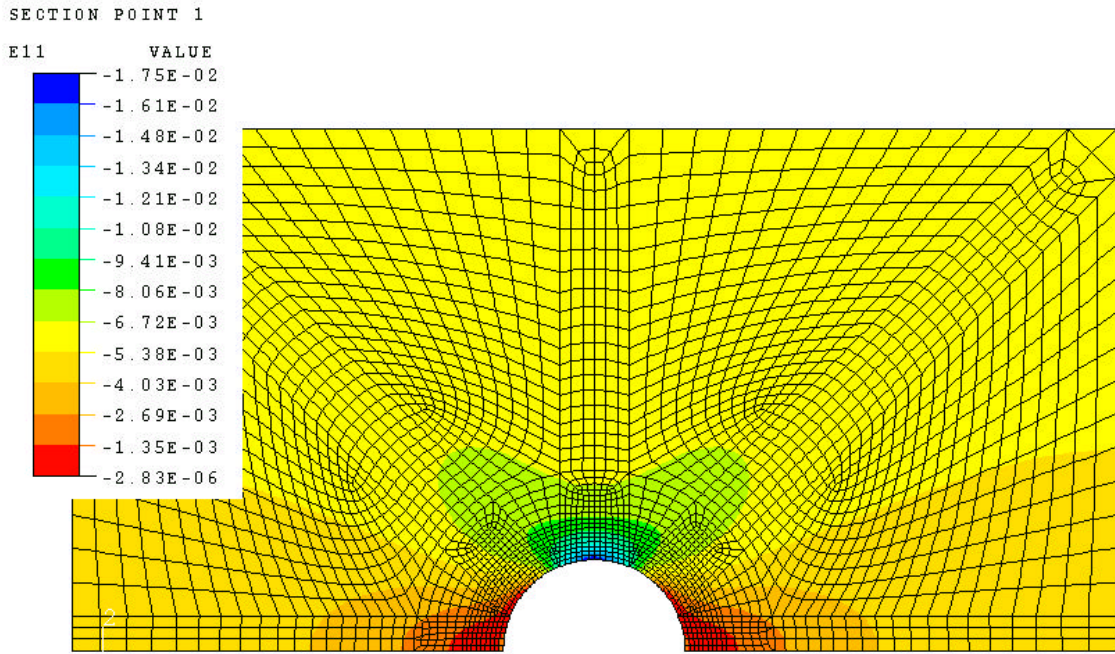


Figure 6.3. Longitudinal strain contours for open hole shell model, gaps centered mesh, no gap run, zero degree layer.

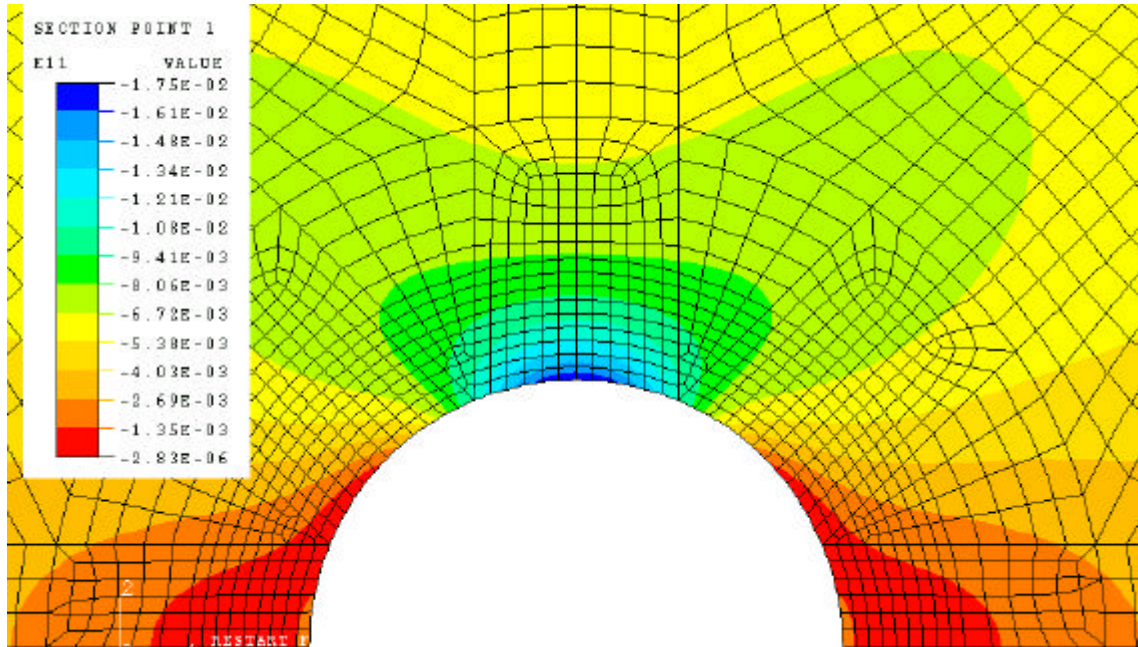


Figure 6.4. Longitudinal strain contour detail region for open hole shell model, centered gap mesh, no gap run, zero degree layer.

A Whitney-Nuismer failure criterion was used to determine failure in the hole models [Agarwal and Broutman, (1990)]. The OHC failure strain reported by Boeing was used to calculate the displacement that was applied to the model. Boeing reported an OHC failure strain for the given laminate of 0.00595 [Avery, (1999)]. This was multiplied by the gauge length section of 1.5 in to get an applied displacement of 0.009 in. Then the results were used to find  $a_0$  for the average-stress criterion. This predicts failure when

$$\frac{1}{a_0} \int_R^{R+a_0} \epsilon_y(r,0) dr = \epsilon_0 \quad (6.1)$$

where  $R$  = the radius of the hole  
 $\epsilon_y$  = the strain from the hole to the sample edge  
 $\epsilon_0$  = the unnotched ply strain  
 $a_0$  = the distance for the averaging to occur over

Plainly stated, failure is predicted when the average stress or strain over the length  $a_0$  past the hole radius reaches the unnotched failure strength/strain. So, the ungapped case was loaded at the know OHC failure strain, and then the distance from the hole where the averaged strain reached the unnotched failure strain was found. A linear strain gradient was found for each element along the ligament of the hole to the sample edge. The strain was plotted against this distance. The area under these curves divided by  $a_0$  was equal to the average experimental strain to failure of an unnotched laminate. An  $a_0$  was determined based on satisfying equation 6.1. The  $a_0$  value calculated from this analysis was 0.056 in. This was assumed to be a laminate constant for later use when

gaps were introduced into the model. A plot of the strain vs. the distance from the hole edge is in Figure 6.5, as predicted by the FE model.

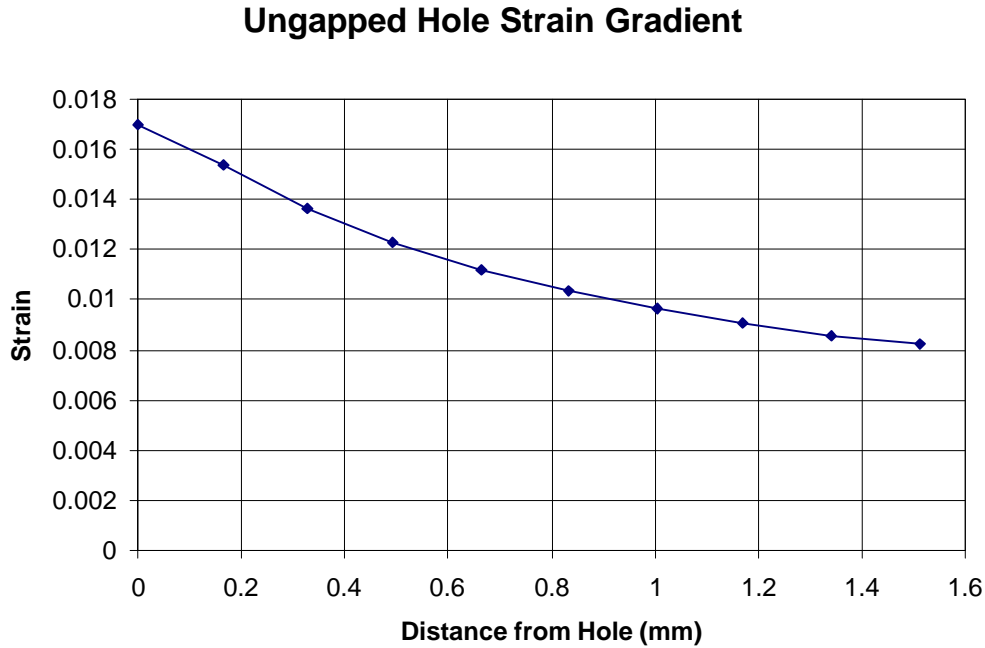


Figure 6.5. Strain as a function of the distance from the hole edge.  
(nominal strain = 0.006)

The experimental failure strain was known for the ungapped case. This allowed the  $a_0$  to be calculated for the given laminate gap geometry. The failure criterion was then used to predict the gapped model failures. The four gap model was the first gap model evaluated.

A detail region of a  $0^\circ$  ply longitudinal strain contour plot for the 4 gap run is shown in Figure 6.6. The contours are significantly different from the no gap run. The edges of the  $90^\circ$  gap area of the mesh have increased strain. This is attributed to resin in that area in the surrounding  $45^\circ$  layers. So, those layers can not carry as much load in

that area, and more of that load has to be carried by the zero ply in that area. Using the  $a_0$  from the ungapped run, the strain was averaged over that distance, and was  $-0.01066$ , almost 8% lower than the ungapped case. However, this was based on strain, and all of the experimental data was compared on a stress basis, since the gapping increases the compliance of the specimen. So, the results needed to be converted from strain to stress.

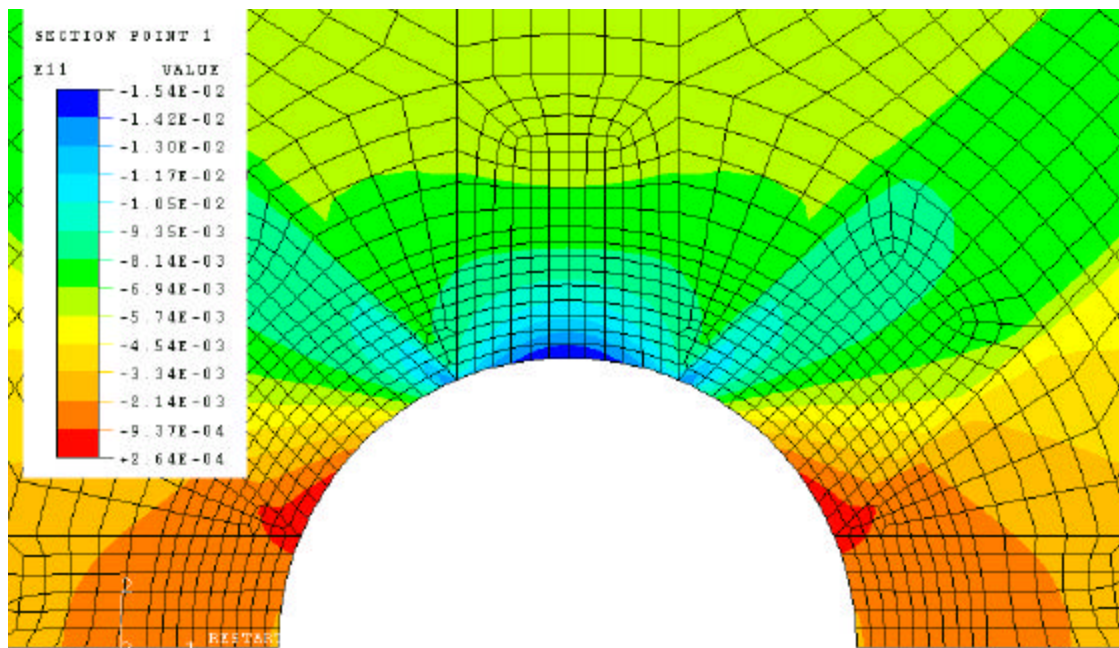


Figure 6.6. Detail of longitudinal strain contours for an open hole model, centered gap mesh, 4 gap run.

First, the reaction forces at the fixed edge of the model were extracted from the results. Forces were converted to stress by dividing by the net area of the model cross section. The stresses were not all at the predicted failure, so they were linearly scaled such that the average strain from the Whitney-Nuismer failure criterion equaled the unnotched compressive strength. These stresses were then divided by the stress of the ungapped OHC run. The 4 gap run failed at nearly the same stress as the ungapped run.

So the gaps did not seem to influence the predicted failure. The same analysis was done for the 1, 2, and 3 gap runs. Results are in Table 6.1.

Table 6.1. Comparison of predicted failure stresses in centered gap mesh runs, open hole model.

Run	Predicted Failure Stress MPa (ksi)	Run stress/ungapped stress (%)
no gaps	388 (56.31)	100.0
1 gap 0°	409 (59.33)	105.4
1 gap 90°	364 (52.77)	93.7
2 gaps 0°/90°	387 (56.16)	99.7
3 gaps 0°/90°/45°	390 (56.51)	100.4
4 gaps	392 (56.86)	101.0

The 4, 3, and 2 gap runs followed a consistent trend; they all were nearly equal to the ungapped run. However, the 1 gap case deviated from this trend. First, the 1 gap case was run with the gap in the 0° plies, producing a failure stress 5% above the ungapped case. This was not expected, because all of the other runs, each with more gaps, had not significantly changed the failure stress. So, the model was run with the gap in the 90° plies. This produced nearly the opposite effect. The stress was approximately 6% *below* the ungapped failure stress. These results were confusing and seemed incorrect, but mesh dependencies were not apparent in the ungapped run. The only straightforward explanation was that in the 4, 3, and 2 gap runs, the gap influence was spread throughout the composite and around the hole perimeter by buffering the hole stress concentration. This allowed the entire gauge section to absorb the gap effects. The 1 gap runs localized the gap effects much more, and so may have been able to concentrate the gap influence.

The centered gap mesh runs were then complete. An  $a_0$  was found to apply the Whitney-Nuismer failure criterion, and, save the 1 gap runs, the presence of resin gaps



With the empirically determined  $a_0$ , failure was predicted in the gapped runs. The first run was with 4 gaps. Strain plots in the loading direction are in Figures 6.8 and 6.9.

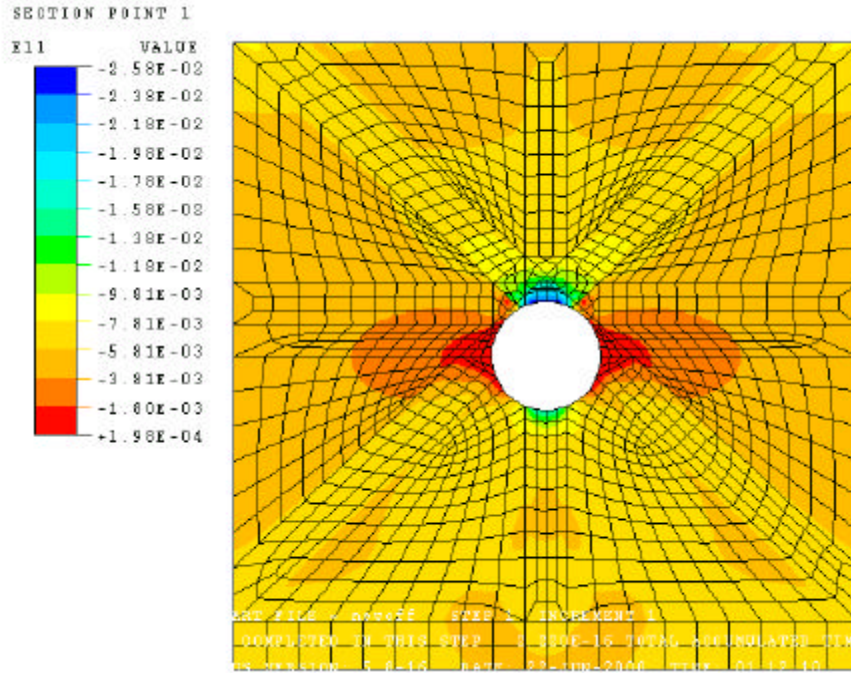


Figure 6.8. Loading direction strain contours for a open hole shell model, offset gaps mesh, 4 gap run.

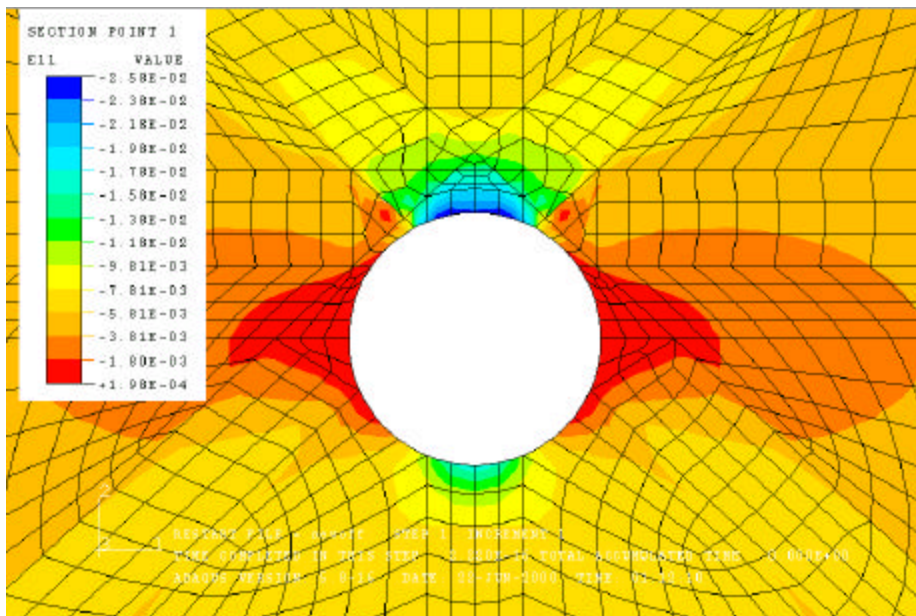


Figure 6.9. Detail of loading direction strain contours for a open hole shell model, offset gaps mesh, 4 gap run.

The strain is quite different from the no gap case. The strain is very high in the gapped region on the hole circumference. The small, half octagon is solid resin throughout the entire laminate thickness, and contained the highest strains. However, the highest strains do not correspond to failure. The resin is more compliant than the fiber direction in the composite, and its stress was further from failure than the surrounding composite. This is easily seen in a maximum stress plot, shown in Figure 6.10.

The closest stresses to failure were the fibers on the ungapped side of the hole. The next highest was where the fibers began again after the gap in the  $0^\circ$  layer. This made sense, since the resin area around the hole did not carry as much load, forcing the other side of the hole carry more. This phenomenon also dictated that the ungapped side of the hole be used for the failure analysis.

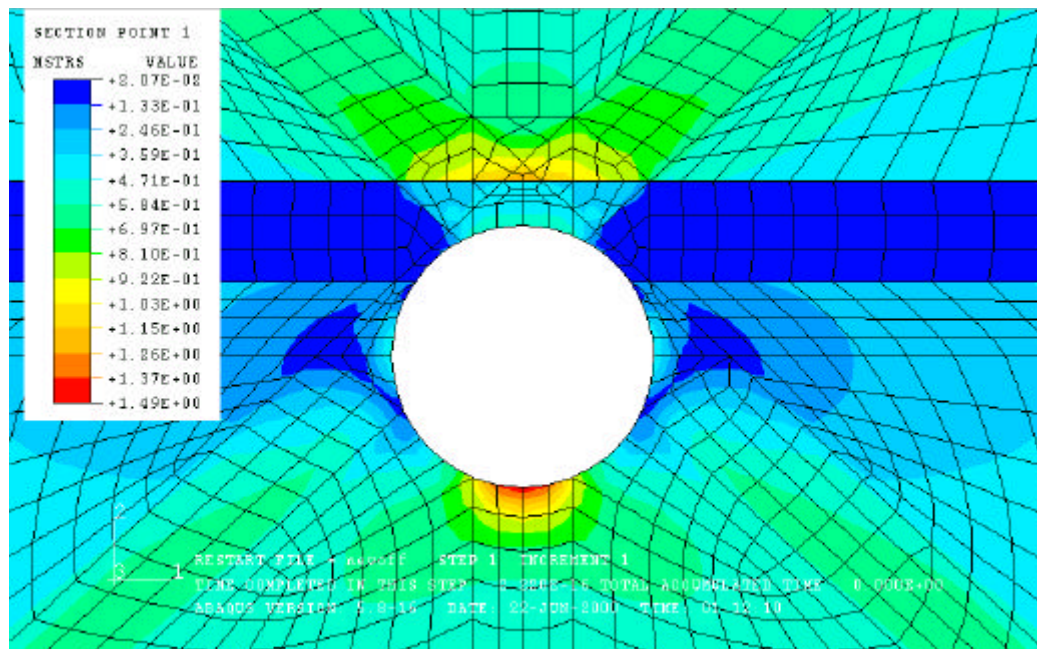


Figure 6.10. Zero degree ply maximum stress contour plot of an open hole shell model, offset gap mesh, 4 gap run.

The Whitney-Nuismer average stress(or strain) failure was again used. The  $a_0$  from the ungapped case was used to calculate the average strain. Again, the results were scaled to failure and converted to stress. The failure stress was (49.82 ksi), 12% lower than the ungapped failure stress. 3, 2, and 1 gap cases were also run. The results are presented in Table 6.2.

Table 6.2. Comparison of predicted OHC failure stresses in offset gap, open hole model.

<b>Run</b>	<b>Predicted Net Failure Stress MPa (ksi)</b>	<b>Run stress/ungapped stress (%)</b>
no gaps	389 (56.40)	100.0
1 gap 0°	373 (54.11)	95.9
1 gap 90°	366 (53.06)	94.1
2 gaps 0°/90°	350 (50.80)	90.1
3 gaps 0°/90°/45°	347 (50.42)	89.4
4 gaps	343 (49.82)	88.3

For this mesh, a consistent trend is seen. The 4 gap run had the lowest strength, with the strengths increasing toward the ungapped configuration. It was discussed previously why the 4 gap case caused higher strains. The compliant gaps made the opposite side of the hole carry more load, and consequently fail prematurely. This effect was decreased with fewer resin gaps in the run.

The offset gap geometry resulted in predicted failure at a lower net stress than an ungapped sample. Typically, this observation was not made in the centered gap case. So comparisons were made between the results of the two different gap geometries.

### Comparison of Centered and Offset Meshes

Several of the data points compared well. The first comparison was between the  $a_0$  parameters calculated in each of the ungapped cases. In the ungapped case, each model had identical stacking sequence, symmetry, and geometry and should have produced nearly identical results despite the asymmetry in the meshing. This was the case with the calculation of  $a_0$ ; the aforementioned values were less than 1% from each other.

The only other case where each of the models had the exact same geometry was in the 1 gap 90° case. Again, these results should have compared well; the difference in the failure stresses was less than 1%. These results gave considerable confidence in the accuracy of the two meshes, and the lack of mesh dependence on the results. However, when different geometries were modeled, they produced significantly different results.

The 4 gap runs for both meshes produced different results. The centered gap case did not change failure from the ungapped case, while the offset gap case produced a 12% decrease in failure stress. However, the entire gap interaction region in the centered gap mesh was removed by the hole. It was not removed in the offset gap mesh. So, the gap effects in the centered gaps mesh were spread out around the hole perimeter more, while the offset gaps had more gap interaction, and this interaction was localized more. A comparison chart is shown in Figure 6.11. Generally, the centered gap mesh runs had predicted failure stresses equal to the ungapped run, and the predicted offset gap strengths fell below the ungapped.

### Comparison of Centered and Offset Mesh Results

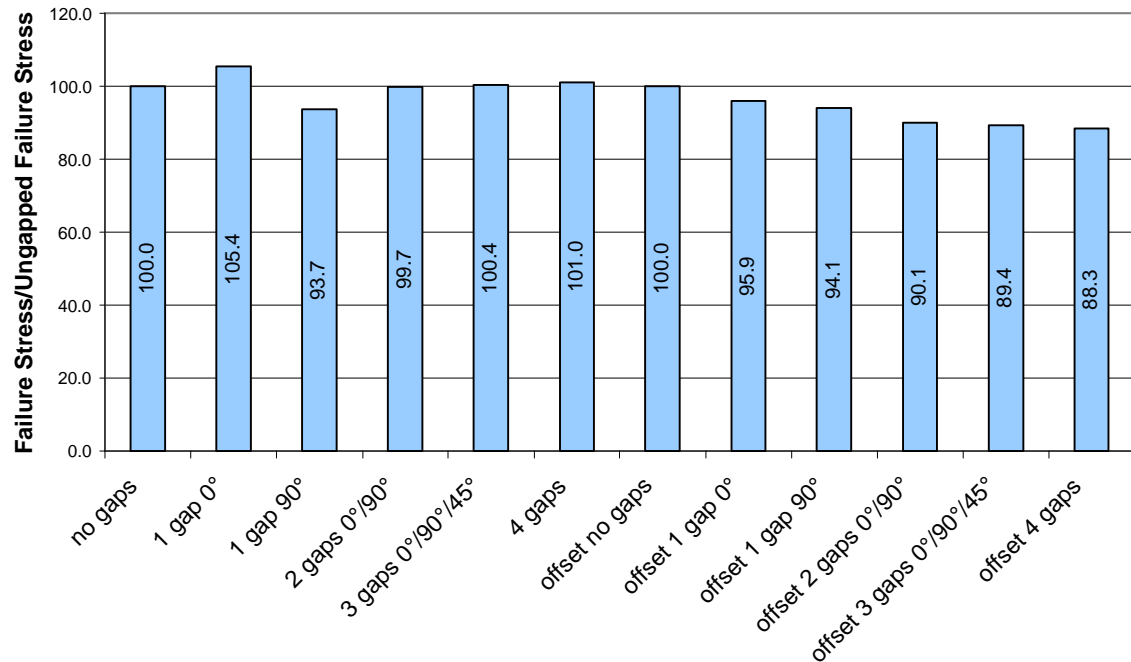


Figure 6.11. OHC stress based numerical prediction comparisons.

Numerical model comparisons were made. They compared well where they were expected to, and gave interesting results otherwise. Nevertheless, the most important results were how the computer models compared to the experimental results.

#### Experimental and Numerical Comparisons

It was important to compare the computer simulations with the test results. This allowed the validity of the computer simulations to be established and gave insight on failure mechanisms. When possible, the results were compared in three different ways. The first was to compare the elastic strain data. This was only possible when photoelastic measurements had been made. The next way was to compare damage. This allowed

comparisons of when and where damage occurred in the composite, both experimentally and numerically. Finally, the failures were compared.

Unnotched Compression. The first comparisons made were the unnotched compression tests. These samples were not tested photoelastically, and so elastic strain field measurements were not made. Additionally, the samples failed catastrophically, so the tests could not be stopped before ultimate failure occurred. So, a damage or failure initiation was not possible. An ultimate failure comparison was performed.

Zero and three gap samples were tested. Obviously, the ungapped finite element runs predicted the experiment only as well as the material properties used. The material properties were calculated from the Boeing published results and so the unnotched, ungapped numerical and Boeing experimental results matched by definition. Given this, the numerical results and MSU experimental results were off by the same amount as the MSU experimental results were off of the Boeing data. This was discussed in chapter 5.

Three-gap tests and computer simulations were run. Experimentally, the 3 gap tests failed at a 9% lower stress than the MSU ungapped data. This 9% reduction was compared to the 3% reduction found numerically. Therefore, the experimental tests produced a greater reduction in strength than was predicted with the finite element models. This was partially expected, because the numerical models did not incorporate any bending effects, nor did they incorporate any out of plane ply waviness. These two factors were expected to further reduce the strength of the laminate. These are discussed in more detail later in the chapter. The next comparisons were made between open hole compression results.

Open Hole Compression. Open hole comparisons were made in all of the categories. The first comparison was between the elastic strain results.

The photoelastic results validated the trends that were seen in the numerical study. The strains in the gapped material were higher than the ungapped strain, with the strain contours notably influenced by the gaps in the photoelastic pictures and in the numerical strain contour plots. A preliminary quantitative comparison was also performed, and is consistent with the numerical trends. The details are in Appendix B.

The next comparison was made between OHC damage results. The first evaluation was when damage initiated. In all of the experimental tests, the first audible cracking in the samples was heard between 44 to 58 kN (10 to 13 kips). This corresponded to 234 to 300 MPa (34 to 44 ksi) net (hole area excluded) stress. The first damage noted in the finite element models was at a net stress of 232 MPa (33.6 ksi). This was acceptably close, but was on the low side. This was expected, because the damage during the tests was the first audible damage, while the damage in the FE runs was simply the first damage calculated. Therefore, damage occurring that was not heard over the room noise (hydraulic pumps, etc.) would cause the experimental damage recorded to be higher than the numerical one.

The experimental results presented in Chapter 5 showed damage in the samples. Nearly every major damage site in these samples was in 0° plies. So, numerical damage prediction was expected in these plies as well. The 0° plies in the finite element models contained the damage initiation sites. Of course, no fiber failure modes were predicted by the models, but failure was indicated in the zero degree plies. The predicted failure

stress changed in magnitude between the various gap geometries, however the locations of these failures did not. The microscope examination of the damaged samples rendered the same result.

The final comparison concerned sample failure. The results were compared to the experimental values. A chart of the experimental and numerical results is in Figure 6.12.

### OHC Experimental/Numerical Comparisons

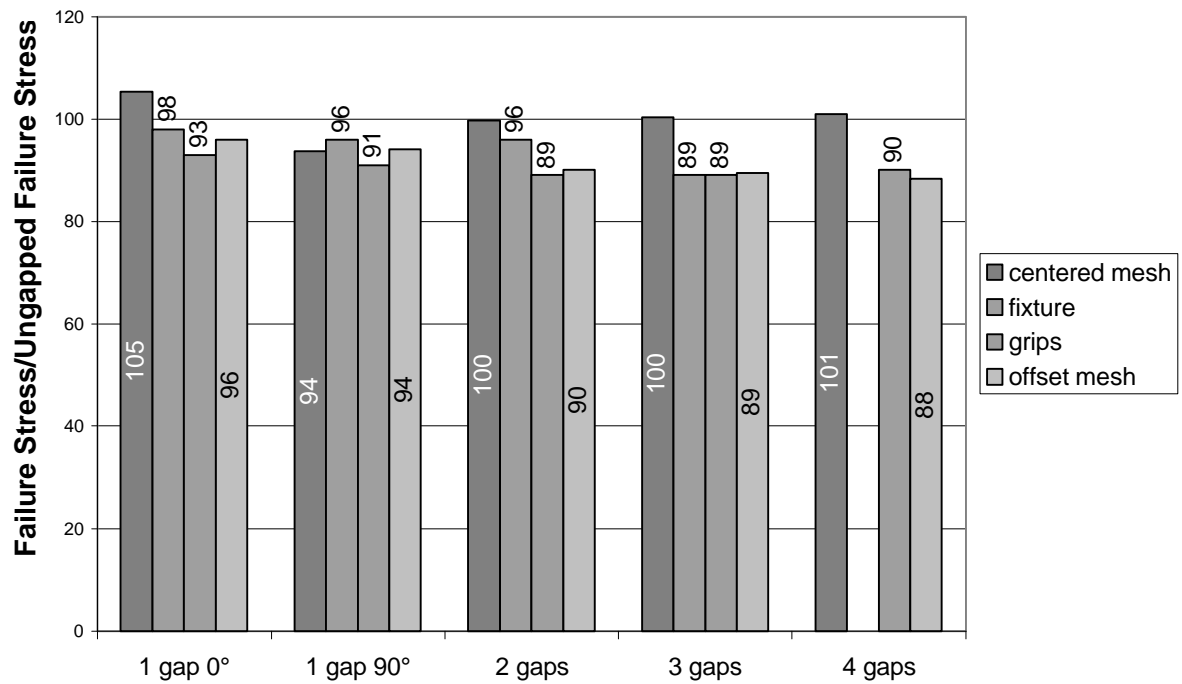


Figure 6.12. OHC stress based experimental/numerical comparisons.

The percentage of the ungapped OHC failure stress (Boeing and/or fixture data) that a sample or model attained or predicted is shown in Figure 6.12. The only case that significantly exceeded 100% was the centered gap model, 1 gap 0° run. All of the other tests fell below the ungapped OHC failure. The two different mesh geometries bounded

the gap influence analytically. The largest numerical failure strength reduction was in the 4 gap run of the offset gap model, at 88%. The largest failure strength increase was with the 1 gap 0° run of the centered gap model, at 105%.

The experimental range was not the same. The 2 and 3 gap cases showed the worst behavior, at 89% of the ungapped failure strength. The 1 gap 0° case produced the highest results, at 98% of the ungapped failure strength. The experimental results usually saw reductions slightly greater than predicted numerically. The offset gap model typically predicted the experimental failure stresses better, although it was rare that the test samples had the gap severity of the offset model. This was attributed to something that was not included in the models.

Two different properties were candidates for the reduction: bending during the tests and out of plane waviness. The fixture attempted to eliminate any bending introduced into the sample. However, the samples themselves may have introduced bending. Sample thickness results were presented in chapter 5. They indicated that the gaps affected the thickness of the laminate by as much as 0.3 mm (0.01 in). This was approximately 5% of the laminate thickness. The thickness variations happened at the ends of the sample and at the center of the sample. A basic schematic of these two scenarios is in Figure 6.13.

It is seen in these side view drawings how bending was introduced into the samples due to their varying thickness. Using a thickness variation of .25 mm (0.01 in), a load of 67 kN (15 kips), and basic statics, a bending moment of 8.5 N-m (75 in-lbs) was approximated from the eccentric loading. This was a significant bending moment. This

moment was input into the laminated plate program Laminate Analysis (P. Minguet, 1992). It reduced the predicted failure of an unnotched, ungapped sample by 9%.

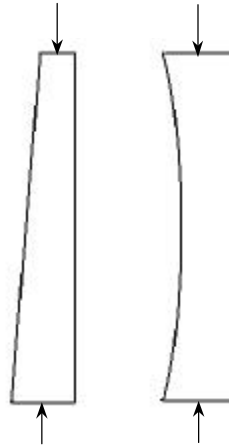


Figure 6.13. Schematics of samples with varying thickness.

Out of plane ply waviness was another factor that may have reduced the laminate strength. Work performed by Adams and Hyer was discussed in Chapter 2. They used amplitude ( $\delta$ ) and wavelength ( $\lambda$ ) of the ply wave to characterize the ply waviness. The ratio  $\delta/\lambda$  was used compare the strength reductions of unnotched compression tests. The data published ranged from a  $\delta/\lambda$  ratio of 0.02 to 0.08, with strength reductions ranging from 1 to 36%.

Measurements similar to Adams and Hyer's were taken from samples containing gaps (Figure 6.14). The  $\delta/\lambda$  ratios ranged from as small 0 to as large as 0.08, depending on the number of gaps and gap width, etc. So, while the waves were formed differently and Adams and Hyer's waviness was much more controlled, similar wave severities were observed in the gapped laminates. Likewise, reductions of 0 to 16% were seen in the gapped laminates, which were within Adams and Hyer's ranges. This is seen in Figure 6.15. The shaded area is the range that the MSU gapped data fell in. These results

indicated that the ply waviness in a gapped laminate was severe enough to cause a strength reduction, and also showed agreement with prominent research in that area.

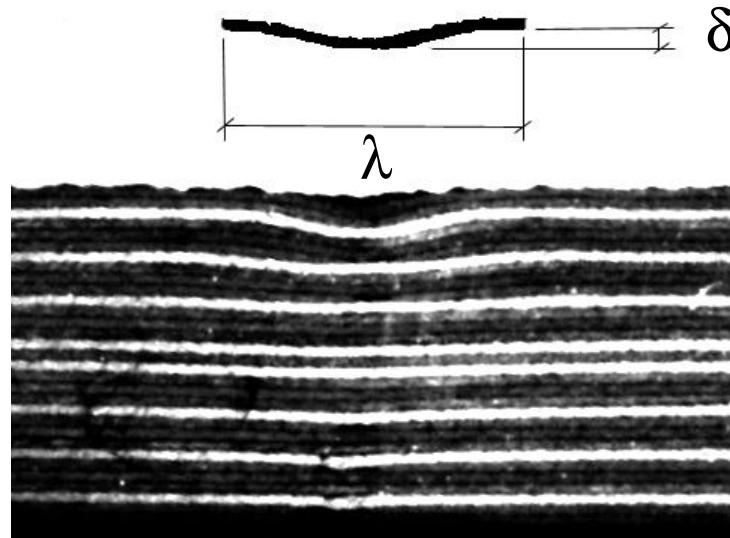


Figure 6.14. Example of layer waviness in a gapped laminate.

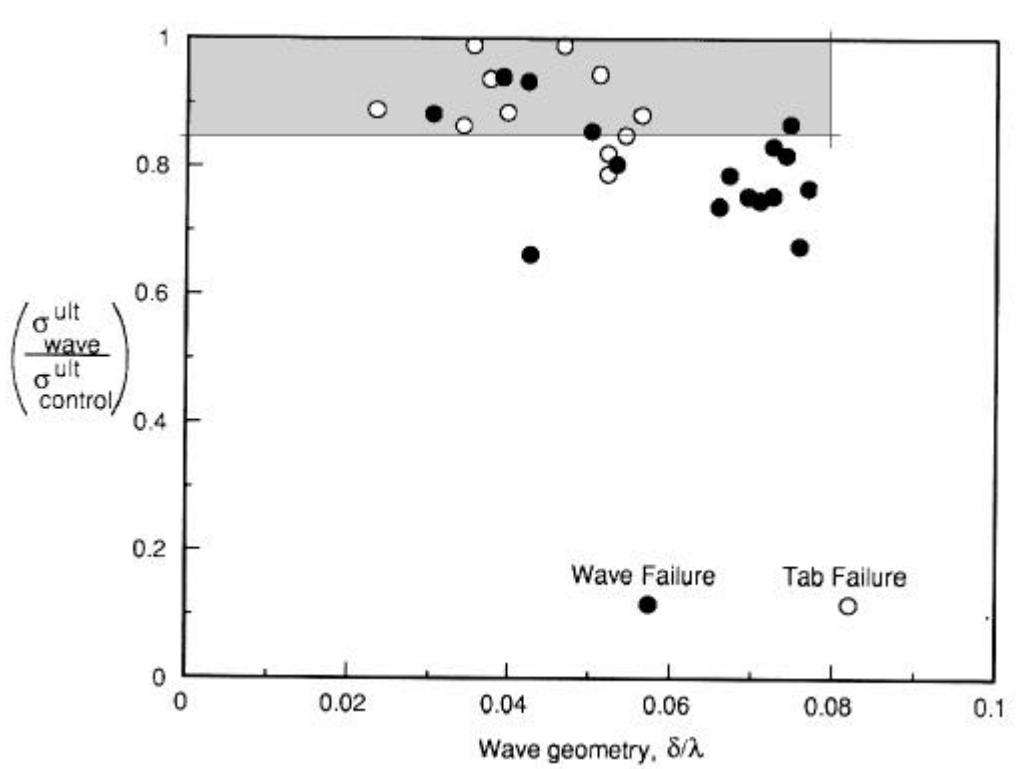


Figure 6.15. Strength reduction range (shaded area) for gapped samples with out of plane waviness. Adapted from Adams and Hyer.

## CHAPTER 7

## CONCLUSIONS AND RECOMMENDATIONS

Motivations, methods, and results have been presented on the effects of gaps on the strength of toughened carbon/epoxy prepreg composites. The results are summarized in this chapter, and recommendations that follow from those are made. These recommendations serve to apply the results to the composites and aerospace industry.

ResultsExperimental

The unnotched tension tests showed significant reductions in strength. The ungapped samples reached a failure stress of 980 MPa (142 ksi). The samples tested with 3 gaps were nearly 16% lower, at 830 MPa (120 ksi). The open hole tension tests were unaffected by the presence of gaps, with a net failure stress of 490 MPa (71 ksi). This was attributed to the hole effect dominating the gap effects.

The unnotched compression strength was reduced 4% from ungapped to 3 gap samples. This was lower than the unnotched tension reduction, but bending caused by sample asymmetry influenced the tests, and may have overshadowed the effect of the gaps. The ungapped tests were 19% below the UNC strength reported by Boeing [Avery, (1999)].

The open hole compression tests were hydraulically gripped and loaded in a compression fixture. The gripped ungapped OHC results were 6% lower than the Boeing published value. Again, sample induced bending was attributed to this. The gap reductions for the machine gripped and gapped OHC tests were 2%, 5%, 5%, and 3% for 1, 2, 3, and 4 gaps respectively. Staggered gap tests were also performed, with a strength reduction of 7%. Generally, the more gaps that were present in the sample, the more the strength was reduced.

The fixture OHC tests showed similar trends. However, the ungapped fixture OHC results were only 1% below the strengths reported by Boeing. Failure strength reductions of 2%, 3%, and 11% were observed for 1, 2, and 3 gaps, respectively. Again, the more gaps that were present in the sample, the more the strength was reduced. While the ungapped, 1 gap, and 2 gap cases were higher in the fixture OHC tests than the machine gripped OHC tests, the 3 gap values were the same. This implied that at a certain level of defects, the defects controlled the failure so much that the test method was inconsequential.

Photoelastic OHC tests were also run. The effects of the gaps were seen in the strain contours. It was also noted that gaps in the surrounding plies influenced the strain, with the gapped areas of those plies changing the contours as well. The strain gradient from the hole edge to the edge sample was compared to the numerical gradients. The trends compared well, with the gapped samples having higher strains than the ungapped. This validated the numerical trends that were observed.

OHC damage progression samples revealed nearly all of the damage present in these samples was in the zero degree plies. This damage was usually in the form of

compressive kink bands, although some delaminations were seen in the zero degree plies as well. No delaminations were observed between plies. The material was toughened between plies with thermoplastic particles, and the absence of delaminations between layers showed the effectiveness of the toughening mechanism. However, delaminations were seen within the plies, indicating that the delamination circumvented the toughened zones.

### Numerical

The unnotched cases were modeled with solid linear elements. Three and four gap cases were run. They had increased strain in the gaps and in the composite surrounding the gaps. The reduction in predicted failure stress was 4% and 7%, for 3 and 4 gap runs, respectively. The run times were fairly long for the 31 layers of solid elements, averaging around an hour.

Stacked shell quadratic elements were used in the open hole models. Shells were used to reduce the computer run times, especially because the complexity of the model geometry was increasing. Independent layers of shells were used so damage modeling could be possible. The shells significantly reduced the model run times, and are recommended for composite applications where transverse loading is negligible, and where the laminate stacking sequence is not a concern.

Two different gap geometries bounded the options of the relationship of the hole and gap locations: offset and centered. An average stress Whitney-Nuismer failure criterion was used. The centered gap model typically predicted smaller reductions in failure stress. The reductions predicted were 5% over and 6% under the OHC ungapped

failure stress for the 1 gap 0° and 1 gap 90° cases, respectively. The other gap cases in this model had failure stresses equal to the ungapped case. The offset gap model showed considerably more reductions. Reductions of 4%, 5%, 10%, 11%, and 12% were predicted for the 1 gap 0°, 1 gap 90°, 2, 3, and 4 gap cases, respectively.

While the models predicted quite different results for the two different gap/hole geometries, two of the gap cases for the models modeled the exact same geometry: no gaps and 1 gap 90°. In both of these cases, the predicted failure stresses in each model were within 1% of each other. This gave confidence in the numerical predictions and verified FE mesh insensitivity. The large difference in the results of the other gap cases showed that the failure predictions were dependant on the gap locations and the number of gaps. Typically, the more gaps present, the lower the failure stress. In both models and all of the gap cases, failure was predicted in the zero degree plies.

The two numerical models typically bounded the experimental results. The offset gap model was usually much closer to the experimental data, although it was rare that the test samples had the gap severity of the offset model. This indicated that other factors might have reduced the strength as well. Layer waviness and thickness variations were considered and determined to be likely factors. However, it appear that there is little interaction, since the experimental results are within the prediction of each mode (inhomogeneity, waviness, or bending).

### Design and Manufacturing Recommendations

Based on the experimental and numerical results, a four gap case was shown to have only a small difference from the three gap case. Therefore, the three gap data are

used to recommend strength values for design. Design allowables are recommended based on the results above. The unnotched tension, open hole tension, and unnotched compression values should be reduced 16%, 0%, and 9%, respectively. However, these numbers should be used cautiously, because only 3 to 5 samples were tested in these categories. They should be used for general trends and to initiate more tests in those areas to have a statistically justifiable failure strength reduction. The open hole compression tests had significantly more samples tested. The results showed that in this case, a laminate with unstaggered gaps had a higher failure stress than a one with staggered gaps. So, if the staggered gap orientation is used, the OHC strength reduction should be 12%.

This research brought up many manufacturing considerations. First, as stated above, the unstaggered orientation gave higher OHC strength results than the staggered configuration. While the strengths were only off by around 1%, it still indicated that the staggered orientation was not adding any strength to the laminate. This is magnified by the fact that the staggered arrangement places more constraints on the layup sequence and contour tape layup machine programming. It appears that many of these constraints may be removed without any reduction (or with a potential increase) of the OHC strength.

Characterization of the material samples also revealed other manufacturing considerations. The gaps caused out of plane layer waviness and thickness variations. These were briefly studied and related to applicable research. At a first glance, these defects seemed capable of reductions of 10% or more, but do not interact to produce a worst scenario of a greater than 30% strength reduction. If steps were taken to eliminate

either of these during manufacturing, the compressive strength values are expected to rise.

### Future Work

Many questions have been answered through the results of this research. However, questions have also arisen from it. These could be answered with further study. Some of these are addressed below.

The unstaggered OHC failure stress was higher than the staggered one. A switch to an unstaggered layup may be warranted based on the results presented. However, the OHC test had a gauge section of 38 by 38 mm (1.5 by 1.5 in.). The staggered configuration filled this entire gauge section with defects. The lower failure stress observed may have been an artifact of the high defect density in the sample. That high concentration of defects on a volumetric basis would not necessarily be present in a structure. Tests with larger gauge sections would address this issue damage stability and hole interactions.

It was unclear how much the resin gaps themselves were responsible for the strength reductions. Much of the reductions could have come from the geometric perturbations that the gaps induced: out of plane layer waviness and thickness variations. Flat panels with gaps could be manufactured with rigid mold surfaces on the top and the bottom of the laminate (the current process has a rigid plate only on one side, with the other vacuum bagged). This may eliminate both the waviness and the thickness variations. Tests from these panels would isolate the sole effects of the gaps.

Finally, a small number of tests were run in unnotched tension, open hole tension, and unnotched compression. More tests in each of these areas would give the results more statistical strength.

## REFERENCES CITED

- Adams, D.O., and M.W. Hyer. 1994. "Effects of Layer Waviness on the Compression Resopnse of Laminates", *ASTM STP 1185: Compression Response of Composite Structures*, p. 65-77.
- Agarwal, Bhagwan D., and Lawrence J. Broutman. 1990. *Analysis and Performance of Fiber Composites*. John Wiley and Sons, Inc.
- Avery, William. 1999. Personal correspondence. Boeing Commercial Airplane Group.
- Cairns, Douglas S., Ilcewicz, Larry B., and Tom Walker. 1993. "Far-Field and Near-Field Strain Response of Automated Tow-Placed Laminates to Stress Concentrations", *Composites Engineering*, 3-11:1087-1097
- Cairns, D.S. 1990. "Mechanisms of Fracture and Toughening in Multiphase Materials", *22<sup>nd</sup> International SAMPE Technical Conference*, November 6-8, p 432-445.
- Camponeschi, Eugene T. Jr. 1991. "Compression of Composite Materials: A Review", *ASTM STP 1110, Composite Materials: Fatigue and Fracture, Third Volume*, p. 550-578.
- Coguill, Scott L. and Donald F. Adams. 2000. "A Comparison of Open-Hole Compression Fixtures by Experimental Evaluation", *Book 1, 45<sup>th</sup> International SAMPE Symposium*, p 1095-1105.
- Dally, James W., and William F. Riley. 1965. *Experimental Stress Analysis*. McGraw-Hill Book Company.
- Dominguez, Fred S. 1987. "Unidirectional Tape Prepregs," *Engineering Materials Handbook, Volume 1, Composites*, pp. 143-145.
- Edens, Michael and Douglas Cairns. 2000. Effects of Tape Gaps and Stagger on the Strength and Stiffness of Composite Laminates: Final Report.
- Gosnell, Rex B. 1987. "Thermoplastic Resins," *Engineering Materials Handbook, Volume 1, Composites*, pp. 97-104.
- Grant, Carroll G. 2000. "Fiber Placement Process Utilization within the Worldwide Aerospace Industry", *Book 1, 45<sup>th</sup> International SAMPE Symposium*, p 709-720.
- Groves, Scott E., and Alton L. Highsmith. 1994. *Compression Response of Composite Stuctures: ASTM STP 1185*. ASTM.

- Herakovic, Carl T. 1998. *Mechanics of Fibrous Composites*. John Wiley and Sons, Inc.
- Jones, Robert M. 1975. *Mechanics of Composite Materials*. Taylor and Francis.
- Lessard, Larry B. and Fu-Kuo Chang. 1991. "Damage Tolerance of Laminated Composites Containing an Open Hole and Subjected to Compressive Loadings: Part II—Experiment," *Journal of Composite Materials*, 25:49.
- Measurements Group: Photoelastic Division. 1992. *030 Series Photoelastic System Instruction Manual*.
- Odagiri, N., Kishi, H., and M. Yamashita. 1996. "Development of TORAYCA Prepreg P2302 Carbon Fiber Reinforced Plastic for Aircraft Primary Structural Materials", *Advanced Composite Materials*, 5:249-252.
- Peterson, R. E. 1974. *Stress Concentration Factors*. John Wiley and Sons.
- Phillips, Joseph L., and Robert T. Parker. 1987. "Fastener Hole Considerations," *Engineering Materials Handbook, Volume 1, Composites*, pp. 712-715.
- Pirrung, Paul F. 1987. "Flat Tape Laying," *Engineering Materials Handbook, Volume 1, Composites*, pp. 624-630.
- Sawicki, A.J., and P.J. Minguet. 1998. "The Effect of Intraply Overlaps and Gaps Upon the Compression Strength of Composite Laminates", *Collection of Technical Papers—AIAA/ASME/ASCE/SHS/ASC Structures, Structural Dynamics & Materials Conference*, v 1 Apr 20-23, p 744-754.
- "Standard Test Method for Open Hole Tensile Strength of Polymer Matrix Composite Laminates, D 5766 –95", 1997 Annual Book of ASTM Standards, Vol. 15.03, 1997, pp. 296-300.
- "Standard Test Method for Compressive Properties of Polymer Matrix Composite Materials with Unsupported Gage Section by Shear Loading, D 3410M – 95", 1997 Annual Book of ASTM Standards, Vol. 15.03, 1997, pp. 116-137.
- Turoski, Luke. 2000. Unpublished report, MSU Composites Group.
- Whishart, Rod. 1999. Intec internal composite drilling procedure.
- Williams, Lynn A. III. 1987. "Contoured Tape Laying," *Engineering Materials Handbook, Volume 1, Composites*, pp. 631-635.

APPENDICES

APPENDIX A

Test Results

## All Test Data

Hole dia. 0.25  
Nom thick 0.234

Sample	Defects	Geometry	Notch	Test	Width (in)	Thick-ness (in)	Max Force (kips)	Stress (ksi)	Norm-alized Net Stress (ksi)	Notes
3I9	no gaps	small radius	none	tension	1.045	0.235	25.26	102.86	n/a	routed
3FG67	max(4) gaps	small radius	none	tension	1.025	0.235	23.49	97.52	n/a	routed
3IJ67	max(4) gaps	small radius	none	tension	1.016	0.235	20.3	85.02	n/a	routed
3C2	no gaps	normal	none	tension	1.516	0.238	28.88	80.04	n/a	no tabs/grip failure/90 direction
3C9	no gaps	normal	none	tension	1.537	0.232	44.1	123.67	n/a	grip failure
3B9	no gaps	long/radius	none	tension	0.855	0.238	29.22	143.68	n/a	routed
3I2	no gaps	long/radius	none	tension	0.845	0.2395	28.55	141.06	n/a	routed
3G9	no gaps	long/radius	none	tension	0.844	0.2395	27.03	133.72	n/a	routed
avg	no gaps	long/radius	none	tension				139.49	n/a	
2IJ9	3 gaps	long/radius	none	tension	0.86	0.228	24.35	124.18	n/a	routed
2IJ5	3 gaps	long/radius	none	tension	0.845	0.226	24.19	126.67	n/a	routed/mold surface torn
2IJ8	3 gaps	long/radius	none	tension	0.868	0.228	23.81	120.31	n/a	routed
avg	3 gaps	long/radius	none	tension				123.72	n/a	
2F5	no gaps	long(8")	.25 hole	tension	1.515	0.237	25.18	70.13	85.06	
2H3	no gaps	long(8")	.25 hole	tension	1.514	0.237	24.87	69.31	84.08	
2C5	no gaps	long(8")	.25 hole	tension	1.519	0.236	25.29	70.55	85.17	
avg	no gaps	long(8")	.25 hole	tension				70.00	84.77	

Sample	Defects	Geometry	Notch	Test	Width (in)	Thick-ness (in)	Max Force (kips)	Stress (ksi)	Norm-alized Net Stress (ksi)	Notes
2IJ2	3 gaps	long(8")	.25 hole	tension	1.579	0.231	26.42	72.43	84.96	
2BC910	3 gaps	long(8")	.25 hole	tension	1.47	0.234	24.42	70.99	85.54	
2IJ4	3 gaps	long(8")	.25 hole	tension	1.447	0.231	23.81	71.23	85.01	
avg	3 gaps	long(8")	.25 hole	tension				71.55	85.17	
3C8	no gaps	normal	none	compression	1.517	0.235	31.04	87.07	n/a	
3F8	no gaps	normal	none	compression	1.51	0.238	29.99	83.45	n/a	no tabs/grip failure
3I8	no gaps	normal	none	compression	1.517	0.237	27.52	76.57	n/a	
3G8	no gaps	normal	none	compression	1.494	0.24	26.57	74.1	n/a	no tabs/grip failure
3DE89	max(4) gaps	normal	none	compression	1.518	0.2315	27.2	77.40	n/a	
3DE12	max(4) gaps	normal	none	compression	1.545	0.235	23.07	63.54	n/a	no tabs
3B5	no gaps	narrow(1")	none	compression	0.992	0.234	21.57	92.92	n/a	inst 8501
3G4	no gaps	narrow(1")	none	compression	0.99	0.236	18.06	77.30	n/a	mts
2B5	no gaps	narrow(1")	none	compression	0.993	0.237	18.77	79.76	n/a	mts
2B4	no gaps	narrow(1")	none	compression	1.002	0.235	16.59	70.45	n/a	mts
2H7	no gaps	narrow(1")	none	compression	1.002	0.236	16.83	71.17	n/a	mts
avg	no gaps	narrow(1")	none	compression				78.32	n/a	
3AB5	1 vertical	narrow(1")	none	compression	0.983	0.233	20.05	87.54	n/a	inst 8501
3C67	1 horizontal	narrow(1")	none	compression	0.99	0.233	20.76	90.00	n/a	inst 8501
2AB78	3 gaps	narrow(1")	none	compression	0.895	0.23	15.4	74.81	n/a	mts
2AB45	3 gaps	narrow(1")	none	compression	0.995	0.23	17.39	75.99	n/a	mts
2BC5	3 gaps	narrow(1")	none	compression	1.02	0.231	16.45	69.82	n/a	mts
2AB56	3 gaps	narrow(1")	none	compression	1.02	0.23	17.09	72.85	n/a	mts
avg	3 gaps	narrow(1")	none	compression				73.37	n/a	

Sample	Defects	Geometry	Notch	Test	Width (in)	Thick-ness (in)	Max Force (kips)	Stress (ksi)	Norm-alized Net Stress (ksi)	Notes
3DE5	1 verticle	narrow(0.5")	none	compression	0.508	0.233	9.452	79.86	n/a	inst 8501
3F67	1 horizontal	narrow(0.5")	none	compression	0.511	0.233	10.4	87.35	n/a	inst 8501
3F5	no gaps	normal	.25 hole	fixture comp.	1.549	0.236	18.81	51.45	61.88	me inst
3I4	no gaps	normal	.25 hole	fixture comp.	1.52	0.238	18.21	50.34	61.28	me inst
3D5	no gaps	normal	.25 hole	fixture comp.	1.509	0.236	16.79	47.15	56.99	me inst
3C3	no gaps	normal	.25 hole	fixture comp.	1.503	0.236	16.74	47.19	57.09	me inst
3D9	no gaps	normal	.25 hole	fixture comp.	1.5	0.236	16.94	47.85	57.91	me inst
avg	no gaps	normal	.25 hole	fixture comp.				48.80	59.03	
3FG5	3 gaps	normal	.25 hole	fixture comp.	1.554	0.235	17.33	47.45	56.79	me inst
3EF78	3 gaps	normal	.25 hole	fixture comp.	1.548	0.231	16.88	47.21	55.58	me inst
3FG8	3 gaps	normal	.25 hole	fixture comp.	1.6	0.234	16.29	43.51	51.57	me inst
3CD910	3 gaps	normal	.25 hole	fixture comp.	1.575	0.232	15.49	42.39	49.96	me inst
3FG910	3 gaps	normal	.25 hole	fixture comp.	1.59	0.231	15.33	41.74	48.89	me inst
avg	3 gaps	normal	.25 hole	fixture comp.				44.46	52.56	
3IJ5	2 gap(x)	normal	.25 hole	fixture comp.	1.63	0.231	18.18	48.28	56.30	me inst
3F3	2 gap(x)	normal	.25 hole	fixture comp.	1.565	0.233	17.11	46.92	55.60	me inst
3GH67	2 gap(+)	normal	.25 hole	fixture comp.	1.503	0.233	17.32	49.46	59.07	me inst
3AB34	2 gap(+)	normal	.25 hole	fixture comp.	1.542	0.232	17.36	48.53	57.42	me inst
3B12	2 gap(+)	normal	.25 hole	fixture comp.			14.79			
avg	2 gaps	normal	.25 hole	fixture comp.				48.30	57.10	
3DE6	1 gap(vert)	normal	.25 hole	fixture comp.	1.499	0.235	17.24	48.94	58.99	me inst
3DE4	1 gap(vert)	normal	.25 hole	fixture comp.	1.525	0.237	17.49	48.39	58.62	me inst
3I67	1 gap(hrzn)	normal	.25 hole	fixture comp.	1.51	0.236	17.44	48.94	59.15	me inst
3G67	2 gap(hrzn)	normal	.25 hole	fixture comp.	1.516	0.235	17.07	47.91	57.62	me inst
3EE89	3 gap(hrzn)	normal	.25 hole	fixture comp.	1.514	0.236	16.2	45.34	54.77	me inst
avg	1 gap	normal	.25 hole	fixture comp.				47.91	57.83	

Sample	Defects	Geometry	Notch	Test	Width (in)	Thick-ness (in)	Max Force (kips)	Stress (ksi)	Norm-alized Net Stress (ksi)	Notes
2G9	no gaps	normal	.25 hole	compression	1.488	0.24	16.07	45.00	55.47	inst/slight breakthrough
3G3	no gaps	normal	.25 hole	compression	1.511	0.237	17.46	48.76	59.17	inst 8501
2I9	no gaps	normal	.25 hole	compression	1.488	0.24	17.22	48.22	59.44	inst 8501
2I8	no gaps	normal	.25 hole	compression	1.521	0.237	16.84	46.72	56.62	
2G8	no gaps	normal	.25 hole	compression	1.522	0.237	16.76	46.46	56.31	
2F8	no gaps	normal	.25 hole	compression	1.522	0.237	16.61	46.05	55.80	
2D3	no gaps	normal	.25 hole	mts2 comp.	1.496	0.237	15.34	43.27	52.61	
2G6	no gaps	normal	.25 hole	mts2 comp.	1.5	0.236	16.6	46.89	56.75	
3B4	no gaps	normal	.25 hole	mts2 comp.	1.495	0.236	16.4	46.48	56.29	
2D4	no gaps	normal	.25 hole	mts2 comp.	1.5	0.237	16.04	45.12	54.84	slight delams on ms hole edge
2B9	no gaps	normal	.25 hole	mts2 comp.	1.488	0.235	16.25	46.47	56.09	
2C9	no gaps	normal	.25 hole	mts2 comp.	1.525	0.237	16.7	46.21	55.97	
3B9	no gaps	normal	.25 hole	mts2 comp.	1.497	0.237	16.35	46.08	56.03	
3C4	no gaps	normal	.25 hole	mts2 comp.	1.495	0.237	15.9	44.88	54.58	
2EE3	no gaps	normal	.25 hole	mts2 comp.	1.497	0.237	15.63	44.05	53.56	
2D9	no gaps	normal	.25 hole	mts2 comp.	1.524	0.234	16.18	45.37	54.27	
2F9	no gaps	normal	.25 hole	mts2 comp.	1.498	0.237	16.31	45.94	55.85	
2I5	no gaps	normal	.25 hole	mts2 comp.	1.495	0.237	16.69	47.10	57.29	
3F4	no gaps	normal	.25 hole	mts2 comp.	1.5	0.237	16.25	45.71	55.56	
2G5	no gaps	normal	.25 hole	mts2 comp.	1.497	0.237	15.94	44.93	54.63	
avg	no gaps	normal	.25 hole	compression				45.99	55.86	
2DE89	max(4) gaps	normal	.25 hole	compression	1.522	0.23	16.07	45.91	53.99	inst 8501
2IJ67	max(4) gaps	normal	.25 hole	compression	1.519	0.225	16.03	46.90	53.98	hole centered/gaps precise
avg	max(4) gaps	normal	.25 hole	compression				46.40	53.99	
2D67	3 gaps	normal	.25 hole	compression	1.521	0.227	15.7	45.47	52.79	porosity on back/edge on gap
3D67	3 gaps	normal	.25 hole	compression	1.493	0.232	16.27	46.97	55.94	inst/slight porosity
2EE67	3 gaps	normal	.25 hole	compression	1.494	0.228	15.8	46.38	54.28	inst/considerable porosity
2H67	3 gaps	normal	.25 hole	compression	1.472	0.23	14.86	43.89	51.97	inst/considerable porosity

Sample	Defects	Geometry	Notch	Test	Width (in)	Thick-ness (in)	Max Force (kips)	Stress (ksi)	Norm-alized Net Stress (ksi)	Notes
3B67	3 gaps	normal	.25 hole	compression	1.487	0.228	14.66	43.24	50.65	inst/considerable porosity
3H67	3 gaps	normal	.25 hole	compression	1.494	0.233	16.01	45.99	55.00	inst 8501
3EE67	3 gaps	normal	.25 hole	compression	1.49	0.23	15.08	44.00	51.97	inst
2EF910	3 gaps	normal	.25 hole	mts2 comp.	1.444	0.234	15.74	46.58	56.34	slight gap porosity
2EF23	3 gaps	normal	.25 hole	mts2 comp.	1.482	0.232	14.85	43.19	51.51	gap porosity
3F12	3 gaps	normal	.25 hole	mts2 comp.	1.49	0.23	14.69	42.87	50.63	glass tabs
2C12	3 gaps	normal	.25 hole	mts2 comp.	1.296	0.229	12.97	43.70	52.99	glass tabs/slight ms porosity
3DE7	3 gaps	normal	.25 hole	mts2 comp.	1.319	0.23	13.67	45.06	54.65	glass tabs
3DE3	3 gaps	normal	.25 hole	mts2 comp.	1.363	0.23	14.16	45.17	54.37	glass tabs
3IJ34	3 gaps	normal	.25 hole	mts2 comp.	1.54	0.23	15.21	42.94	50.39	
3IJ910	3 gaps	normal	.25 hole	mts2 comp.	1.497	0.227	15.63	46.00	53.56	
3IJ8	3 gaps	normal	.25 hole	mts2 comp.	1.517	0.232	15.72	44.67	53.02	slight delam bulge on mold side
2DE12	3 gaps	normal	.25 hole	mts2 comp.	1.398	0.232	14.08	43.41	52.41	gap porosity
2EF34	3 gaps	normal	.25 hole	mts2 comp.	1.451	0.232	14.69	43.64	52.27	
2BC8	3 gaps	normal	.25 hole	mts2 comp.	1.486	0.232	14.8	42.93	51.17	slight gap porosity
2FG23	3 gaps	normal	.25 hole	mts2 comp.	1.486	0.233	15.56	44.94	53.80	
2DE6	3 gaps	normal	.25 hole	mts2 comp.	1.457	0.231	14.78	43.91	52.33	considerable ms gap porosity
2FG910	3 gaps	normal	.25 hole	mts2 comp.	1.43	0.232	15.11	45.54	54.72	
2DE45	3 gaps	normal	.25 hole	mts2 comp.	1.435	0.23	14.85	44.99	53.55	slight hole delam, mold gap porosity
avg	3 gaps	normal	.25 hole	compression				44.59	53.06	
2D5	2 gaps x	normal	.25 hole	mts2 comp.	1.44	0.232	14.04	42.03	50.42	
2B3	2 gaps x	normal	.25 hole	mts2 comp.	1.485	0.231	15.12	44.08	52.32	slight ms por in gap
3C3	2 gaps x	normal	.25 hole	mts2 comp.	1.609	0.229	17.05	46.27	53.62	no tabs
2I3	2 gaps x	normal	.25 hole	mts2 comp.	1.436	0.232	14.72	44.18	53.04	slight ms por in gap
2FG89	2 gaps +	normal	.25 hole	mts2 comp.	1.53	0.233	16.29	45.70	54.39	slight delam around hole
2BC12	2 gaps +	normal	.25 hole	mts2 comp.	1.457	0.235	14.79	43.20	52.37	

Sample	Defects	Geometry	Notch	Test	Width (in)	Thick-ness (in)	Max Force (kips)	Stress (ksi)	Norm-alized Net Stress (ksi)	Notes
3FG12	2 gaps +	normal	.25 hole	mts2 comp.	1.53	0.235	15.55	43.25	51.92	no tabs
2GH67	2 gaps +	normal	.25 hole	mts2 comp.	1.435	0.234	15.14	45.09	54.60	
avg	2 gaps	normal	.25 hole	mts2 comp.				44.22	52.83	
2H12	1 gap -	normal	.25 hole	mts2 comp.	1.519	0.2235	16.78	49.43	56.51	
2D12	1 gap -	normal	.25 hole	mts2 comp.	1.525	0.235	16.08	44.87	53.90	
2C67	1 gap -	normal	.25 hole	mts2 comp.	1.525	0.236	16.3	45.29	54.63	
2EE12	1 gap -	normal	.25 hole	mts2 comp.	1.525	0.235	15.34	42.80	51.42	
2FG7	1 gap l	normal	.25 hole	mts2 comp.	1.499	0.236	15.87	44.86	54.30	
2CD8	1 gap l	normal	.25 hole	mts2 comp.	1.487	0.236	15.89	45.28	54.90	
2CD3	1 gap l	normal	.25 hole	mts2 comp.	1.489	0.235	16.46	47.04	56.77	
2BC3	1 gap l	normal	.25 hole	mts2 comp.	1.435	0.236	15.25	45.03	55.00	
avg	1 gap	normal	.25 hole	mts2 comp.				45.58	54.68	
1DE45	stagger	normal	.25 hole	mts2 comp.	1.485	0.232	14.24	41.33	49.28	
1IJ910	stagger	normal	.25 hole	mts2 comp.	1.482	0.235	14.84	42.61	51.48	
1GH89	stagger	normal	.25 hole	mts2 comp.	1.48	0.232	15.28	44.50	53.09	
1IJ34	stagger	normal	.25 hole	mts2 comp.	1.482	0.232	14.31	41.62	49.64	
1DE12	stagger	normal	.25 hole	mts2 comp.	1.48	0.232	14.86	43.28	51.63	
1FG34	stagger	normal	.25 hole	mts2 comp.	1.482	0.231	14.63	42.74	50.75	
1BC910	stagger	normal	.25 hole	mts2 comp.	1.483	0.232	15.36	44.64	53.24	
1BC67	stagger	normal	.25 hole	mts2 comp.	1.48	0.232	14.69	42.78	51.04	
1GH12	stagger	normal	.25 hole	mts2 comp.	1.48	0.232	14.86	43.28	51.63	
1AB89	stagger	normal	.25 hole	mts2 comp.	1.484	0.233	15.85	45.84	54.89	
1FG67	stagger	normal	.25 hole	mts2 comp.	1.484	0.234	14.85	42.76	51.43	
1DE89	stagger	normal	.25 hole	mts2 comp.	1.482	0.232	15.1	43.92	52.38	
1GH45	stagger	normal	.25 hole	mts2 comp.	1.483	0.231	14.94	43.61	51.78	
1EF23	stagger	normal	.25 hole	mts2 comp.	1.482	0.232	15.23	44.30	52.83	
avg								43.37	51.79	

<b>Sample</b>	<b>Defects</b>	<b>Geometry</b>	<b>Notch</b>	<b>Test</b>	<b>Width (in)</b>	<b>Thick- ness (in)</b>	<b>Max Force (kips)</b>	<b>Stress (ksi)</b>	<b>Norm- alized Net Stress (ksi)</b>	<b>Notes</b>
3D3	no gaps	Boeing	.25 hole	compression	1.501	0.2385	17.75	49.58	60.64	Boeing OHC
3E3	no gaps	Boeing	.25 hole	compression	1.5	0.2385	16.93	47.32	57.88	Boeing OHC
avg	no gaps	Boeing	.25 hole	compression				48.45	59.26	

APPENDIX B

Quantitative Photoelastic Results

### Quantitative Photoelastic Analysis

The photoelastic results were used qualitatively for comparison in Chapter 6. However, a preliminary quantitative analysis was performed.

Strain values from the FE models and the photoelastic tests were compared for the no, 2, and 3 gaps cases. The photoelastic applied stress (gross) was 70 MPa (10 ksi). The FE data was from the ungapped model. This was used to compare to all of the photoelastic tests. The gapped FE results were not used for comparison, because the specific gap configuration found in the samples was not modeled. The finite element results were scaled to photoelastic gross stress. The no gap case is shown in Figure 1.

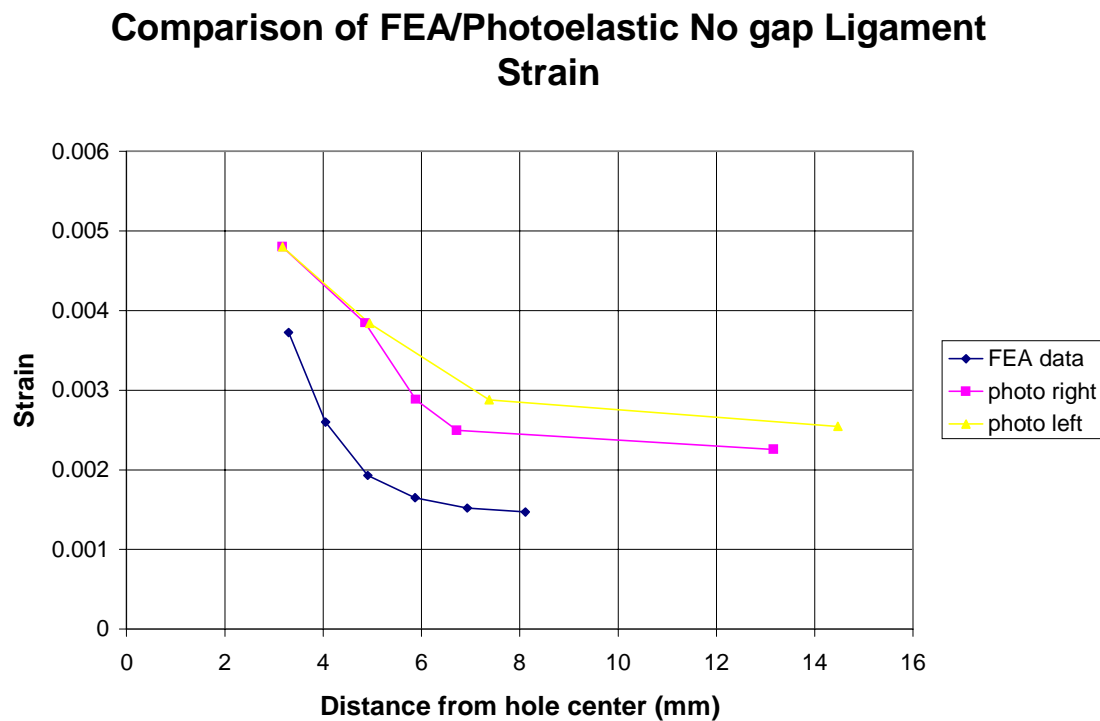


Figure 1. Comparison of FEA/Photoelastic no gap ligament strain.

Strains were extracted from the photoelastic measurements with the methods outlined in Dalley and Riley [(1965)], and in the polariscope manufacturer handbook [Measurements group, (1992)]. The equation used to extract these strains was

$$\varepsilon_x - \varepsilon_y = f \cdot N$$

where  $\varepsilon_x$  = principle strain  
 $\varepsilon_y$  = principle strain  
 $f$  = fringe value of coating(calibration or manufacturer)  
 $N$  = fringe order

The last two series plotted on the graphs were the data taken from the left and right sides of the hole of the photoelastic images. The data did not match perfectly. It was noted in Chapter 5 that the tests did not have back to back strain gauges, so the fixture was not accurately shimmed to eliminate bending from the loading. That could explain the offset of the curves. The strain decay with distance from the hole edge matched fairly well. The data points at the hole edge were not expected to match well because the resolution in the photoelastic pictures near the hole edge was poor, which limited how accurately the fringe order was determined. Next, the two and three gap cases were compared.

The two gap photoelastic sample had gaps in the 45 and -45 plies. The strains are shown in Figure 2.

### Comparison of FEA/Photoelastic 2 gap Ligament Strain

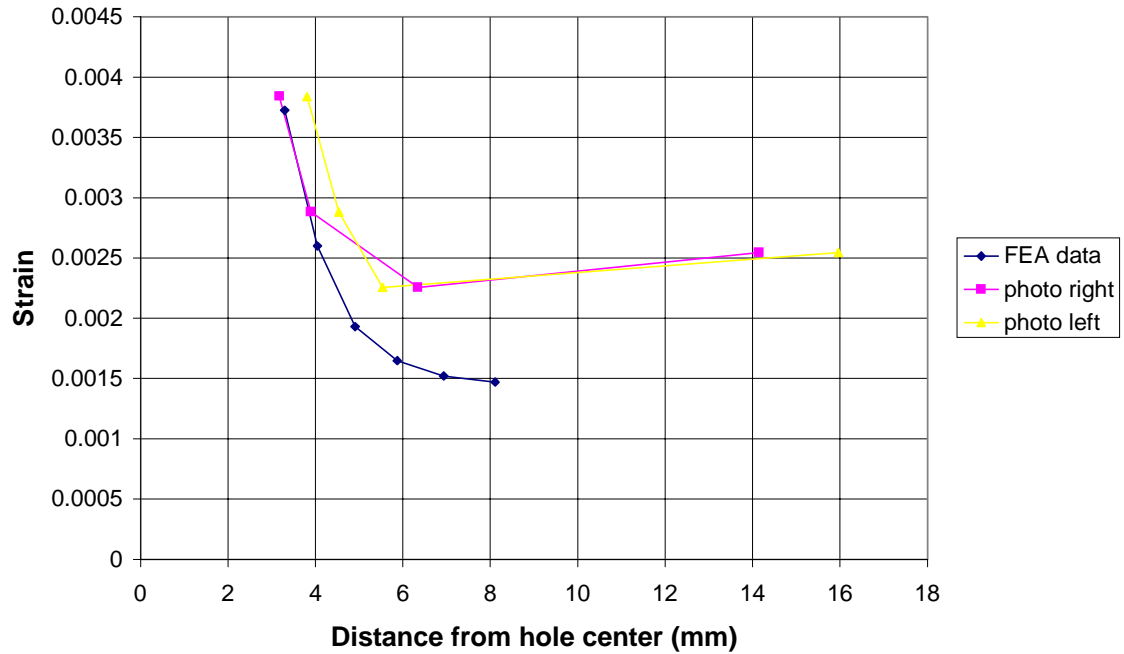


Figure 2. Comparison of FEA/photoelastic 2 gap ligament strains.

The data at the hole edge matches more closely than was expected. The trends matched fairly well near the hole, but the FE ungapped strain drops off more, away from the hole. The higher overall strains correspond to the gapped numerical models discussed earlier in this chapter. The numerical results had higher strains overall, and predicted failure before an ungapped case, and the results are consistent. Finally, the 3 gap configuration was compared. The photoelastic sample had a triangular gap configuration. The strains are shown in Figure 3.

### Comparison of FEA/Photoelastic 3 gap Strain

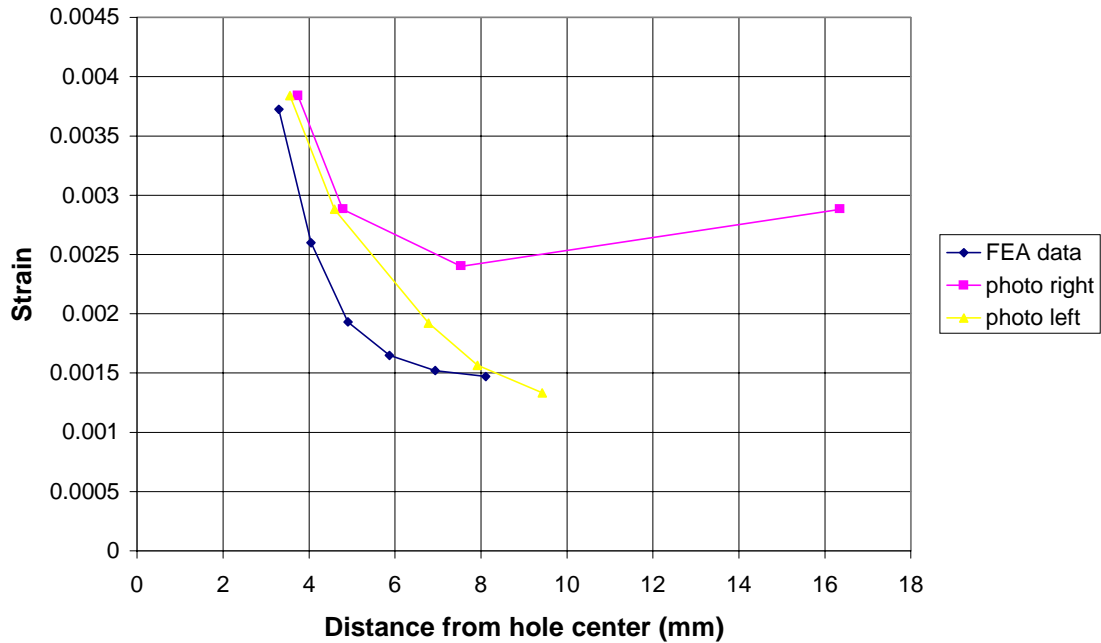


Figure 3. Comparison of FEA/photoelastic 3 gap strain.

Again, the data point at the hole edge matched well. The two different sides of the photoelastic sample were markedly different. However, the geometry was not symmetric for this sample, so the strains on the opposite sides could have been different. This comparison shows that the strains, especially away from the hole, were larger than the FE strains, similar to the two gap case, and the numerical trends seen earlier in Chapter 6.

This analysis has some validity and shows promise that photoelastic measurement methods can be used quantitatively for gapped materials, but warrant further work. Recommendations for refinement were more tests, to apply the photoelastic material on the mold side of the samples, and to use a larger zoom lens for the pictures taken, so more contour detail can be recorded.